ENGINEERING TARGETED PROTEINS FOR INTRACELLULAR DELIVERY OF BIOTHERAPEUTICS

MASSACHUSETTS INSTITUTE OF TECHNOLOGY
JUL 10 2012
LIBRARIES
ARCHIVES

By

Christopher M. Pirie

B.S., Bioengineering
University of Washington, 2006

Submitted to the Department of Biological Engineering
in Partial Fulfillment of the Requirements for the Degree of

Doctor of Philosophy in Biological Engineering

at the

Massachusetts Institute of Technology

September 2011

© 2011 Massachusetts Institute of Technology
All rights reserved

Signature of Author: .....
Department of Biological Engineering
August 31st, 2011

Certified by: .....
K. Dane Wittrup
C.P. Dubbs Professor of Chemical Engineering & Biological Engineering
Thesis Advisor

Accepted by: .....
Forest M. White
Assistant Professor of Biological Engineering
Co-Chair, Department Graduate Program Committee

Thesis committee members:

Doug Lauffenburger
Ford Professor and Head of Biological Engineering
Massachusetts Institute of Technology

Michael G. Rosenblum
Professor of Experimental Therapeutics, Division of Cancer Medicine
The University of Texas M.D. Anderson Cancer Center

Engineering Targeted Proteins for Intracellular Delivery of Biotherapeutics

By Christopher M. Pirie

Submitted to the Department of Biological Engineering on
August 22st, 2011 in Partial Fulfillment of the Requirements for the
Degree of Doctor of Philosophy in Biological Engineering

ABSTRACT

Biotherapeutics have revolutionized medicine with their ability to achieve unprecedented molecular recognition and mediate complex biological responses. The intracellular delivery of biotherapeutics is an unmet scientific challenge and medical need. A wide variety of different treatment modalities depend on not only on the ability to achieve intracellular delivery, but to do so in a targeted manner.

An independently-targeted, two-molecule system was developed to accomplish intracellular delivery in a uniquely specific manner. Immunotoxins were designed based on the plant toxin gelonin and targeted towards the canonical cancer-specific antigens: epidermal growth factor receptor and carcinoembryonic antigen. Using quantitative internalization flow cytometry matched with controlled exposure cytotoxicity, the number of internalized gelonin immunotoxins required to induce apoptosis in a single cell was found to be ~$5x10^6$ molecules. This threshold to cytotoxicity was conserved across all gelonin constructs regardless of antigen target, binding scaffold, affinity, or cell line. Next, cholesterol-dependent cytolysins were targeted to the same antigens by genetic fusion to engineered fibronectin domains. When combined *in vitro*, targeted gelonin and cytolysin had synergistic cytotoxic effects and the presence of cytolysin reduced the intracellular barrier to cytotoxicity to < 10^4 immunotoxin molecules. *In vivo*, these molecules induced non-specific, dose-limiting toxicities at varying levels and were cleared from the plasma at rates consistent with their molecular weight. Dosed individually, neither compound was capable of controlling tumor xenografts, but when combined in a delayed dosing scheme they inhibited tumor growth and induced apoptosis throughout xenografts as confirmed by histology. Mathematical modeling was informed by *in vivo* experiments and provided insight in dosing and tumor exposure overlap.

These results emphasize the necessity of a targeted intracellular delivery system and support the merit of the described approach. Additional research into the safety and efficacy of these molecules as well as the design of new constructs will certainly improve the clinical relevance of this technique.

Thesis Supervisor: K. Dane Wittrup
Title: C.P. Dubbs Professor of Chemical Engineering & Biological Engineering

Acknowledgements

The work that follows is the product of years of hard work. But none of it would have been possible without the help and support of a great number of people. I would be remiss if I started by thanking anyone other than my advisor Dane Wittrup. He accepted me into a lab and a technical area in which I had little experience and through his patience and wisdom I've learned to be a half-decent scientist. For that I am eternally grateful. In addition I was the fortunate beneficiary of research insight and scientific perspective from two other thesis committee members Doug Lauffenburger and Michael Rosenblum. As leaders in their respective fields they both have very full schedules and I can't thank them enough for taking the time to help instill in me some of their scientific acumen.

Surrounding me during the research journey that was my graduate school career were some of the brightest and friendliest people anyone could ask for. I am indebted to all of the students I have worked with past and present. Each of them has contributed to my work in one small way or another from sharing a reagent to feedback during group meetings. The congeniality in our lab is unrivaled and it makes coming in every morning and working odd hours infinitely more enjoyable. I should extend a special thanks to members who have contributed most directly to my research: Greg Thurber initiated the collaboration with the Rosenblum Lab that became my project. Michael Schmidt guided me in my earliest modeling work and provided the scFv's for my first immunotoxins. Benjamin Hackel was the father of fibronectin engineering in the lab and provided variants for later immunotoxins and fusions. David Liu's work in siRNA delivery built off of my own cytolysin discoveries and helped directly improve upon my work. And I thank my long-time, close-quarters officemates Jamie Spangler and Jordi Mata-Fink for putting up with me. During my time in the lab I was able to work with a number of promising young undergraduate students Sarah Gomez, Stephanie Bachar, Emanuel Quiroz, and Yuan Zhou as well as two marvelous masters' students Charlotte Varenne and Gabriela Pregernig. I'd like to acknowledge funding from a few different sources including the National Cancer Institute and the National Science Foundation.

Last, but certainly not least, I want to thank my friends and family. My first year in Cambridge was pretty tough between moving across the country and facing the rigors of core classes. I got through it only with the help of a special group of people: Scott Carlson, Lorenna Buck, Ranjani Paradise, Kristen Bernick, and Phil Bransford who has also been an outstanding roommate for most of my time here. Thanks to the members of the MIT Graduate Soccer Team and the MIT Entrepreneurship Review for always making sure I had something to take my mind off of research when the going was tough. I owe gratitude to my siblings Nick and Shannon for their continued support in so many different ways. And finally to my parents Mike and Claire: without you I wouldn't be here. Your love and approval means more to me than you can possibly know.

Dedicated to my nana, Lilian Mary Woodward,
whose love, patience, and sense of duty
I've tried to emulate in life and in science.

Table of Contents

List of Figures & Tables

Chapter 1 – Intracellular delivery of biotherapeutics

1.1 – The biotechnology revolution and biotherapeutics

The pharmaceutical industry is in the process of undergoing a radical change in not only their business models but in the way they conduct research and development. In the second half of the 20th century, these companies reaped the rewards of advances in organic chemistry processes and small molecule therapeutics. But in recent years the small molecule well has gone relatively dry and the rise of biotechnology has led to the development of a new class of therapeutics synthesized biologically. These biotherapeutics represented a significant fraction (~30%) of the drugs approved in 2010 (1). It seems likely that biologics will continue to take a greater share of Food and Drug Administration approvals each year in the future as pharmaceutical companies shift their research foci towards this area through mergers, acquisitions, and restructuring.

Antibodies are the most prevalent biotherapeutics in use today with 32 approved drugs for a variety of indications (2). In their IgG format, antibodies exists as 150 kDa proteins with specific bivalent binding to an antigen target (Figure 1.1). Over the years, variations on this format have emerged: from Fab (single binding arm) to scFv (variable regions connected by a linker) constructs. And more recently smaller scaffolds such as fibronectin domains (3, 4), darpins (5, 6), and affibodies (7, 8) have been diversified and engineered to attain monovalent antigen binding affinities equal to the bivalent avidity of early antibodies.

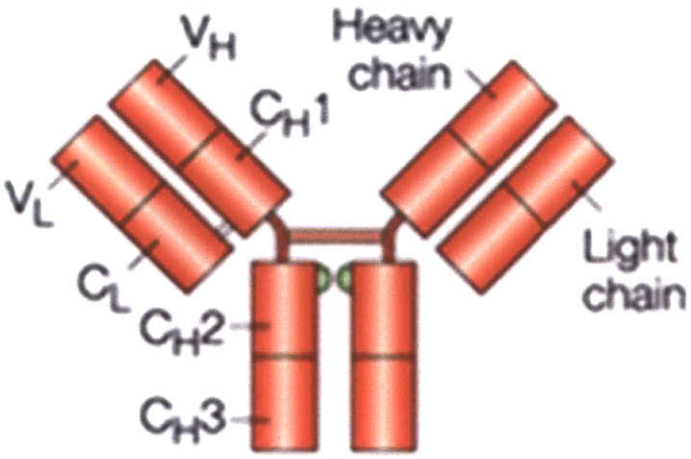

Figure 1.1 – Antibody structure. The structure of an IgG including the heavy and light chains as connected through inter-domain disulfide bonds and their breakdown into variable and constant domains. V = variable, C = constant, X_L = light chain, X_H = heavy chain (9).

Therapeutics targeted by molecular recognition, like antibodies, have been medicine's closest realization of Paul Ehrlich's dream of a "magic bullet" to treat disease (10). As antibody technologies matured, researchers began to investigate various methods of enhancing their potency (Figure 1.2). Recent developments have begun to build upon the basic IgG structure highlighted by the European Medicines Agency approval of the first bispecific therapeutic Catumaxomab in 2009 (11) and by numerous other multi-valents (12), antibody drug conjugates (13, 14), and empowered antibodies (15, 16) in clinical and preclinical trials. The next generation of targeted therapeutics will soon be broadly available in the clinic and making a difference in the lives of patients. Another member of this category of targeted therapeutics is immunotoxins, which combine an antibody fragment or other antigen binding domain with a plant or bacterial toxin.

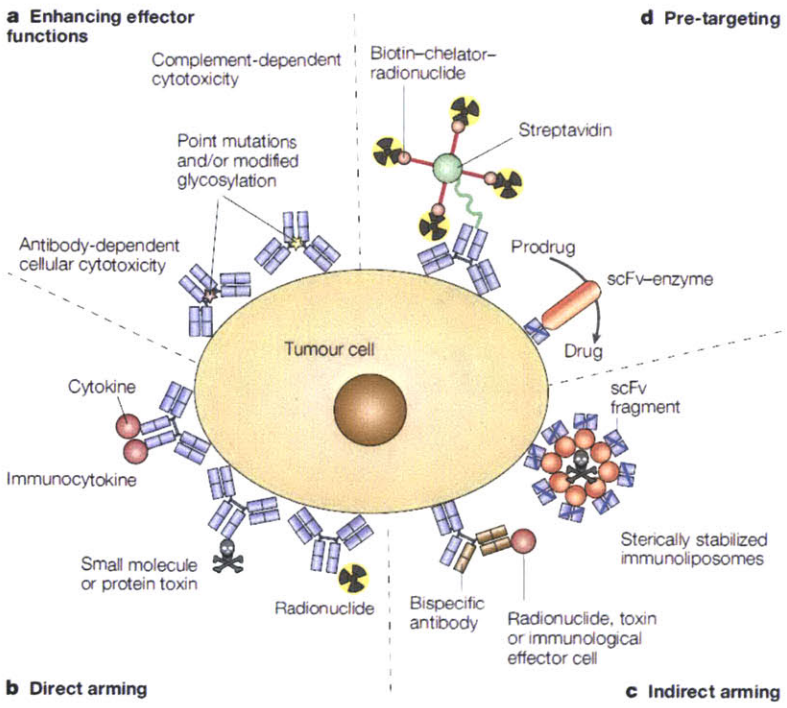

Figure 1.2 – Antibodies advanced. Antibodies can be adapted for increased efficacy by (A) engineering effector functions, (B) fusing or conjugating to toxins, (C) tangential modalities, or (D) primary/secondary approaches (9). This work begins by developing a direct arming variant based on fibronectin domain targeting of a protein toxin and goes on to develop something more akin to a pre-targeting approach using a fibronectin targeted bacterial delivery protein as a secondary agent.

1.2 – Immunotoxins

For over two decades, researchers have envisioned a highly effective immunotoxin for cancer therapy (17). Initially, toxins were purified from their primary source, either bacteria or plants, and conjugated to monoclonal antibodies using chemical techniques. Thanks to the great diversity of evolution there is a wide array of toxins to select from including type-I and type-II ribosome inactivating proteins (RIPs), apoptosis inducers, and inhibitors of other cellular mechanisms. In addition there are numerous antibodies and antibody fragments with specificity for a broad

selection of cancer specific antigens. Thus the possible combinations of toxin and antibody are enormous and while researchers have investigated scores of permutations, there are still many variations yet to be studied. Currently there has only been one immunotoxin approved by the FDA: Ontak™ (recombinant interleukin-2/diphtheria toxin, Ligand Pharmaceuticals) (18). It is indicated for treatment of cutaneous T-cell lymphoma.

The greatest successes in the use of immunotoxins have been achieved when treating hematological cancers that avoid the transportation obstacles encountered when targeting a solid tumor. There are currently more than a dozen immunotoxins in clinical trials, most of which have failed to meet expectations (19), but there is still evidence for successful treatment of solid tumors with immunotoxins (20). In a tumor there are a myriad of barriers against macromolecular access including non-uniform capillary distribution and blood flow, high interstitial pressure, low diffusion constants, and antigen binding. Despite these issues, free IgG has been used with success in the treatment of solid tumors, as exemplified by the anti-ErbB2 drug Herceptin™ (21). Treatment in this manner requires labeling of a cancer cell with enough antibodies to activate antibody-dependent or complement-dependent cytotoxicity or enough to block signaling from the ligand/antigen. These mechanisms often require significant antibody saturation of the tumor. Since intoxication of a cancer cell involves only a few immunotoxin molecules inside the cytoplasm, an ideal immunotoxin would require neither tumor saturation nor the assistance of immune cells.

Gelonin is a plant toxin found in the seeds of *Gelonium multiflorum*, native to Asia. As a type-I RIP it contains no binding domain and likely evolved as an apoptotic mechanism for infected plant cells that would store it in a vacuole. Like all plant RIPs, gelonin is an RNA glycosidase that cleaves a specific adenine residue from 28s rRNA. It does so with a catalytic efficiency such that only a few molecules in the cytoplasm of a eukaryotic cell will inhibit protein synthesis to the point that the cell initiates apoptosis. However, because gelonin is a type-I RIP and contains neither binding nor translocation domains, it is non-toxic up to micromolar extracellular concentrations. An approximately 30 kDa protein, gelonin was first produced in a recombinant form in 1993 (22) allowing for simple insertion as a fusion protein with antibodies. Researchers working with Dr. Michael Rosenblum have previously used gelonin in immunotoxins with antibodies against melanoma gp240 (ZME-018) (23, 24), anti-CD33 (M195) (25, 26), and histocompatibility leukocyte antigen (Lym-1) (27). The properties of gelonin make it ideal for this application since its conjugation has only a small effect on plasma half-life of free antibody and its immunotoxins exhibit limited reticuloendothelial uptake. By comparison, ricin A chain toxin-containing conjugates have significantly lowered half-lives and elevated uptake in both the liver and spleen (28, 29). Ricin A chain must be separated from the binding moiety for efficacy.

When treating cells with very high expression levels of an internalizing antigen, immunotoxins with binding domains of moderate affinity may accumulate in intracellular compartments at sufficient levels to facilitate stochastic

translocation of the few molecules needed to induce apoptosis. However, if an antibody has too low affinity or, as may more often be the case, the target antigen is not sufficiently over-expressed, then not enough immunotoxin will be internalized and cytotoxicity will never be achieved. The choice of binding target and specific binding affinity for that target are therefore important parameters that can influence the *in vivo* toxicity and overall efficacy of an immunotoxin.

1.3 – Biotherapeutic intracellular delivery

A major challenge in the clinical application of many biotherapeutics is endosomal escape: instead of entering the main body of a cell, the molecules become trapped in isolated compartments called endosomes where they are eventually destroyed (30, 31). Fundamentally, it is the ability of the toxin to escape the endosomal compartment holding it following internalization that ultimately determines the potency of the immunotoxin. Because of the extreme efficiency of ribosome inactivation, immunotoxins without a native translocation mechanism are ideal tools for querying intracellular delivery. Advances in the design of proteins that bind to disease-specific markers have given researchers the ability the send drugs to the appropriate tissue and get inside the endosome, but for many therapeutics, specifically those that are active only in the cytoplasm or nucleus, this is not enough. Finding ways to enhance escape from endosomes in a targeted manner is recognized as a central challenge not only for for type-I immunotoxins (32) but also for siRNA and gene therapy (33, 34).

Early developers of immunotoxins diverged in their use of different types of toxins; those generally working with type II toxins such as diphtheria toxin, ricin, or pseudomonas exotoxin didn't worry about intracellular delivery because these toxins incorporate their own translocation mechanisms facilitating cytoplasmic access (35-37). Others working with type I toxins such as gelonin or saponin investigated various small molecule and protein based methods for enhancing translocation with moderate success *in vitro* (38-43).

Many methods of achieving intracellular delivery of immunotoxins have been tested (41), including small molecule potentiators (42, 44-46), proteins (47-49), and peptides (50-52). These enhancers have shown mixed results, and are often limited by immunogenicity or lack of potency. Of the different protein domains used to affect intracellular delivery cholesterol-dependent cytolysins have been some of the most promising (53-56). Structural homologs of human perforin, which is involved in delivery of granzyme B (57), these cytolysins have evolved in bacteria as a tool for escape from the phagosomes of macrophages (58) and have now been harnessed to facilitate intracellular delivery of various biotherapeutics. In some cases they have been directly attached to a therapeutically active molecule (59) or incorporated into a combined liposomal formulation (37, 54). We've taken an entirely different approach to using these membrane active proteins for targeted intracellular delivery.

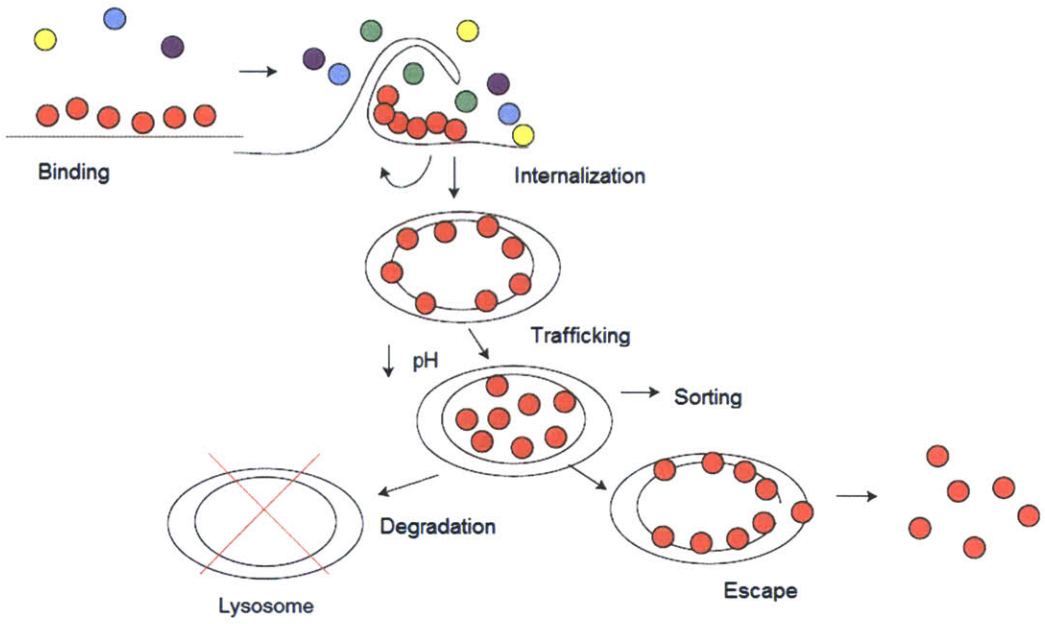

Figure 1.3 – The intracellular delivery pathway. When a targeted biotherapeutic binds to a cell surface it will, after some period of time, become internalized by one of a variety of different mechanisms. Following internalization the endosomal compartment is trafficked and may fuse with other sub-cellular compartments while the conditions within begin to change, most important of which is a decrease in pH. Most of these compartments will progress to lysosomes where enzymes will degrade the contents, unless the biotherapeutic is released into the cytoplasm by some other mechanism.

1.4 – Thesis overview

In this thesis, we describe a new intracellular biotherapeutic delivery system that shows promise as a generalizable approach across antigen targets and active therapeutic components. Beginning in Chapter 2, a new type of immunotoxin is built that targets the plant toxin gelonin to cancer antigens with engineered scFvs and fibronectin domains. We extend the standard characterization of immunotoxins by quantitatively matching their internalization and cytotoxicity,

which defines the precise number of molecules required to induce apoptosis. With this new assay, we demonstrate conclusively that endosomal escape is the rate limiting step of cytotoxicity for our gelonin immunotoxins. In Chapter 3 we introduce our new intracellular delivery tool, targeted cytolysin, and demonstrate its *in vitro* efficacy when administered in combination with gelonin immunotoxins. Chapter 4 extends the system into *in vivo* experiments. And finally, in Chapter 5, we briefly discuss the mathematical modeling techniques used to predict the dynamics of the two-agent system *in vivo* and its therapeutic potential.

1.5 – Citations

1. Division of Business Analyses and Reporting, O. of B. I. (2011) [online] http://www.fda.gov/downloads/Drugs/DevelopmentApprovalProcess/HowDrugsareDevelopedandApproved/DrugandBiologicApprovalReports/UCM242677.pdf (Accessed August 9, 2011).

2. The Immunology Link (2011) [online] http://www.immunologylink.com/FDA-APP-Abs.html (Accessed August 9, 2011).

3. Main, A. L., Harvey, T. S., Baron, M., Boyd, J., and Campbell, I. D. (1992) *Cell* **71**, 671-678

4. Koide, A., Bailey, C. W., Huang, X., and Koide, S. (1998) *J. Mol. Biol* **284**, 1141-1151

5. Kawe, M., Forrer, P., Amstutz, P., and Plückthun, A. (2006) *J. Biol. Chem* **281**, 40252-40263

6. Stumpp, M. T., and Amstutz, P. (2007) *Curr Opin Drug Discov Devel* **10**, 153-159

7. Hansson, M., Ringdahl, J., Robert, A., Power, U., Goetsch, L., Nguyen, T. N., Uhlén, M., Ståhl, S., and Nygren, P. A. (1999) *Immunotechnology* **4**, 237-252

8. Nygren, P.-A. (2008) *FEBS J* **275**, 2668-2676

9. Carter, P. (2001) *Nat. Rev. Cancer* **1**, 118-129

10. Strebhardt, K., and Ullrich, A. (2008) *Nat. Rev. Cancer* **8**, 473-480

11. Heiss, M. M., Murawa, P., Koralewski, P., Kutarska, E., Kolesnik, O. O., Ivanchenko, V. V., Dudnichenko, A. S., Aleknaviciene, B., Razbadauskas, A., Gore, M., Ganea-Motan, E., Ciuleanu, T., Wimberger, P., Schmittel, A., Schmalfeldt, B., Burges, A., Bokemeyer, C., Lindhofer, H., Lahr, A., and Parsons, S. L. (2010) *Int. J. Cancer* **127**, 2209-2221

12. González, G. P., García, I. G., González, J. G., Sánchez, L. P., Mirabal, M. V., Marín, C. C., Ruiz, F. L. G., Iglesias, E. G., de Queralta, R. L., Toirac, R. R., Avila, M. A., Díaz, A. L., Saura, P. A. L., Gavilondo, J. V., and González, J. P. O. (2011) *Cancer Biother. Radiopharm* **26**, 353-363

13. Krop, I. E., Beeram, M., Modi, S., Jones, S. F., Holden, S. N., Yu, W., Girish, S., Tibbitts, J., Yi, J.-H., Sliwkowski, M. X., Jacobson, F., Lutzker, S. G., and Burris, H. A. (2010) *J. Clin. Oncol* **28**, 2698-2704

14. Younes, A., Bartlett, N. L., Leonard, J. P., Kennedy, D. A., Lynch, C. M., Sievers, E. L., and Forero-Torres, A. (2010) *N. Engl. J. Med* **363**, 1812-1821

15. Huang, T.-H., Chintalacharuvu, K. R., and Morrison, S. L. (2007) *J. Immunol* **179**, 6881-6888

16. Nagorsen, D., and Baeuerle, P. A. (2011) *Exp. Cell Res* **317**, 1255-1260

17. Vitetta, E. S., Krolick, K. A., Miyama-Inaba, M., Cushley, W., and Uhr, J. W. (1983) *Science* **219**, 644-650

18. LeMaistre, C. F., Saleh, M. N., Kuzel, T. M., Foss, F., Platanias, L. C., Schwartz, G., Ratain, M., Rook, A., Freytes, C. O., Craig, F., Reuben, J., and Nichols, J. C. (1998) *Blood* **91**, 399-405

19. Pastan, I., Hassan, R., Fitzgerald, D. J., and Kreitman, R. J. (2006) *Nat. Rev. Cancer* **6**, 559-565

20. Pai, L. H., Wittes, R., Setser, A., Willingham, M. C., and Pastan, I. (1996) *Nat. Med* **2**, 350-353

21. Baselga, J. (2001) *Eur. J. Cancer* **37 Suppl 1**, 18-24

22. Nolan, P. A., Garrison, D. A., and Better, M. (1993) *Gene* **134**, 223-227

23. Rosenblum, M. G., Murray, J. L., Cheung, L., Rifkin, R., Salmon, S., and Bartholomew, R. (1991) *Mol. Biother* **3**, 6-13

24. Mujoo, K., Cheung, L., Murray, J. L., and Rosenblum, M. G. (1995) *Cancer Immunol. Immunother* **40**, 339-345

25. McGraw, K. J., Rosenblum, M. G., Cheung, L., and Scheinberg, D. A. (1994) *Cancer Immunol. Immunother* **39**, 367-374

26. Xu, Y., Xu, Q., Rosenblum, M. G., and Scheinberg, D. A. (1996) *Leukemia* **10**, 321-326

27. O'Boyle, K. P., Colletti, D., Mazurek, C., Wang, Y., Ray, S. K., Diamond, B., Rosenblum, M. G., Epstein, A. L., Shochat, D., and Dutcher, J. P. (1995) *J Immunother Emphasis Tumor Immunol* **18**, 221-230

28. Bourrie, B. J., Casellas, P., Blythman, H. E., and Jansen, F. K. (1986) *Eur. J. Biochem* **155**, 1-10

29. Fulton, R. J., Tucker, T. F., Vitetta, E. S., and Uhr, J. W. (1988) *Cancer Res* **48**, 2618-2625

30. Shim, M. S., and Kwon, Y. J. (2010) *FEBS J* **277**, 4814-4827

31. Lu, Y., Yang, J., and Sega, E. (2006) *AAPS J* **8**, E466-478

32. Sandvig, K., and van Deurs, B. (2005) *Gene Ther* **12**, 865-872

33. Lares, M. R., Rossi, J. J., and Ouellet, D. L. (2010) *Trends Biotechnol* **28**, 570-579

34. Varkouhi, A. K., Scholte, M., Storm, G., and Haisma, H. J. (2011) *J Control Release* **151**, 220-228

35. Giles, R. V., Spiller, D. G., Grzybowski, J., Clark, R. E., Nicklin, P., and Tidd, D. M. (1998) *Nucleic Acids Res* **26**, 1567-1575

36. Walev, I., Bhakdi, S. C., Hofmann, F., Djonder, N., Valeva, A., Aktories, K., and Bhakdi, S. (2001) *Proc. Natl. Acad. Sci. U.S.A* **98**, 3185-3190

37. Provoda, C. J., Stier, E. M., and Lee, K.-D. (2003) *J. Biol. Chem* **278**, 35102-35108

38. Kelley, V. E., Bacha, P., Pankewycz, O., Nichols, J. C., Murphy, J. R., and Strom, T. B. (1988) *Proc. Natl. Acad. Sci. U.S.A* **85**, 3980-3984

39. Bjorn, M. J., Groetsema, G., and Scalapino, L. (1986) *Cancer Res* **46**, 3262-3267

40. Seon, B. K. (1984) *Cancer Res* **44**, 259-264

41. Wu, M. (1997) *Br. J. Cancer* **75**, 1347-1355

42. Wu, Y. N., Gadina, M., Tao-Cheng, J. H., and Youle, R. J. (1994) *J. Cell Biol* **125**, 743-753

43. Vitetta, E. S., Cushley, W., and Uhr, J. W. (1983) *Proc. Natl. Acad. Sci. U.S.A* **80**, 6332-6335

44. Mollenhauer, H. H., Morré, D. J., and Rowe, L. D. (1990) *Biochim. Biophys. Acta* **1031**, 225-246

45. Ippoliti, R., Ginobbi, P., Lendaro, E., D'Agostino, I., Ombres, D., Benedetti, P. A., Brunori, M., and Citro, G. (1998) *Cell. Mol. Life Sci* **54**, 866-875

46. Griffin, T. W., Childs, L. R., FitzGerald, D. J., and Levin, L. V. (1987) *J. Natl. Cancer Inst* **79**, 679-685

47. Hong, S. S., Gay, B., Karayan, L., Dabauvalle, M. C., and Boulanger, P. (1999) *Virology* **262**, 163-177

48. Medina-Kauwe, L. K., Maguire, M., Kasahara, N., and Kedes, L. (2001) *Gene Ther* **8**, 1753-1761

49. Goldmacher, V. S., Blättler, W. A., Lambert, J. M., McIntyre, G., and Stewart, J. (1989) *Mol. Pharmacol* **36**, 818-822

50. Wadia, J. S., Stan, R. V., and Dowdy, S. F. (2004) *Nat. Med* **10**, 310-315

51. Meyer, M., Zintchenko, A., Ogris, M., and Wagner, E. (2007) *J Gene Med* **9**, 797-805

52. Moore, N. M., Sheppard, C. L., Barbour, T. R., and Sakiyama-Elbert, S. E. (2008) *J Gene Med* **10**, 1134-1149

53. Browne, K. A., Blink, E., Sutton, V. R., Froelich, C. J., Jans, D. A., and Trapani, J. A. (1999) *Mol. Cell. Biol* **19**, 8604-8615

54. Sun, X., Provoda, C., and Lee, K.-D. (2010) *J Control Release* **148**, 219-225

55. Gottschalk, S., Tweten, R. K., Smith, L. C., and Woo, S. L. (1995) *Gene Ther* **2**, 498-503

56. Provoda, C. J., and Lee, K. D. (2000) *Adv. Drug Deliv. Rev* **41**, 209-221

57. Thiery, J., Keefe, D., Boulant, S., Boucrot, E., Walch, M., Martinvalet, D., Goping, I. S., Bleackley, R. C., Kirchhausen, T., and Lieberman, J. (2011) *Nat. Immunol* **12**, 770-777

58. Portnoy, D. A., Tweten, R. K., Kehoe, M., and Bielecki, J. (1992) *Infect. Immun* **60**, 2710-2717

59. Saito, G., Amidon, G. L., and Lee, K.-D. (2003) *Gene Ther* **10**, 72-83

Chapter 2 – Endosomal escape limitations of immunotoxins

2.1 · Abstract

Gelonin-based immunotoxins vary widely in their cytotoxic potency as a function of antigen density, target cell internalization and trafficking kinetics, and conjugate properties. We have synthesized novel gelonin immunotoxins using two different binding scaffold types targeting two different tumor antigens. Constructs were characterized using an antigen negative cell line, cell lines positive for each antigen, and a cell line positive for both antigens. Immunotoxins exhibited K_d values between 8-15 nM and showed 20-2000 fold enhanced cytotoxicity compared to gelonin (IC_{50} ~ 0.25-30 nM vs. 500 nM). We quantified internalization of gelonin and gelonin-based immunotoxins and aligned the data with cytotoxicity measurements made at equivalent concentration and exposures. When matched internalization and cytotoxicity data were combined, a conserved internalized cytotoxicity curve was generated, which was common across experimental conditions. Considerable variations in antigen expression, trafficking kinetics, extracellular immunotoxin concentration, and exposure time display a single potency curve on the basis of internalized immunotoxin. Fifty-percent cytotoxicity occurred when ~$5x10^6$ toxin molecules were internalized regardless of the mechanism of uptake. A threshold for apoptosis suggests that endosomal escape is a common, highly inefficient rate-limiting step following internalization by any means tested. Methods designed to enhance endosomal escape might be utilized to improve the potency of gelonin based immunotoxins.

2.2 - Introduction

Immunotoxins are a promising approach to the targeted delivery of highly potent, cancer-specific cytotoxic agents. Immunotoxins are frequently composed of a targeting moiety (derived from antibodies or other cell-binding proteins) either chemically conjugated or genetically fused to highly cytotoxic plant or bacterial protein toxins. Clinical success for immunotoxins has been mostly limited to hematological malignancies due to transport limitations in solid tumors (1). Such limitations have been extensively studied experimentally (2) and with several computational models (3,4).

The potency of a particular immunotoxin is dependent on the ability to deliver the toxin to the cytoplasm, which is commonly considered to be the rate limiting step. For some native toxins such as ricin, intracellular delivery is achieved through lectin binding followed by internalization and toxin release with membrane fusion or retrograde trafficking (5). Immunotoxins attempt to recreate this scenario by replacing the indiscriminate lectin binding with cancer-specific antigen binding as a means of targeting and internalization (6). Subsequent intracellular trafficking, release, and endosomal escape is often achieved using existing toxin characteristics, translocation domains, protease cleavage sites, disulfide bonds and/or signaling peptides (7-10). However, the inclusion of toxins with domains facilitating cytoplasmic access can also lead to increased non-specific toxicity *in vivo* (11,12).

Gelonin is a plant toxin and classified as a type I ribosome inactivating protein because it lacks any cell-binding or cytoplasmic delivery domains. Recombinant gelonin (rGel) is a ~30 kDa *N*-glycosidase with activity similar to ricin A chain but exhibiting better stability and lower immunogenicity (13,14). The use of rGel in tumor targeted cytotoxic agents has been well studied (15,16). Further, rGel has been shown to be active without cleavage from the binding domain, and without negative impact on the targeting agent's pharmacokinetics (17). The necessity of internalization for activity of rGel immunotoxins and the antigen to which it is directed have been previously demonstrated (18,19).

Carcinoembryonic antigen (CEA) is a 180 kDa membrane glycoprotein which exhibits depolarized overexpression in numerous epithelial tumor types (20). The utility of CEA as a tumor targeting tool for both therapy and imaging has been well-established (21-23). Experiments in our laboratory have shown that CEA is internalized with a half-life between 10 and 16 hours and thus represents a potential target for immunotoxins (24). CEA has previously been used as a target for the early development of immunotoxins (25-27). Epidermal growth factor receptor (EGFR) has a strikingly faster internalization rate (~30 minutes). However, many such internalized molecules return to the cell surface by recycling (28). Like CEA, EGFR is a well established cancer-associated antigen. EGFR has also been used as a target for designed immunotoxins (29,30). Previous studies have suggested that antigens displaying similar expression levels but different internalization rates can lead to profoundly different immunotoxin potencies (6).

MFE-23 is an antibody single chain variable fragment (scFv) directed against CEA. Originally identified by phage library selection, this scFv was later humanized by resurfacing and engineered in yeast for greater stability, and solubility (shMFE) as well as affinity (sm3E) (31-33). Both of these engineered molecules are well-expressed in yeast and have K_d's of ~7nM and ~30pM respectively. The 10th human fibronectin type III domain (Fn3) has been designed using various directed evolution approaches for specific affinity towards numerous different targets (34-36). We describe engineered fibronectin fragments binding EGFR and CEA (designated E246 and C743 respectively).

In this study we generated several novel immunotoxins targeting CEA and EGFR, including the first published report of Fn3-based immunotoxins. Comparing the different immunotoxin constructs, we investigated the mechanisms of cellular intoxication including the cell-binding-dependent internalization of immunotoxins and the subsequent loss of cell viability. Using a novel analysis of viability versus net internalized antigen, a universal potency relationship was found which was independent of the antigen, binding affinity/scaffold, internalization/recycling rate, external immunotoxin concentration, and incubation time. This work may be useful in understanding the mechanisms of immunotoxin-based cell killing and what factors influence cellular intoxication. With a better understanding of these mechanisms and factors we can engineer more effective agents as cell-targeted therapeutics for cancer.

2.3 – Methods

2.3.1 – Cell lines

The human fibrosarcoma cell line HT-1080 was used throughout as an antigen negative control. HT-1080 cells were transfected with a plasmid for CEA expression and those cells, denoted HT-1080(CEA), were maintained under antibiotic selection pressure from geneticin as previously described (24). The human epidermoid carcinoma cell line A431 was used as an EGFR positive line and the human colorectal carcinoma cell line HT-29 was used as a double positive cell line for both CEA and EGFR.

2.3.2 – Construction of expression plasmids

The gene encoding the recombinant form of the gelonin toxin was codon-optimized for *E. coli* expression and ordered from DNA 2.0 (Menlo Park, CA). The gene was digested out of the synthetic vector using designed *Pst*I and *Hind*III restriction sites and cloned into the pMal-c2x expression vector encoding a maltose binding protein (MBP) fusion product. Into this construct, Fn3 clones were inserted by amplification of Fn3s out of their own expression vectors and using the purified amplification products as primers for a Quikchange™ insertion similar to the protocol described by Geiser *et al.* (37). The linker between the Fn3 and rGel was modified to consist strictly of the amino acids encoded for by the necessary restriction sites for binder cloning and a G_4S linker sequence. In this setting, various Fn3 and scFv genes could be inserted by restriction digestion and cloning

using *Nhe*I and *Bam*HI. As an alternative vector for expression we cloned the immunotoxin construct by *Eco*RI and *Hind*III digestion into pET32a (Novagen) expressing the product as a TrxA fusion. We further modified this vector by mutating the protease site designed to remove the fusion tag from enterokinase to tobacco etch virus.

2.3.3 – Protein expression and purification

The pMal-c2x vector containing the rGel gene was transformed into Origami 2 (DE3) (Novagen, San Diego, CA) and grown on LB agar plates containing ampicillin and tetracycline. Colonies were picked from the plate and grown overnight at 37 °C in 5 mL aliquots of selective media, which were then used to seed 1 L of antibiotic free rich LB media and allowed to grow to logarithmic phase. Once the culture reached an OD_{600} between 0.5 and 1.0, 5 mL 0.1 M IPTG was added and the induction was allowed to continue at 37 °C for 4hrs. Following induction cultures were centrifuged at 15,000 xg for 12 min and cell pellets frozen at -20 °C. Pellets were resuspended in amylose column buffer containing Complete EDTA-free protease inhibitor (Roche, Indianapolis, IN) and then sonicated on a Branson Sonifier 450A at 50% duty cycle and power level 5 for three, one-minute intervals. The resulting solution was centrifuge at 50,000 xg for 30 min to pellet cell debris and the supernatant was applied to an amylose column as described by the manufacturer (New England Biolabs, Ipswich, MA). Purified recombinant proteins were concentrated and buffer exchanged into Factor Xa digestion buffer using

Amicon columns with a 30 kDa MWCO then incubated overnight at room temperature with 5 µL Factor Xa (New England Biolabs). rGel (Appendix reference - A.1) was isolated from the removed MBP and Factor Xa by ion-exchange chromatography with a HiTrap Q column (GE Healthcare, Piscataway, NJ).

For production of immunotoxins, the Rosettagami 2 (DE3) bacterial host cell line was used and chloramphenicol was added to plates and overnight growth media as a selection agent. For Fn3-rGel immunotoxins, all other purification steps were the same as for rGel expression. In the case of scFv immunotoxins the TrxA fusion construct was used to facilitate more efficient formation of stabilizing disulfide bonds. In this case, induction was carried out in standard LB media using 10 mL 0.1 M IPTG at 20 °C for 6 hrs. Purification of TrxA-scFv-rGel was achieved using IMAC with TALON resin (Clontech, Mountain View, CA). The TrxA tag was removed by digestion with TEV protease and the scFv-rGel was isolated from TrxA and TEV by size-exclusion chromatography on Superdex 200 and 75 10/300 columns connected in series.

Yields for rGel were approximately ~3 mg/L after all purification steps. We synthesized two Fn3 immunotoxins, one targeting CEA (C7rGel – A.2) and one targeting EGFR (E4rGel – A.3), based on the affinity matured parent Fn3s C743 and E246. Yields for C7rGel and E4rGel respectively were ~2.2 and ~3 mg/L. We synthesized two scFv immunotoxins, both targeting CEA, 3ErGel (A.4) and FErGel (A.5), based on disulfide stabilized versions of the affinity matured scFv's sm3E and shMFE (33). Yields for 3ErGel and FErGel respectively were ~125 and ~750 µg/L.

Relative yields of each of the different immunotoxins and analysis by polyacrylamide gel electrophoresis suggests that the primary reason for differences in yields may be the proper folding and solubility for each immunotoxin. The disulfide-stabilized scFv's appeared to disrupt folding, and thus soluble expression yields, to a greater degree than Fn3s (although some of this difference may be due to alternative fusion partners TrxA versus MBP). Similarly, the 3E scFv destabilizes to a greater extent than the FE scFv in the context of the immunotoxin.

2.3.4 – Antigen binding affinity titration

Immunotoxins were biotinylated using amine reactive EZ-Link Sulfo-NHS-LC-biotin (Pierce, Rockford, IL). Antigen positive cell lines HT-1080(CEA) and A431 were lifted from culture plates with trypsin and resuspended in 4% formalin for 30 min before being washed and stored in phosphate buffered saline with 1% (w/v) bovine serum albumin (PBSA). Fixed cells were incubated with varying concentrations of biotinylated immunotoxins overnight at 37 °C, washed once and resuspended in 250 µL of PBSA with 1 µL goat anti-biotic FITC (Sigma, St. Louis, MO) for 1 hr at 4 °C. Cells were washed once again and resuspended in 150 µL PBSA before being analyzed for fluorescence on an Accuri C6 flow cytometer. For each titrating concentration, the median fluorescent intensity was determined and data sets for each immunotoxin were fitted to a standard binding isotherm using least-squares regression.

Early attempts to titrate directly-labeled immunotoxins on fixed cells resulted in a high non-specific background signal. Alternative approaches to titration were attempted before we eventually arrived at the secondary detection method described above. Titrations of all immunotoxins were performed on either fixed HT-1080(CEA) cells or A-431 cells. Titration of the scFv immunotoxins 3ErGel and FErGel resulted in fitted K_d's of 8 nM and 15 nM respectively, which were somewhat higher than the titrated affinity of their parental sm3E and shMFE scFv's (K_d's ~ 30 pM and 9 nM, respectively, data not shown). We fitted the titration data for Fn3 immunotoxins C7rGel and E4rGel and found K_d values of 10 nM and 13 nM respectively. These K_d's were also slightly higher than those found for the parent Fn3s, 2 nM for C743 and 3 nM for E246. Differences in overall signal were attributed to differences in the degree of biotinylation of immunotoxins. Biotinylated rGel showed no significant signal when titrated over the same range of concentrations.

2.3.5 – Cytotoxicity assays

Log-phase tumor cells were removed by trypsinization, counted, and seeded on 96-well plates at 2,500 cells per well. Cells were allowed to adhere overnight after which fresh growth media containing varying concentrations of rGel or immunotoxin was added to triplicate wells. Toxins were incubated with the cells for 72 h before the toxin containing media was removed and replaced with media containing the WST I reagent (Roche). The red/ox solution was allowed to develop

for 1-3 h under normal culture conditions after which plates were measured for absorbance at 450 nm. Untreated cells and cells lysed with a 1% Triton-X100 solution were used as positive and negative controls respectively. Measurements were compared to baseline and normalized to control treatments, triplicates averaged, and standard errors calculated. Time dependent cytotoxicity data were obtained by treating cells as described, removing toxin containing media, washing once with PBS, then replacing with fresh media for wells at each time point then following identical assay procedures after 72 h. rGel cytotoxicity measurements were made on concentrations between $1x10^{-9}$ and $3x10^{-6}$ M and times between 1 and 72 h. High antigen expressing cells were incubated with 10 nM either scFv immunotoxin or 30 nM either Fn3 immunotoxin, while the low antigen expressing line was incubated with 30 nM immunotoxin, with all incubations lasting between 12 and 72 h.

2.3.6 – Quantitative internalization

Cell lines were incubated with immunotoxins directly labeled with AlexaFluor 488. At various times, cells were washed with PBS and incubated for 30 min with the quenching rabbit anti-AlexaFluor 488 (Invitrogen, Carlsbad, CA). Cells were then scraped from the wells, washed again with PBS, and analyzed for internal fluorescent signal. Quantum Simply Cellular anti-Mouse IgG beads (Bangs Laboratories, Fishers, IN) with different quantified binding capacities were incubated with AlexaFluor 488 labeled mouse IgG for 30 min, washed with PBS,

then measured for fluorescence. The number of fluorescent molecules per protein on both immunotoxins and mouse IgG was determined using absorbance measurements at 280 and 494 nm. Bead fluorescence measurements were used to generate a standard curve for fluorescence signal per fluorescent molecule. Immunotoxin internalization data were quantified by mapping fluorescence signal to the bead fit converting signal to fluorescent molecules and then translated into immunotoxin molecules using the labeling ratio.

2.3.7 – Internalized cytotoxicity

Data obtained in time dependent cytotoxicity experiments were combined with those from quantitative internalization experiments and plotted to suggest the former as the dependent variable and the latter as the independent variable. Accumulated results were fitted using non-linear least squares regression of an exposure-response curve with variable slopes using MATLAB (The MathWorks, Natick, MA). From this fitting, half-maximum and near-full response metrics were calculated and reported.

2.4 – Results

2.4.1 – Novel gelonin-based immunotoxins

Four new immunotoxins were constructed which target CEA or EGFR. Three different immunotoxins targeting CEA were constructed, using antibody scFv fragments (3ErGel and FErGel), or a newly selected fibronectin scaffold-based binding domain with specificity for CEA (C7rGel). The 3ErGel incorporates a high affinity anti-CEA scFv sm3E described previously (33), while the FErGel incorporates a lower-affinity precursor scFv, shMFE. As separate scFv molecules, the affinities of these two binding modules are 30 pM (sm3E) and 9 nM (shMFE). Using a yeast-displayed library of fibronectin scaffold proteins with randomized loops, a new binding module targeting CEA was isolated (C743), with a K_d of 2 nM, and another module that binds EGFR (E246) was isolated with a K_d of 3 nM. Each of these four binding modules were expressed as N-terminal fusions to recombinant gelonin, and binding of the resultant immunotoxin constructs was assessed with tumor cell lines (Figure 2.1).

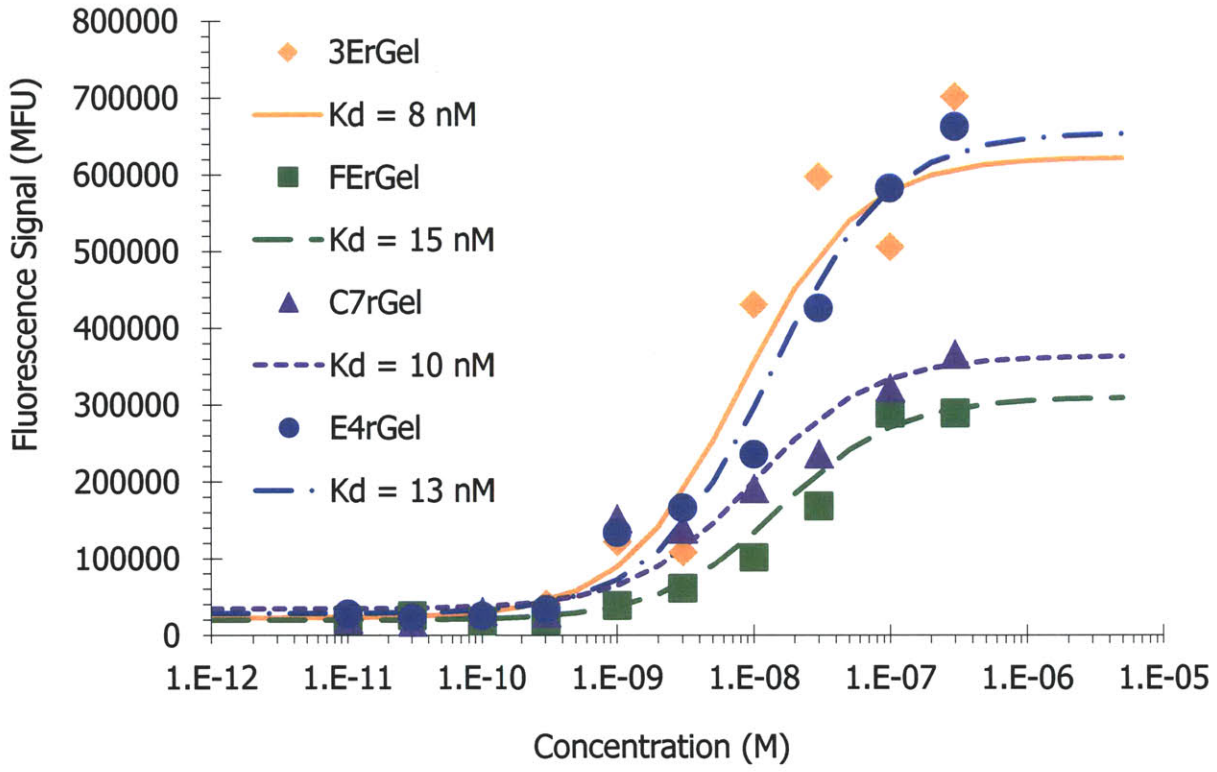

Figure 2.1 – Immunotoxin affinity. Antigen affinity of binding fragments is retained in their respective immunotoxin constructs. Four immunotoxins targeted towards either CEA or EGFR via either scFv or Fn3 domain. The 3E and FE scFv clones targeting CEA, the C7 fibronectin clone targeting CEA, and the E4 fibronectin clone targeting EGFR were each fused to rGel and titrated for binding affinity on HT-1080(CEA) or A431 for CEA or EGFR respectively. Binding on fixed cells was detected with goat anti-biotin FITC by flow cytometry. Data was fitted using least-squares regression with a binding isotherm giving K_d's of 8nM for 3ErGel, 15nM for FErGel, 10nM for C7rGel, and 13nM for E4rGel.

2.4.2 – Cytotoxicity of rGel and immunotoxins

Results of concentration dependent cytotoxicity (Figure 2.2) suggest that immunotoxin potency varies over two orders of magnitude, and is determined by a complex combination of antigen density, binding affinity, binding scaffold, and antigen internalization/recycling rate. On all cell lines tested gelonin shows IC_{50} values around 500nM (Figure 2.2A). We find that all immunotoxins have an IC_{50} of approximately 1 μM on the antigen negative HT-1080 cell line (Figure 2.2B). When incubated with the double positive, low antigen expressing HT-29 cell line, all of the immunotoxins again display IC_{50} values greater than or equal to 1 μM (Figure 2.2C). The exposure response curves on high antigen-expressing cell lines (Figure 2.2D) are consistent with previous results that apparent immunotoxin potency varies widely when expressed solely as a function of extracellular concentration of the agent and that each of the immunotoxins displayed a different IC_{50} against either HT-1080(CEA) or A431 (3ErGel = 250 pM, FErGel = 1.5 nM, C7rGel = 8 nM, E4rGel = 30 nM).

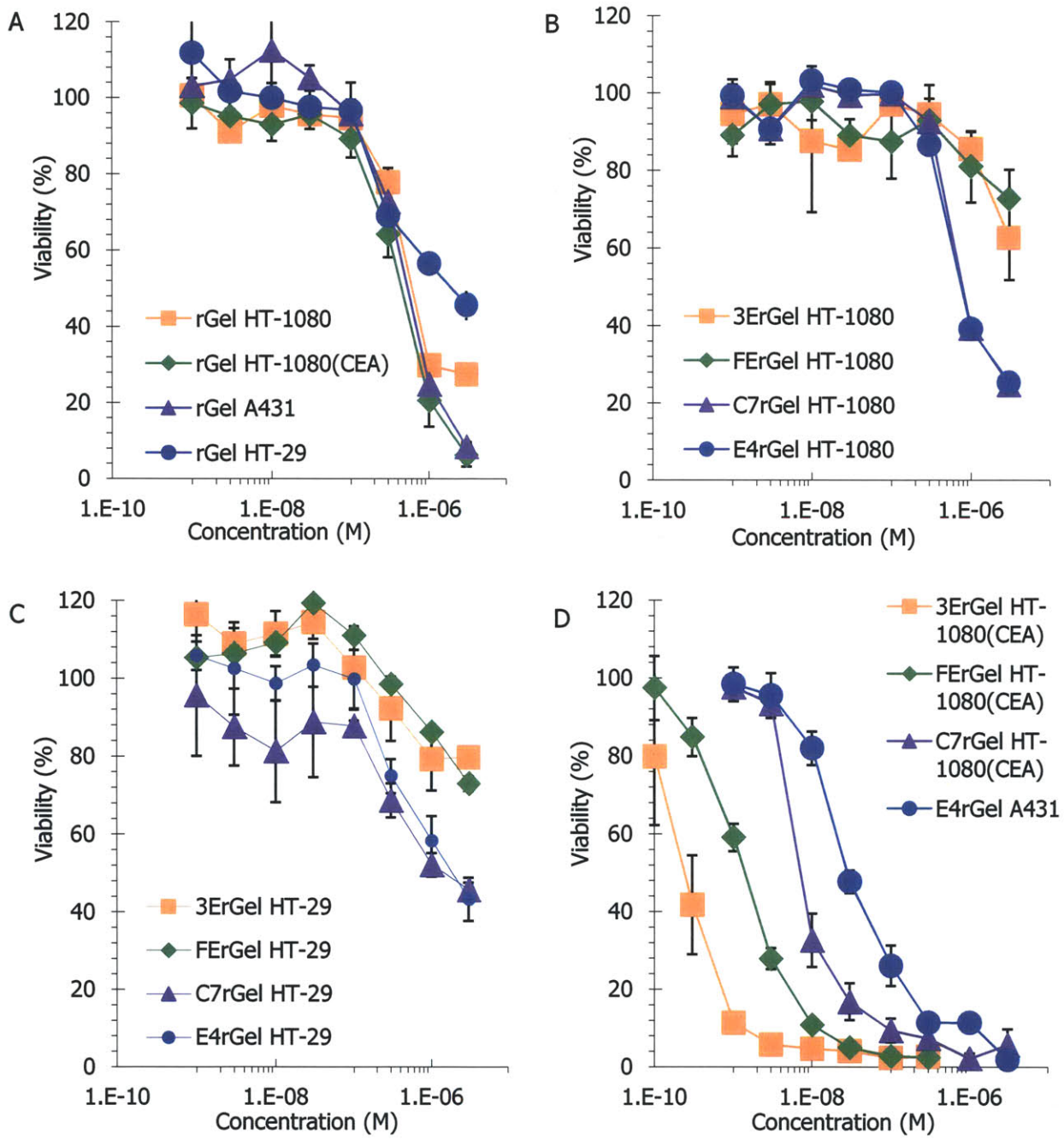

Figure 2.2 – Immunotoxin cytotoxicity. scFv and Fn3 immunotoxins show enhanced cytotoxicity specific for antigen positive cells. (A) The IC_{50} of soluble rGel was ~500nM on all four cell lines used in the study. (B) Antigen negative cells (HT-1080) were treated with the four different immunotoxins which displayed roughly equivalent potency to soluble toxin. (C) Immunotoxins tested for cytotoxicity on the double positive, low-antigen density HT-29 cell line. Surprisingly, none of the immunotoxins show enhanced cytotoxicity compared to the IC_{50} of rGel. (D) On high antigen expressing cells (HT-1080(CEA) and A431) greater potency is observed.

2.4.3 – rGel time dependent internalization and cytotoxicity

rGel was incubated with HT-1080 cells for various lengths of time up to 72 h and assessed for both internalization and cytotoxicity as described above, after which data were combined to determine the internalized cytotoxicity profile (Figure 2.3). Time dependent quantitative internalization results (Figure 2.3A) indicate that for very low concentrations and very short times a minimum signal of roughly $1x10^4$ molecules can be detected, likely due to autofluorescence from the cells above the baseline bead autofluorescence. As treatment concentrations and incubation times are increased the number of rGel internalized increases, peaking at nearly $1x10^7$ molecules at 3 μM for more than 24 h. Time dependent cytotoxicity results (Figure 2.3B) show a similarly consistent theme in which low concentration, short time treatments consistently result in viabilities between 80 and 100%. At the highest concentrations and longest times, viability drops as low as 10%, while 50% viability is achieved either by 3 μM concentration treatment for 12 h or by lower concentration treatments for somewhat longer durations. By combining time dependent quantitative internalization and cytotoxicity data to remove time as a variable, an internalized cytotoxicity profile is obtained (Figure 2.3C). For the HT-1080 cells treated with rGel, we found a wide variation in uptake and viability as a function of concentration and time (Figures 2.3A & B). This data collapsed to a fairly tight relationship between viability and the number of internalized gelonin molecules and we noted a steep reduction in viability at approximately $5x10^6$ internalized molecules (Figure 2.3C).

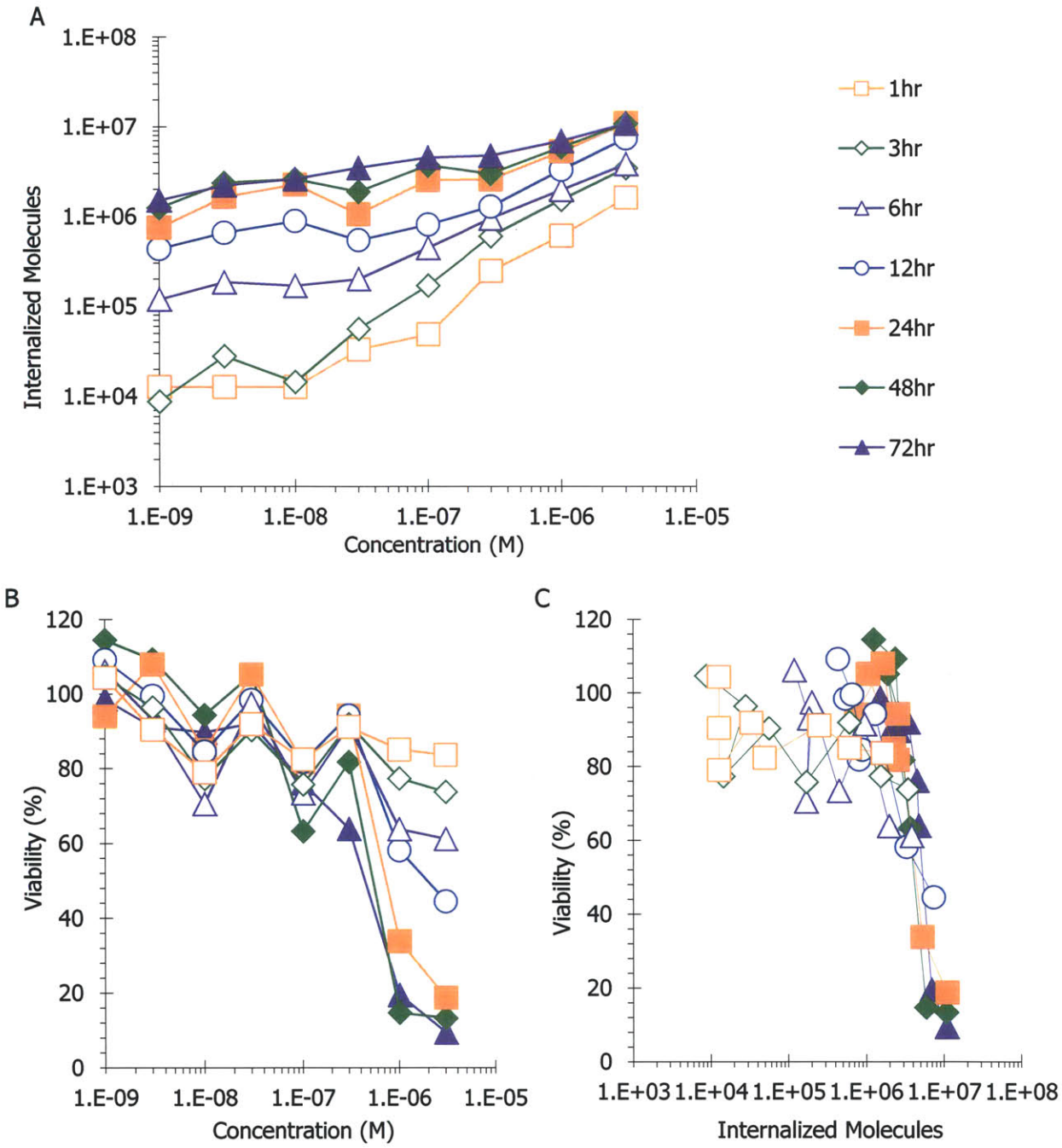

Figure 1.3 – rGel molecular cytotoxicity. Correlated internalization and cytotoxicity measurements indicate a precise number of rGel molecules must be internalized by a single cell before cytotoxicity is observed. (A) Time and concentration dependence of rGel internalization by HT-1080 using the described quantitative internalization flow cytometry assay. (B) Concentration and exposure matched cytotoxicity was measured using the WST assay. (C) Data from A and B were combined and plotted to show the dependence of cytotoxicity on the number of internal gelonin resulting in the determination of the TN_{50} near $5x10^6$.

2.4.4 – Immunotoxin time dependent internalization and cytotoxicity

High antigen-expressing HT-1080(CEA) and A-431 cell lines as well as the low antigen-expressing, double positive HT-29 cell line were incubated with immunotoxins targeting the appropriate antigens for various times at concentrations selected to show a wide change in viability over the range in time. We assessed cells for immunotoxin internalization as well as viability following incubations as described above and the data from the two measurements were combined to determine the internalized cytotoxicity of the immunotoxins (Figure 2.4). Wide variation in uptake and viability with the different cell lines and immunotoxins was observed (Figures 2.4A & B). However, the combined data for internalized cytotoxicity surprisingly produced a curve consistent with that for pinocytosed rGel, with a sharp reduction in viability once cells internalized more than $5x10^6$ molecules (Figure 2.4C).

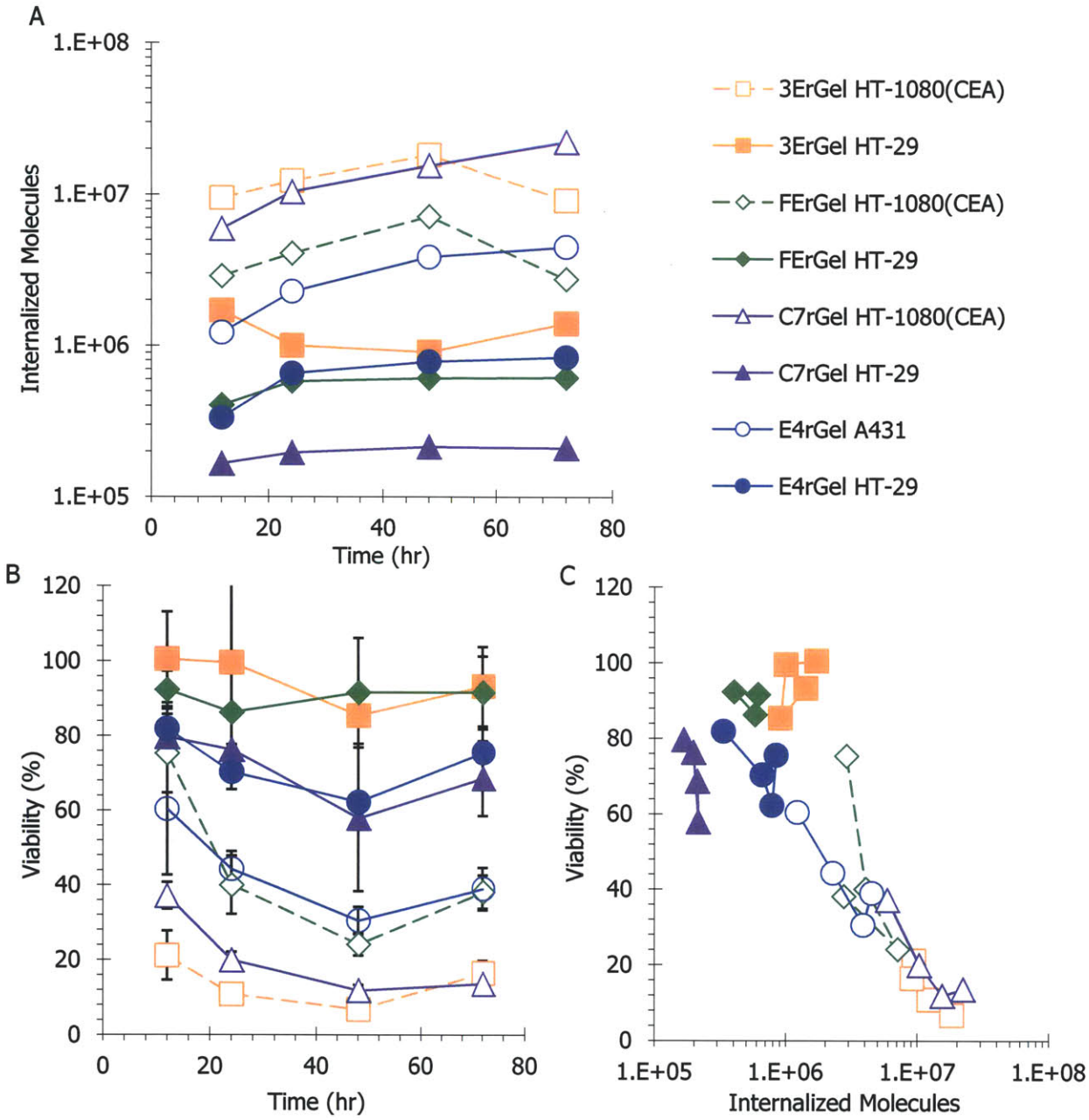

Figure 2.4 – Immunotoxin molecular cytotoxicity. Rate-limiting endosomal escape in scFv and Fn3. (A) The internalization of immunotoxins by antigen positive cells was measured by quantitative internalization flow cytometry at varying times and concentrations. All HT-29 treatments and C7rGel/E4rGel treatments on HT-1080(CEA) and A431 were made at 30nM while 3ErGel and FErGel treatments on HT-1080(CEA) were made at 10nM. Antigen-dependent internalization is reported by subtracting signal from cells blocked with unlabeled competitor. (B) Concentration and exposure matched cytotoxicity from the WST assay. (C) Data from A and B were combined and plotted to show the dependence of cytotoxicity on the number of internal immunotoxins resulting in a TN_{50} of ~$3x10^6$ for all species.

2.4.5 – Cumulative internalized cytotoxicity

Data collected from multiple experiments using each of the described cell lines with various concentrations and exposures of rGel or one of the immunotoxins were matched for internalized toxin levels and cytotoxicity as described and combined into one cumulative internalized cytotoxicity plot (Figure 2.5). The entire data set was accounted for irrespective of experimental conditions and used to fit an exposure-response curve with variable slopes of the form:

$$y = \frac{100}{[1 + (x / TN_{50})^{slope}]}$$

where both TN_{50} and slope are fitted parameters. Fitting the exposure-response curve parameters resulted in a $TN_{50} = 4.68 \times 10^6$ and a *slope* = 1.86. The TN_{50} fit describes the number of internalized immunotoxins necessary to induce a 50% loss of viability. Additionally, in situations such as this where we observe a strong step-function response characterized by a large slope parameter, it is useful to consider values associated with a more complete response. Here we consider the TN_{90} as calculated from the fit using the equation:

$$TN_{90} = TN_{50}\left(\frac{90}{100-90}\right)^{1/slope}$$

The resulting TN_{90} indicates that 1.53×10^7 molecules of toxin must be internalized on average for 90% of the population to undergo apoptosis. In other words, when the average population uptake reaches the TN_{90}, only one-tenth of the population has failed to achieve the ~5×10^6 molecule limit for toxicity. The plotted cumulative

internalized cytotoxicity data are each a median value of a Gaussian distribution of cells internalizing different numbers of toxin molecules as measured by flow cytometry (Figure 1.5). Thus, for each data point, half of the cells in the treatment population internalized more than the recorded number and half took up less. So at the TN_{50}, 50% of the cells died, and 50% internalized at least ~$5x10^6$ molecules indicating that this is indeed the average threshold for loss of viability in a single cell.

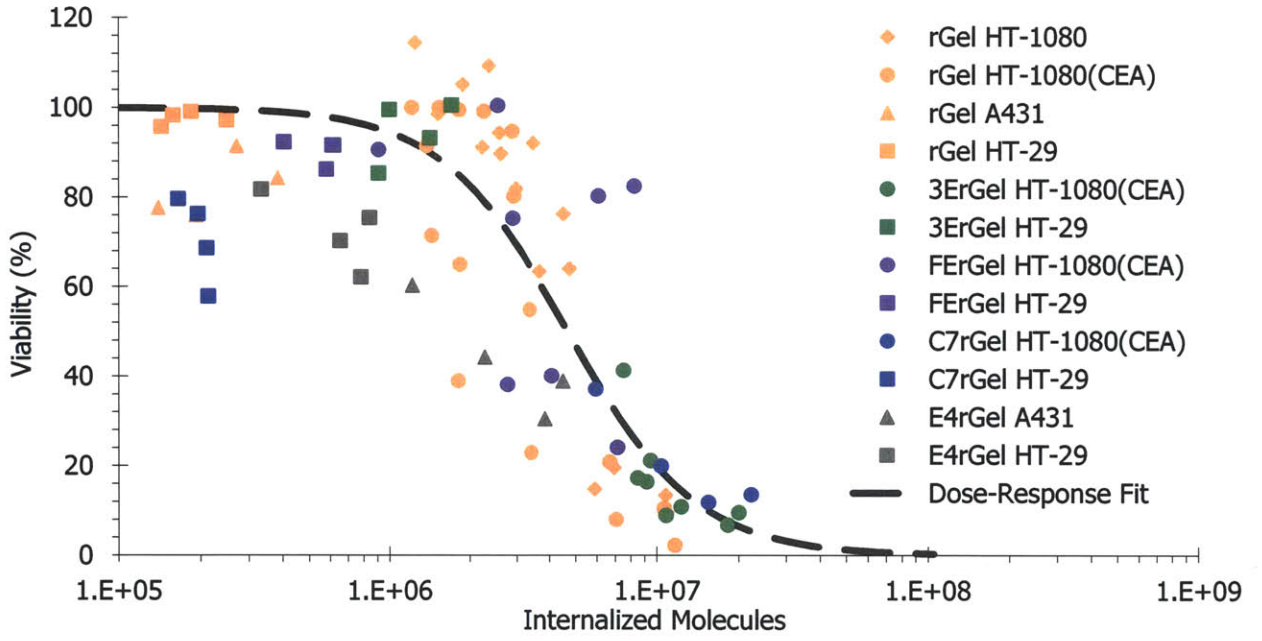

Figure 2.5 – Cumulative molecular cytotoxicity. Aggregated data from experiments using different binding scaffolds, antigen targets, affinities, and cell lines all converge to the same TN_{50} curve. Accumulated internalized cytotoxicity data for rGel on all cell lines and immunotoxins on antigen high and antigen low cells. The cumulative data set was fit using an exposure response curve with variable slopes giving a TN_{50} of $4.7x10^6$ and with an exponential decay curve giving a k value of $1.6x10^{-7}$ which can be converted to a half-decay or TN_{50} of $4.3x10^6$.

2.5 – Discussion

The importance of internalization for the efficacy of immunotoxins is well appreciated (6,18,39,40). However, these studies clearly indicate that a type I toxin such as gelonin exhibits quantitatively the same low intracellular potency regardless of the particular pathway which drives internalization. Delivery of the cytotoxic domain of an immunotoxin to the cytoplasm of a cell is dependent upon a series of steps, each with a varying degree of efficiency depending on the cell type, antigen density, binding affinity, internalization/recycling, and sub-cellular trafficking or endosomal escape. Due to the enzymatic potency of ribosome inactivating proteins, only a few toxin molecules successfully delivered to the cytoplasm (or ribosomal compartment) may be lethal to the cell (41). Quantitative measurement of levels this low is exceedingly difficult and it is therefore difficult to directly determine a rate of translocation or escape of molecules into the active compartment. Alternatively, we chose to quantify the total intracellular level of immunotoxins, and infer their cytoplasmic access by the resulting cytotoxicity. Strikingly, there is an apparently near-universal requirement for approximately $5x10^6$ gelonin molecules to be internalized in order to kill a tumor cell, regardless of the route of vesicular internalization.

Buildup of such a significant number of toxins intracellularly, given the efficiency of the enzyme once in the cytoplasm, suggests not only that binding and internalization of immunotoxin is quite efficient, but also that endosomal escape is the rate-limiting step in the process of intoxication. If endosomal escape were more

efficient, cells would become intoxicated much faster and such high levels of internalization would not be observed. Nevertheless, it should be acknowledged that these data might also be explained by a rate limiting degradation of toxin assuming retention of fluorescence.

Here we have synthesized a novel set of immunotoxins based on binding domain fusions to the plant toxin gelonin. We have used ds-scFv's engineered for affinity towards CEA as well as Fn3s engineered for affinity towards CEA and EGFR. To our knowledge, this is the first published report of Fn3-targeted immunotoxins. Studies describing rGel fusions with fibronectin fragments targeting IGF1R were recently reported (AACR 2010). We examined the ability of these binding scaffolds to retain affinity within the fusion construct and found that while affinity is retained to a considerable degree, there was some loss of affinity compared to the parent molecule likely attributable to partial misfolding and instability in the fusion construct. This is consistent with work by others designing direct fusion immunotoxins (42,43). We believe that this misfolding and instability also influences the synthetic yields of each of the immunotoxins. Those constructs showing the greatest loss of parent affinity also have the lowest yields. Despite losses of relative affinity, all of the immunotoxins still bound their respective antigens with low nanomolar affinities.

Development of the new class of Fn3-based immunotoxins is an attempt to overcome two of the most substantial limitations to immunotoxin therapy. Commonly, these therapies are limited by vascular toxicity and a failure to

infiltrate the tumor mass. The smaller Fn3 scaffold (~10 kDa) should allow for more rapid clearance from the vasculature thereby minimizing exposure, and maximize the diffusion coefficient to optimize tumor penetration under fast clearance conditions. It is well established that molecules smaller than the 60-70 kDa molecular weight cut-off for renal filtration are rapidly cleared (44). And while this clearance itself limits total tumor targeting, our lab's mathematical models suggest that the smaller molecular weight should lead to a more homogenous immunotoxin distribution within the tumor (4). We plan to test whether these hypotheses regarding the pharmacokinetics of Fn3 immunotoxins are validated by *in vivo* experiments. This work and others has shown that Fn3 scaffold is capable of mediating antigen specific binding at affinities on par with scFv or IgG at a fraction of the molecular weight.

Antigen binding by scFv or Fn3 domains was sufficient to enhance gelonin potency towards antigen positive cells between 20 and 2000 fold depending on scaffold, affinity, antigen internalization/recycling and antigen density. Immunotoxins showed no increase in cytotoxicity compared to rGel on antigen negative cells and cells expressing low levels of antigens. These results support previous examples using scFv fusions to enhance toxin potency (17) and validate Fn3 as a new targeting agent with improved stability and expression, due in part to an absence of disulfide bonds, for immunotoxin design. Fn3 based immunotoxins have the added advantage of being smaller in size allowing them to potentially better penetrate tumors due to improved capillary permeability and diffusion.

In an attempt to better understand the subcellular barrier to cytotoxicity, we measured the molecular internalization of rGel in HT-1080 cells. Using identical treatments, we determined the cytotoxicity resulting from the measured internalization. As toxin concentration and incubation time were increased, the number of molecules internalized per cell increased and the population viability decreased. When viability was plotted as a function of internalized molecules a strong non-linear relationship was found, independent of incubation time and concentration. We hypothesize that the number of internalized molecules required to induce a 50% loss in viability, TN_{50}, is determined primarily by the rate of endosomal escape and cytoplasmic access. Conversely, one might have expected that antigen binding might actually deter the rate of intoxication following internalization, based on the success of methods enhancing cytotoxicity by incorporating release elements between binding and toxin domains (45,46). However, the overlap in the internalized immunotoxin cytotoxicity curve for antigen-bound and internalized immunotoxin vs. pinocytosed free gelonin indicates that release of immunotoxins from antigen binding plays a negligible role in intoxication.

The described technique for determining TN_{50} does not address the precise fate of the immunotoxins following endocytosis. Murphy and coworkers have modeled the intoxication process for diphtheria and gelonin immunotoxins in great subcellular detail and fitted model parameters to protein synthesis inhibition data, finding that the translocation rate constant for gelonin, approximately $5x10^{-8}$ min^{-1}

is several orders of magnitude slower than that of diphtheria alternatives and independent of the targeting moiety (16,47,48). In this work, they conclude that for every 10^6 internalized gelonin immunotoxin molecules, only one reaches the cytoplasm (16) - a result in striking quantitative agreement with the measured TN_{50} of ~5 x 10^6 in the present work. It should be noted that those experiments focused on protein synthesis inhibition rather than a direct measure of cell viability. Utilizing the reported technique, it is likely that immunotoxins incorporating toxins with dedicated translocation domains will show lower TN_{50} values depending on the efficiency of their endosomal escape machinery. However, such added functionality is likely to contribute directly to off-target toxicity *in vivo*.

The subcellular barrier to delivery is common to all therapeutic macromolecules requiring cytoplasmic access. Many groups interested in the delivery of siRNA have investigated various tools for overcoming this barrier including endosome disrupting polymers (49). Our measurements of the number of toxin molecules required to achieve a single translocation event should be a useful assay for investigating the potential of these tools to enhance intracellular delivery in a quantitative way.

In the future, assessment of novel immunotoxin constructs should be more thorough when potency is evaluated both by the traditional extracellular concentration response metric and the internalized cytotoxicity measurement presented here. Having designed novel, potent immunotoxins, engineering efforts should now be properly directed either towards designing molecules with improved

intracellular uptake (e.g. tumor delivery/penetration, antigen density, binding affinity, internalization kinetics, and tumor retention), or which have improvements in the efficiency of intracellular trafficking to the biologically active compartment. These results should have a significant impact on the rational design of immunotoxins and their combination therapies.

Notes – This chapter is largely derived from Pirie C.M., Hackel B.J., Rosenblum M.G., Wittrup K.D. (2011) *J Biol Chem* **286**(6), 4165-4172

2.6 – Works cited

1. Pastan, I., Hassan, R., FitzGerald, D. J., and Kreitman, R. J. (2007) *Annu Rev Med* **58**, 221-237

2. Ackerman, M. E., Pawlowski, D., and Wittrup, K. D. (2008) *Mol Cancer Ther* **7**(7), 2233-2240

3. Wenning, L. A., and Murphy, R. M. (1999) *Biotechnol Bioeng* **62**(5), 562-575

4. Thurber, G. M., Schmidt, M. M., and Wittrup, K. D. (2008) *Adv Drug Deliver Rev* **60**(12), 1421-1434

5. Roberts, L. M., and Lord, J. M. (2004) *Mini Rev Med Chem* **4**(5), 505-512

6. Du, X., Beers, R., Fitzgerald, D. J., and Pastan, I. (2008) *Cancer Res* **68**(15), 6300-6305

7. Kondo, T., FitzGerald, D., Chaudhary, V. K., Adhya, S., and Pastan, I. (1988) *J Biol Chem* **263**(19), 9470-9475

8. Keller, J., Heisler, I., Tauber, R., and Fuchs, H. (2001) *J Control Release* **74**(1-3), 259-261

9. Rathore, D., and Batra, J. K. (1996) *Biochem Biophys Res Commun* **222**(1), 58-63

10. Seetharam, S., Chaudhary, V. K., FitzGerald, D., and Pastan, I. (1991) *J Biol Chem* **266**(26), 17376-17381

11. Kreitman, R. J., Hassan, R., Fitzgerald, D. J., and Pastan, I. (2009) *Clin Cancer Res* **15**(16), 5274-5279

12. Kreitman, R. J., Stetler-Stevenson, M., Margulies, I., Noel, P., Fitzgerald, D. J., Wilson, W. H., and Pastan, I. (2009) *J Clin Oncol* **27**(18), 2983-2990

13. Stirpe, F., Olsnes, S., and Pihl, A. (1980) *J Biol Chem* **255**(14), 6947-6953

14. Rosenblum, M. G., Kohr, W. A., Beattie, K. L., Beattie, W. G., Marks, W., Toman, P. D., and Cheung, L. (1995) *J Interferon Cytokine Res* **15**(6), 547-555

15. Scott, C. F., Lambert, J. M., Goldmacher, V. S., Blattler, W. A., Sobel, R., Schlossman, S. F., and Benacerraf, B. (1987) *Int J Immunopharmaco* **9**(2), 211-225

16. Yazdi, P. T., and Murphy, R. M. (1994) *Cancer Research* **54**(24), 6387-6394

17. Rosenblum, M. G., Cheung, L. H., Liu, Y. Y., and Marks, J. W. (2003) *Cancer Research* **63**(14), 3995-4002

18. Goldmacher, V. S., Scott, C. F., Lambert, J. M., McIntyre, G. D., Blattler, W. A., Collnhson, A. R., Stewart, J. K., Chong, L. D., Cook, S., Slayter, H. S., and et al. (1989) *J Cell Physiol* **141**(1), 222-234

19. Lambert, J. M., Senter, P. D., Yau-Young, A., Blattler, W. A., and Goldmacher, V. S. (1985) *J Biol Chem* **260**(22), 12035-12041

20. Hammarstrom, S. (1999) *Semin Cancer Biol* **9**(2), 67-81

21. Wegener, W. A., Petrelli, N., Serafini, A., and Goldenberg, D. M. (2000) *J Nucl Med* **41**(6), 1016-1020

22. Sharma, S. K., Pedley, R. B., Bhatia, J., Boxer, G. M., El-Emir, E., Qureshi, U., Tolner, B., Lowe, H., Michael, N. P., Minton, N., Begent, R. H. J., and Chester, K. A. (2005) *Clin Cancer Res* **11**(2), 814-825

23. Kraeber-Bodere, F., Rousseau, C., Bodet-Milin, C., Ferrer, L., Faivre-Chauvet, A., Campion, L., Vuillez, J. P., Devillers, A., Chang, C. H., Goldenberg, D. M., Chatal, J. F., and Barbet, J. (2006) *J Nucl Med* **47**(2), 247-255

24. Schmidt, M. M., Thurber, G. M., and Wittrup, K. D. (2008) *Cancer Immunol Immun* **57**(12), 1879-1890

25. Levin, L. V., Griffin, T. W., Childs, L. R., Davis, S., and Haagensen, D. E., Jr. (1987) *Cancer Immunol Immunother* **24**(3), 202-206

26. Avila, A. D., Mateo de Acosta, C., and Lage, A. (1989) *Int J Cancer* **43**(5), 926-929

27. Akamatsu, Y., Murphy, J. C., Nolan, K. F., Thomas, P., Kreitman, R. J., Leung, S. O., and Junghans, R. P. (1998) *Clin Cancer Res* **4**(11), 2825-2832

28. Sorkin, A., and Goh, L. K. (2009) *Exp Cell Res* **315**(4), 683-696

29. Di Massimo, A. M., Di Loreto, M., Pacilli, A., Raucci, G., D'Alatri, L., Mele, A., Bolognesi, A., Polito, L., Stirpe, F., and De Santis, R. (1997) *Br J Cancer* **75**(6), 822-828

30. Beers, R., Chowdhury, P., Bigner, D., and Pastan, I. (2000) *Clin Cancer Res* **6**(7), 2835-2843

31. Chester, K. A., Begent, R. H., Robson, L., Keep, P., Pedley, R. B., Boden, J. A., Boxer, G., Green, A., Winter, G., Cochet, O., and et al. (1994) *Lancet* **343**(8895), 455-456

32. Boehm, M. K., Corper, A. L., Wan, T., Sohi, M. K., Sutton, B. J., Thornton, J. D., Keep, P. A., Chester, K. A., Begent, R. H., and Perkins, S. J. (2000) *Biochem J* **346 Pt 2**, 519-528

33. Graff, C. P., Chester, K., Begent, R., and Wittrup, K. D. (2004) *Protein Eng Des Sel* **17**(4), 293-304

34. Koide, A., Bailey, C. W., Huang, X., and Koide, S. (1998) *J Mol Biol* **284**(4), 1141-1151

35. Hackel, B. J., Kapila, A., and Wittrup, K. D. (2008) *J Mol Biol* **381**(5), 1238-1252

36. Koide, A., and Koide, S. (2007) *Methods Mol Biol* **352**, 95-109

37. Geiser, M., Cebe, R., Drewello, D., and Schmitz, R. (2001) *Biotechniques* **31**(1), 88-90, 92

38. Zhang, M., Aguilera, D., Das, C., Vasquez, H., Zage, P., Gopalakrishnan, V., and Wolff, J. (2007) *Anticancer Res* **27**(1A), 35-38

39. Preijers, F. W., Tax, W. J., De Witte, T., Janssen, A., vd Heijden, H., Vidal, H., Wessels, J. M., and Capel, P. J. (1988) *Br J Haematol* **70**(3), 289-294

40. May, R. D., Wheeler, H. T., Finkelman, F. D., Uhr, J. W., and Vitetta, E. S. (1991) *Cell Immunol* **135**(2), 490-500

41. Yamaizumi, M., Mekada, E., Uchida, T., and Okada, Y. (1978) *Cell* **15**(1), 245-250

42. Reiter, Y., Brinkmann, U., Jung, S. H., Lee, B., Kasprzyk, P. G., King, C. R., and Pastan, I. (1994) *J Biol Chem* **269**(28), 18327-18331

43. Thompson, J., Stavrou, S., Weetall, M., Hexham, J. M., Digan, M. E., Wang, Z., Woo, J. H., Yu, Y., Mathias, A., Liu, Y. Y., Ma, S., Gordienko, I., Lake, P., and Neville, D. M., Jr. (2001) *Protein Eng* **14**(12), 1035-1041

44. Deen, W. M., Lazzara, M. J., and Myers, B. D. (2001) *Am J Physiol Renal Physiol* **281**(4), F579-596

45. Neville, D. M., Jr., Srinivasachar, K., Stone, R., and Scharff, J. (1989) *J Biol Chem* **264**(25), 14653-14661

46. Chiron, M. F., Fryling, C. M., and FitzGerald, D. (1997) *J Biol Chem* **272**(50), 31707-31711

47. Wenning, L. A., Yazdi, P. T., and Murphy, R. M. (1998) *Biotechnol Bioeng* **57**(4), 484-496

48. Chan, M. C., and Murphy, R. M. (1999) *Cancer Immunol Immunother* **47**(6), 321-329

49. Convertine, A. J., Benoit, D. S., Duvall, C. L., Hoffman, A. S., and Stayton, P. S. (2009) *J Control Release* **133**(3), 221-229

Chapter 3 – An *in trans* targeted intracellular delivery system

3.1 - Abstract

Molecular targeting technology has led to the advent of macromolecular therapeutics capable of tissue specific intervention. But the use of this technology in the field of intracellular drug delivery has been limited and consequently there exists a need for a broadly applicable targeted intracellular delivery system. We've designed an independently targeted drug delivery system based on engineered fibronectin domains fused to bacterial cytolysins. The designed fusion proteins had binding affinities in the single digit nanomolar range to their respective antigen targets and showed antigen-dependent cytotoxicity correlated with hemolytic activity. Delivery capability of the system was validated using gelonin immunotoxins whose exquisite cytoplasmic activities make them ideal candidates for exhibiting enhancement of intracellular delivery. *in vitro* experiments demonstrated the ability of these fusion proteins to synergize in antigen-specific cytotoxicity, reducing the number of internalized toxins required to induce apoptosis from ~$5x10^6$ to < 10^4. These results convey both the potential of this particular application in cancer therapy and of our general approach to intracellular delivery of therapeutic macromolecules.

3.2 – Introduction

For decades researchers have pursued a means by which to deliver therapeutic macromolecules such as DNA, RNA, and proteins to the cytoplasm of cells in order to affect intracellular targets. The *in vivo* efficacy of any macromolecular therapeutic is fraught with numerous challenges, not the least of which is endosomal escape (1). Within the fields of gene therapy and RNA interference, the challenge of intracellular delivery is appreciated, and the value of accomplishing that delivery in a targeted manner is well understood (2, 3). The same is true for protein drugs(4, 5); delivery of protein antigens to antigen presenting cells for display is also enhanced by various mechanisms of endosomal disruption (6, 7). Despite measured successes, there remains a critical unmet need for an effective, targeted intracellular delivery approach.

Immunotoxins are a class of proteins whose intracellular delivery is of particular importance. Early developers of immunotoxins diverged in their use of various types of toxins, generally working with either type I or type II toxins (8). Researchers working with type II toxins, such as diphtheria toxin, ricin, or pseudomonas exotoxin, never concerned themselves with intracellular delivery because these toxins incorporate their own evolved translocation domains or other components that facilitate endosomal escape (9-11). Meanwhile, those working with type I toxins investigated various small molecule and protein based methods for enhancing translocation(12-17). In some cases, potent intracellular delivery agents

have been identified, but specificity remained elusive and toxicity was often a confounding factor.

The bacterium *Listeria Monocytogenes* produces the unique protein listeriolysin O (LLO) as a tool for endosomal escape from phagosomes in macrophages. What makes LLO unique is that, unlike other cytolysins, it is only active within the lysosomal compartment. Once the bacterium and protein are release into the cytoplasm, LLO is inactivated through a variety of mechanisms (18), the most important of which is due to its pH sensitivity (19). LLO and other cytolysins have been used previously as tools for the delivery of biotherapeutics including DNA and proteins (20-23). LLO has also been used as the cytotoxic component of an immunotoxin (24). Homologs in the cholesterol-dependent cytolysin (CDC) family (25) include perfringolysin O (PFO) and streptolysin O. Because of their mechanism of action and the established difficulty in the delivery of our immunotoxins, we hypothesized that targeted type I immunotoxins and targeted CDCs might synergize through enhanced intracellular delivery.

We have previously designed a set of immunotoxins based on engineered binding affinity variants of the 10th type III human fibronectin (Fn3) domain targeting either the carcinoembryonic antigen (CEA) or the epidermal growth factor receptor (EGFR) fused to recombinant, plant type I ribosome inactivating protein gelonin (rGel) (26). These immunotoxins showed enhanced, targeted cytotoxicity towards highly-expressing antigen positive cells. However, they were impotent against lower-expressing cell lines leading us to investigate and quantify the

endosomal escape efficiency of the immunotoxins. Other work in this field indicates that only ~5 immunotoxin molecules are required to reach the cytoplasm in order to induce apoptosis, yet our findings suggested ~5 million immunotoxin had to be internalized to reach this apoptotic threshold. This result encouraged us design tools capable of inducing targeted endosomal disruption.

Specifically, we sought to develop a system for delivering a therapeutic macromolecule to the cytoplasm of a cell in a targeted manner. Using the same engineered Fn3s as our gelonin immunotoxins, we created targeted fusion proteins with LLO and PFO. The fusion proteins were expressed recombinantly in *E. coli*, conserved antigen-specific binding, and showed some antigen-dependent cytotoxicity. Membrane disruptive hemolysis, a characteristic of CDCs, was also conserved. When combined in cell treatments with gelonin immunotoxins these fusions exhibited potentiating activity, decreasing the IC_{50} values of immunotoxins by several orders of magnitude. Potentiation was observed when the two agents were targeted to the same antigen competitively, when targeted to different antigens known to colocalize, and even when targeted to cells expressing low levels of antigens. We went on to test the ability of fusions to potentiate immunotoxin activity when the two agents were applied to cells at different times and to quantify the reduction in the intracellular barrier to delivery, which was consistent with the improvement in cytotoxicity suggesting that the observed synergistic effects are the result of membrane destabilization or pore-formation by the cytolysins leading to release of immunotoxin.

This *in trans* approach to intracellular delivery is a departure from traditional intracellular delivery methods in which the membrane disruptive agent and the therapeutic payload are directly connected. Two different agents targeting the same cell can become colocalized within the same endosomal compartment where the potentiating agent facilitates the release of the therapeutic payload (Figure 3.1).

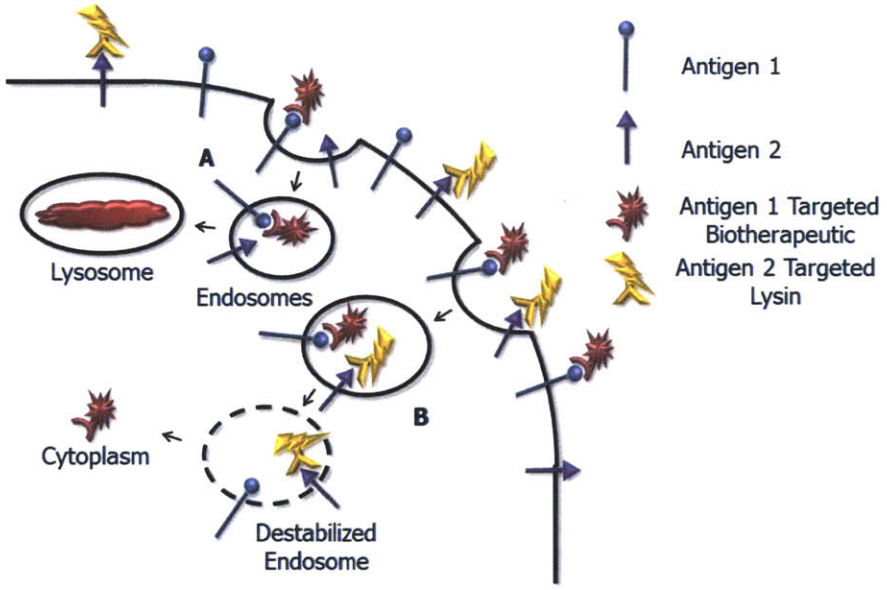

Figure 3.1 – Targeted in trans intracellular delivery. The central concept of this work is that separately targeted membrane disrupting functionality can be delivered to tumor cells via Fn3-cytolysin fusions. Simultaneous targeted delivery of such a potentiator to tumor cells that internalize by endocytosis an independently targeted biotherapeutic will potentiate the immunotoxin by improving its leakage to the cytoplasm, its site of action. By separating the membrane-crossing and toxic moieties, we are able to dramatically improve specificity and potency. The traditional fate of intracellularly active biotherapeutics (A) leads to degradation in the lysosome, but upon compartmental colocalization of biotherapeutic and potentiator (B), the lysins' membrane disruptive characteristics release the biotherapeutic into the cytoplasm

3.3 – Methods

3.3.1 – Cell lines

To obtain an appropriate cross section of the different antigens targeted, we utilized four different established human cancer cell lines. HT-1080 is a human fibrosarcoma cell line negative for CEA. HT-1080(CEA) is a transfected variant of HT-1080 which expresses CEA at high levels (~$2x10^6$ copies/cell) on its surface through the pIRES-CEA plasmid, which is maintained under selective pressure from geneticin at 250 μg/mL. Both HT-1080 and HT-1080(CEA) also express ~$1x10^5$ copies of EGFR. A431 is a human epidermoid carcinoma cell line that highly expresses EGFR (~$3x10^6$ copies/cell) but not CEA. HT-29 is a human colorectal carcinoma cell line that expresses lower levels of both CEA and EGFR (~$1x10^5$ copies/cell).

3.3.2 – Colocalization microscopy

1 x 10^5 HT-29 cells were cultured on MatTek dishes with 0.13mm coverslip bottoms in 200 μL of growth media to which Alexa584-sm3E anti-CEA single-chain antibody variable fragment (7 μM, DOL 1.85) and Alexa488-225 anti-EGFR antibody (5uM, DOL 6) were added with final concentrations of 11.7 nM and 33 nM, respectively. The cells were maintained in this solution under standard culture conditions (37 °C, 5% CO_2) for 15 hours, after which the cells were washed three times with PBS and returned to growth media for 30 minutes before imaging. Cells were serum starved

prior to treatment. Images were taken under 60x magnification on an inverted Olympus X71 Deltavision deconvolution microscope.

3.3.3 – Construction of expression plasmids

Genes encoding LLO and PFO proteins were codon-optimized for expression in *E. coli* and ordered from GenScript (Piscataway, NJ). Genes were amplified by PCR using primers designed with 3' complimentarity to either end. After being purified from an agarose gel, the gene product was inserted into the same fusion construct used previously for our immunotoxin synthesis by the method of Geiser *et al.* (26, 27). The resulting plasmid encoded an open reading frame including, from N-terminus to C-terminus: maltose binding protein, N_{10} linker, Factor Xa protease site, an engineered 10th Type III fibronectin domain, a G_4S linker, and LLO or PFO. Additionally, our PFO gene was truncated to remove an unnecessary secretory sequence and its construct modified to incorporated a tobacco-etch virus protease site N-terminal to the constant Factor Xa site.

3.3.4 – Protein expression and purification

Immunotoxins were synthesized as described previously (26) and Fn3-LLO/PFO (A.6, A.7, A.8, and A.9) production was conducted in a similar manner. Briefly, the appropriate plasmids were transformed into Rosetta (DE3) *E. coli* (Novagen, San Diego, CA) and grown on LB agar plates supplemented with ampicillin and chloramphenicol. Colonies were isolated from the plate and used to inoculate 15 mL

of selective media which incubated overnight at 37 °C. Cultures were used to inoculate 1 L of antibiotic free LB media and grown to an OD_{600} ~ 0.5 at which point 5 mL of 0.1M IPTG was added and the cultures moved to incubate at 30 °C for 6 hours. Following induction, cultures were centrifuged at 15,000 x g for 12 minutes, the supernatant removed, and the cell pellets frozen at -20 °C. Pellets were resuspended in 25mL amylose column buffer containing Complete EDTA-free protease inhibitor (Roche, Indianapolis, IN) and then sonicated on a Branson Sonifier 450A (Branson Ultrasonics, Danbury, CT) at 50% duty cycle and power level 6 for three, one-minute intervals. The resulting solution was centrifuge at 50,000 x g for 30 minutes to pellet cell debris and the supernatant was applied to an amylose column as described by the manufacturer (New England Biolabs, Ipswich, MA). Purified recombinant proteins were concentrated and buffer exchanged into Factor Xa/TEV protease digestion buffer using Amicon columns with a 100 kDa MWCO then incubated overnight at 4°C with 5 µL Factor Xa/TEV protease (New England Biolabs/Invitrogen). Fn3-cytolysin was isolated from the cleaved MBP and Factor Xa/TEV protease by ion-exchange chromatography with a HiTrap Q column (GE Healthcare, Piscataway, NJ).

3.3.5 – Antigen binding affinity titration

Fn3-LLO was biotinylated using amine reactive EZ-Link Sulfo-NHS-LC-biotin (Pierce, Rockford, IL). Antigen positive cell lines HT-1080(CEA) and A431 were lifted from culture plates with trypsin and resuspended in 4% formalin for 30

minutes before being washed and stored in phosphate buffered saline with 1% (w/v) bovine serum albumin (PBSA). Fixed cells were incubated with varying concentrations of biotinylated fusion protein overnight at 37 °C, washed once and resuspended in 250 µL of PBSA with 1 µL streptavidin-phycoerythrin conjugate (Sigma, St. Louis, MO) for 1 hour at 4 °C. Cells were washed once again and resuspended in 150 µL PBSA before being analyzed for fluorescence on an Accuri C6 Flow Cytometer (Accuri Cytometers, Ann Arbor, MI). For each titrating concentration, the median fluorescent intensity was determined and data sets for each immunotoxin were fitted to a standard binding isotherm using least-squares regression with the Excel (Microsoft Corp., Redmond, WA) solver tool.

To titrate Fn3-PFO fusions, CEA (R&D Systems, Minneapolis, MN) was biotinylated using amine reactive EZ-Link Sulfo-NHS-LC-biotin (Pierce). Biotinylated CEA was loaded streptavidin coated magnetic beads (Invitrogen, Carlsbad, CA), and incubated with varying concentrations of C7PFO for 6 hours at 4 °C. EGFR 404SG ectodomain was expressed on the surface of yeast(28), and incubated with varying concentrations of E6PFO for 6 hours at 4 °C. Cells or beads were washed once and resuspended in 50 µL of PBSA with 0.25 µL of rabbit anti-His6 antibody (Abcam, Cambridge, MA) which was labeled with the Alexa 647 Microscale Protein Labeling Kit (Invitrogen) for 30 minutes at 4 °C. Cells or beads were washed twice with 200 µL PBSA before being analyzed for fluorescence by flow cytometry.

3.3.6 – Hemolysis

Experiments were conducted to determine the degree to which Fn3-cytolysin would disrupt red blood cell membranes using a method similar to that described by Henry *et al.* (29). Briefly, purified mouse red blood cells (Fitzgerald, Acton, MA) were washed twice with PBSA at either pH 7.4 or pH 5. Cells were mixed with fusion protein at varying concentrations in the same buffer to a final cell concentration of ~$1x10^9$ cells/ml. Cells and protein were incubated at 37 °C for 1 hour before treatments were centrifuged at 13,500 x g for 5 minutes. Supernatants were transferred to 96-well plates and absorbance read at 540 nm. Results were normalized to a PBS negative control and 1% Triton-X100 positive control.

3.3.7 – Cytotoxicity

Log-phase tumor cells were lifted by trypsinization, counted, and seeded on 96-well plates at 2,500 cells per well. Cells were allowed to adhere overnight, after which fresh growth media containing varying concentrations of Fn3-cytolysin and/or immunotoxin was added to triplicate wells. Cells were incubated in treatment media for 48 hours before being replaced with media containing the WST I reagent (Roche). The red/ox solution was allowed to develop for 1 hour under normal culture conditions after which plates were measured for absorbance at 450 nm. Untreated cells and cells lysed with a 1% Triton-X100 solution were used as positive and negative controls, respectively. Measurements were set to baseline on negative control and normalized to positive control treatments, triplicates averaged, and

standard deviations calculated. Delayed dose or time dependent cytotoxicity data were obtained by treating cells as described for 12 hours with immunotoxin, removing treatment containing media, washing once with PBS, then replacing with fresh media or media containing the potentiating agent for wells at 0, 12, 24, or 48 hours from initial immunotoxin exposure, then following identical assay procedures after 72 hours. In situations where one agent was titrated and the other was fixed or where both agents' concentrations were fixed, the fixed concentration was selected so as to be non-toxic in the absence of the other agent.

3.3.8 – Statistical analyses of synergy

To quantify the extent of synergy between gelonin immunotoxins and targeted cytolysins *in vitro* we used designed cytotoxicity co-titrations to calculate combination index (CI) and cumulative combination data to calculate synergy assessment factor (SAF). The combination index metric was first used to determine the synergistic effects of mutually exclusive and mutually non-exclusive enzyme inhibitors by Chou and Talalay (30, 31). Synergy assessment factor is a more recent treatment of synergistic effects which was inspired by combination index. It was first put forth by Yan *et al.* as it pertained to synergy within signaling networks(32) and is equivalent to the fractional product equation described by Webb(33). For CI calculations we simultaneously titrated immunotoxins and used 0.9 fraction affected as the analysis point.

$$CI = \frac{[IT]}{IT_{90}} + \frac{[P]}{P_{90}} + \frac{[IT] \times [P]}{(IT, P)_{90}}$$

Alternatively, when using SAF we chose to calculate the metric for all titrations and data points then averaged for cell line or immunotoxin/potentiator of interest.

$$SAF = F_A(IT, P) - F_A(IT) \times F_A(P)$$

3.3.9 – Quantitative internalization

Cell lines were incubated with immunotoxins directly labeled with AlexaFluor 488 and unlabeled Fn3-cytolysin. At various times, cells were washed with PBS and incubated for 30 minutes with the quenching rabbit anti-AlexaFluor 488 (Invitrogen). Cells were then scraped from the wells, washed again with PBS, and analyzed for internal fluorescent signal. Quantum Simply Cellular anti-Mouse IgG beads (Bangs Laboratories, Fishers, IN) with different quantified binding capacities were incubated with AlexaFluor 488 labeled mouse IgG for 30 minutes, washed with PBS, then measured for fluorescence. The number of fluorescent molecules per protein on both immunotoxins and mouse IgG was determined using absorbance measurements at 280 and 494 nm. Bead fluorescence measurements were used to generate a standard curve for fluorescence signal per fluorophore. Immunotoxin internalization data were quantified by mapping fluorescence signal to the bead fit, converting signal to fluorescent molecules and then translated into immunotoxin molecules using the labeling ratio.

3.3.10 – Internalized cytotoxicity

Data obtained in time dependent cytotoxicity experiments were combined with those from quantitative internalization experiments and plotted to suggest the former as the dependent variable and the latter as the independent variable as in our previous work (Chapter 2). Accumulated results were fitted using non-linear least squares regression of an exposure-response curve with variable slopes using MATLAB (The MathWorks, Natick, MA). From this fitting, a mid-range response metric was calculated and reported.

3.4 – Results

3.4.1 – EGFR and CEA intracellular colocalization

HT-29 cells express approximately $1x10^5$ copies each of both EGFR and CEA on their surface. These cells were treated with fluorescently labeled anti-EGFR IgG and anti-CEA scFv. Subsequent microscopy images showed that both antigens were bound and internalized showing punctuate staining (Figure 3.2). Further, the merging of the images from the two fluorescent channels indicates strong colocalization. Colocalization was characterized using image analysis software and found to have a positive Pearson's coefficient of correlation of 0.76.

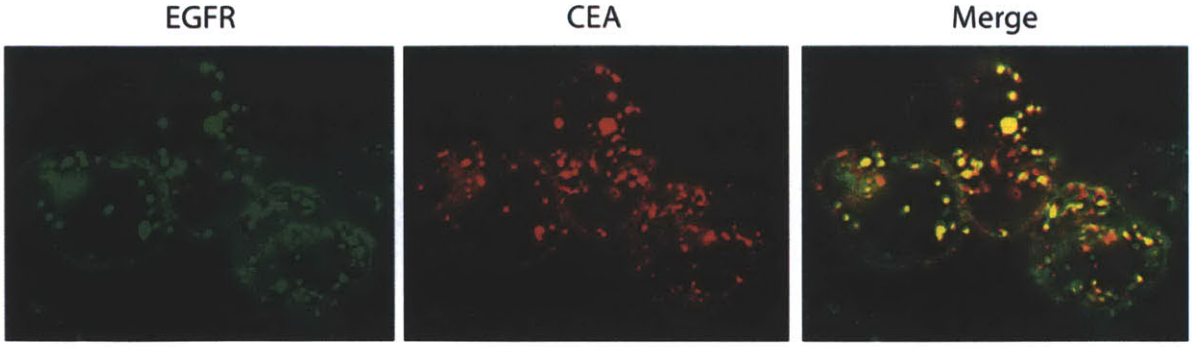

Figure 3.2 - Colocalization of intracellular EGFR and CEA. HT-29 cells that express both EGFR and CEA show that agents targeted to these two receptors will colocalize to a considerable extent to the same intracellular compartments, a necessary condition for the success of the proposed potentiation strategy. An anti-EGFR antibody was labeled with AlexaFluor-488 and an anti-CEA scFv was labeled with AlexaFluor-594 before both were used to label HT-29 cells to observe colocalization.

3.4.2 – Cytolysin fusion synthesis and in vitro characterization

Novel fusion proteins of the Fn3-LLO and Fn3-PFO types were designed with targeting to EGFR and CEA. Fusions were derived from Fn3 clones E626 and C743, which bind to EGFR and CEA with K_d's of 260 pM and 1.8 nM, respectively and were engineered and assayed for antigen affinity as described by Pirie *et al.* (26). The fusions were expressed in *E. coli* at ~100 μg/L for Fn3LLO and ~1.5 mg/L for Fn3PFO. Non-linear regression fitting shows that the K_d's for the fusion proteins are 5.0 nM for E6LLO, 4.1 nM for C7LLO, 4.1 nM for E6PFO and 4.1 nM for C7PFO (Figure 3.3A).

Given our understanding of cytolysin activity and the work of Bergelt *et al.* (24), we realized that it was important to assess the direct cytotoxicity of the Fn3-cytolysins. The independent cytotoxicity of the fusions was tested by titration on a

variety of antigen positive and antigen negative cell lines. Fitting the data with concentration-response curves with variable slopes gave IC_{50} values that correlated inversely with antigen expression level (Figure 3.3B). These data show that targeted LLO and PFO fusions do indeed possess some inherent cytotoxicity and that, much like gelonin fusions, their cytotoxicity is related to specific binding of cell surface antigens.

A

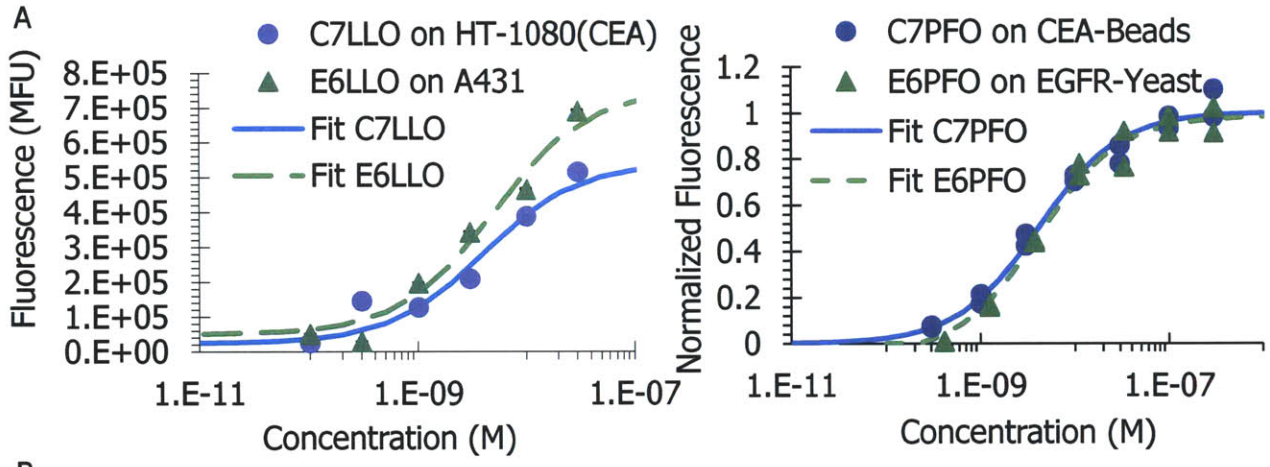

B

IC_{50}'s (M)	Cell Line		
Potentiator	HT-1080(CEA)	A431	HT-29
C7LLO	8.3×10^{-8}	-	$>1 \times 10^{-6}$
E6LLO	2.5×10^{-7}	7.1×10^{-8}	$>1 \times 10^{-6}$
C7PFO	7×10^{-12}	9.8×10^{-12}	1.2×10^{-10}
E6PFO	1×10^{-11}	5.4×10^{-10}	1.5×10^{-11}

Figure 3.3 – Cytolysin fusion binding and cytotoxicity. (A) Biotinylated Fn3-LLO fusions were titrated against fixed A431 or HT-1080(CEA) cells, while Fn3-PFO fusions were titrated against antigen-coated beads or antigen-displaying yeast. Fusions showed binding affinity K_d's in the low nM range, only slightly reduced relative to the parent Fn3 affinity. (B) Fusions were added to growth media on cells with varying antigen expression levels. For each cell type, Fn3-cytolysin cytotoxicity correlated with antigen expression level.

A common assay in the characterization of bacterial CDCs and other membrane disruptive materials is the hemolysis assay. The ability of Fn3-cytolysin fusions to disrupt red blood cells at either physiological or endosomal pH can be representative of non-specific toxicity and activity respectively. We were particularly interested in assessing hemolysis because of work suggesting very low toxicity limits of LLO *in vivo* (19). At pH 7, the EC_{50} for membrane disruption by E6LLO was ~500 nM, while at pH 5 it was ~3 nM. For E6PFO the EC_{50}'s were 25 pM and 4 pM respectively (Figure 3.4). This data is consistent with work by Jones and Portnoy that queried LLO and PFO properties and found similar hemolytic characteristics (34).

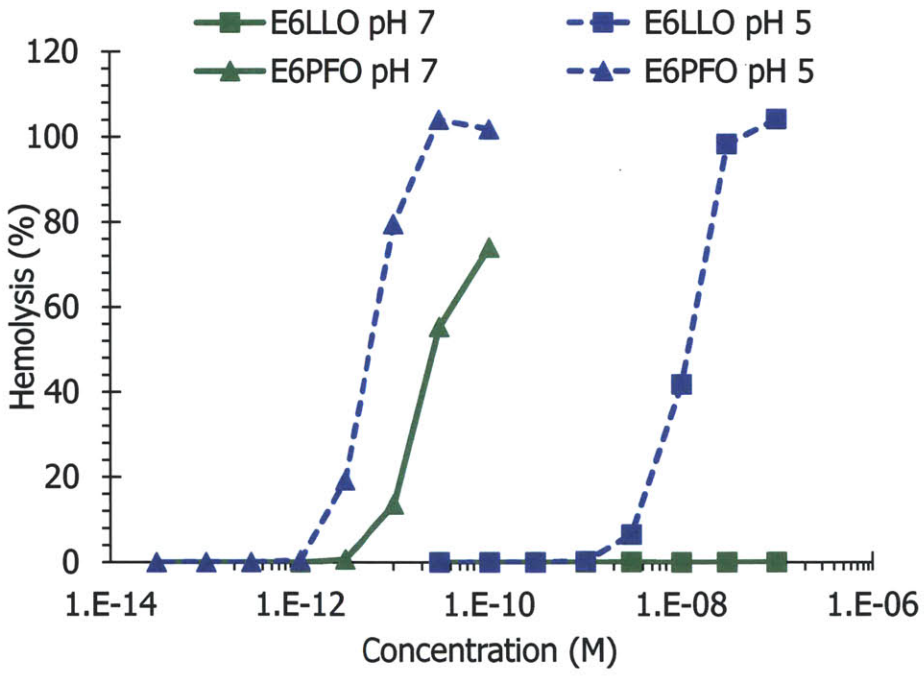

Figure 3.4 – Cytolysin fusion hemolytic activity. Fn3-cytolysins were incubated with mouse red blood cells at either physiological (7) or endosomal pH (5). Fusions showed the expected pH dependent response at concentrations consistent with their non-specific toxicity and potentiating activity.

3.4.3 – Potentiated immunotoxin cytotoxicity in vitro

In this study we've used two different immunotoxins E4rGel and C7rGel targeting EGFR and CEA respectively that have been described previously (26). These immunotoxins show independent IC_{50}'s of approximately 30 nM and 5 nM respectively on cell lines expressing high levels of antigen. However, on HT-29 cells that express low levels of antigen, the immunotoxins appear no more potent than untargeted toxin with IC_{50}'s around 1 μM. Remarkably, when we titrate the immunotoxins in the presence of non-toxic levels of Fn3-cytolysin, the potency is increased by several orders of magnitude. We find that on high antigen expressing cells, the IC_{50} of E4rGel is decreased from 30 nM to ~50 pM and that of C7rGel is potentiated from about 1 nM to the single digit pM range (Figure 3.5). When both agents are titrated at a fixed ratio, the independent titrations are non-toxic, while the combination shows synergistic cytotoxicity. Perhaps most importantly, we were able to show that otherwise ineffective immunotoxin can be activated to an equivalent degree on HT-29 cells where the IC_{50}'s shift from 1 μM to 1 nM (Figure 3.6A). This shift was consistent for both non-competitively co-targeted immunotoxin and potentiator and for differentially targeted components.

To statistically support the observed synergy between gelonin and cytolysin immunotoxins we employed two different metrics: combination index (CI) and synergy assessment factor (SAF). Qualitatively, CI values are characterized as antagonistic when > 1, additive when $= 1$, and synergistic when < 1. Alternatively, SAF will $= 0$ when a combination is additive, > 0 when antagonistic, and < 0 when

synergistic. We report here examples of CI_{90} values less than 1 and negative SAF values indicative of the strong synergy (Figure 3.6B) we observed across all cytolysin fusions when combined with gelonin immunotoxins on any cell line. The strength of each synergy metric tended to show an inverse correlation with the independent potency of the gelonin immunotoxin on the cell line in question.

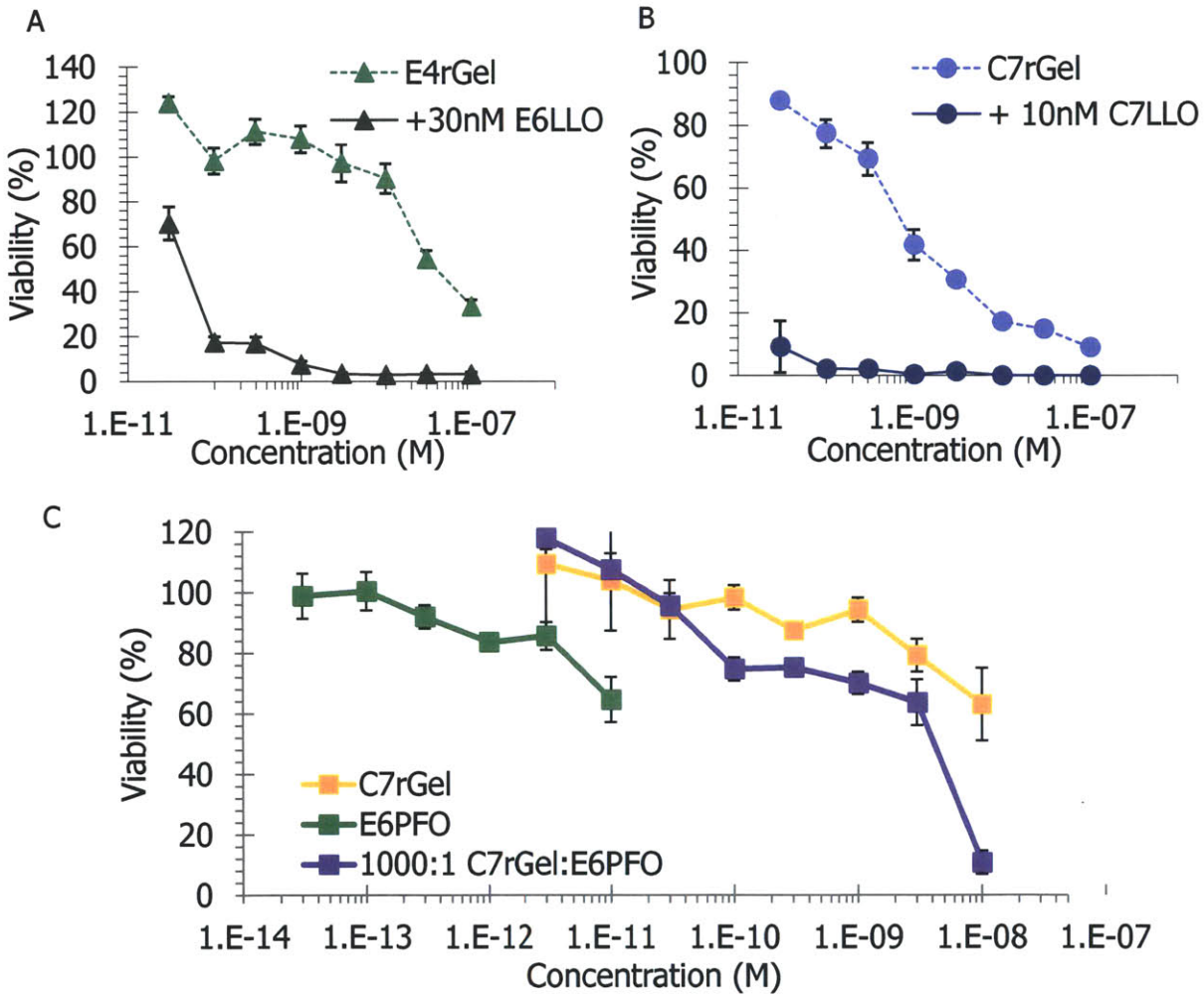

Figure 3.5 – Potentiation of gelonin immunotoxin cytotoxicity. (A) Potentiation of anti-EGFR immunotoxin E4rGel using the non-competitive, co-targeted potentiator E6LLO on A431 cells. (B) anti-CEA immunotoxin C7rGel potentiated by the competitive potentiator C7LLO on HT-1080(CEA) cells. (C) Titrations of C7rGel and E6PFO on HT-29 cells achieve only modest toxicity alone, but when titrated together at the same concentrations, much greater toxicity is observed.

A

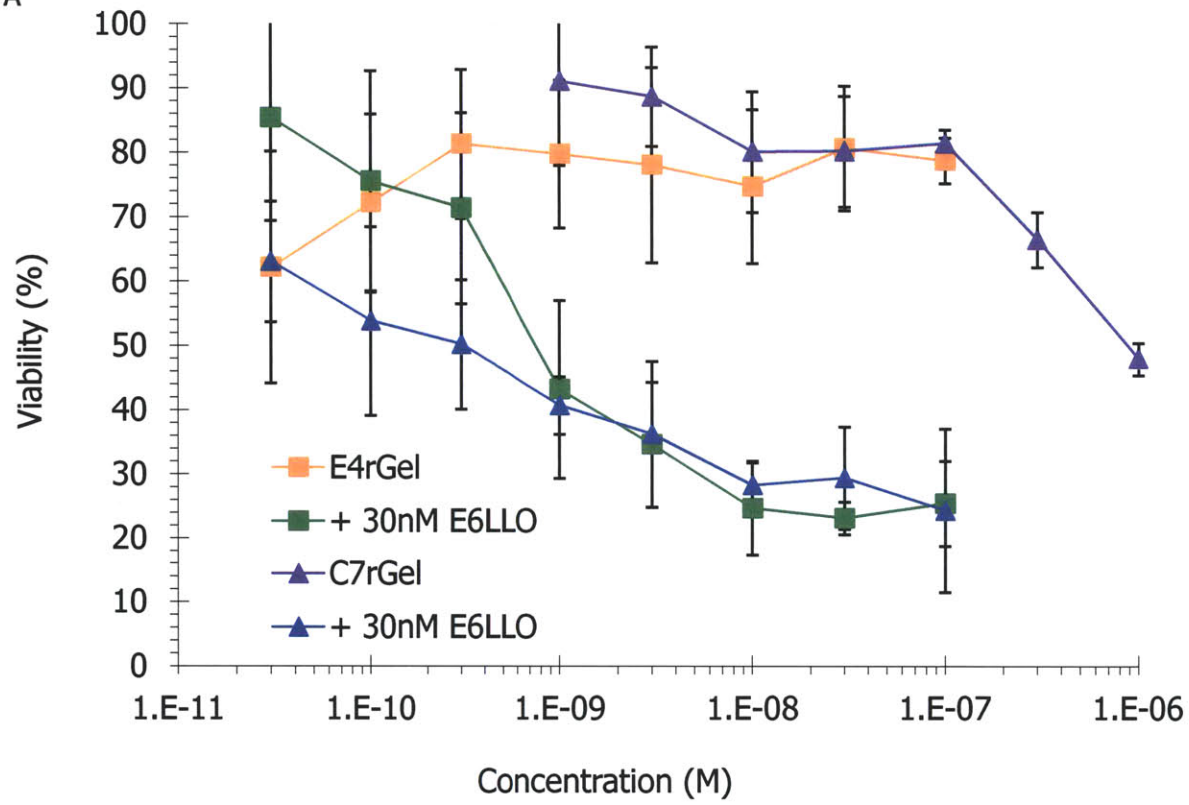

B

Synergy indices Potentiator	Cell line (Index) HT-1080(CEA) (CI)	(SAF)	HT-29 (CI)	(SAF)
E6LLO	0.04	-0.43	0.03	-0.58
E6PFO	0.08	-0.35	0.11	-0.32

Figure 3.6 – in vitro potentiation. Fn3-cytolysins were first tested *in vitro* to show that the fundamental IC_{50} of Fn3-rGel's could be lowered. (A) HT-29 cells titrated with immunotoxins targeting either EGFR or CEA experience only limited cytotoxicity up to μM concentrations. But in the presence of non-toxic levels of potentiator, these same immunotoxins have IC_{50}'s around 1 nM. (B) For two EGFR targeted potentiators, combination index (CI) and synergy assessment factor (SAF) are calculated for their effect on HT-1080(CEA) and HT-29 in the presence of C7rGel.

3.4.4 – Internalized cytotoxicity with potentiated TN_{50}

Previously we have shown that there is an intracellular barrier to immunotoxin potency which requires that ~$5x10^6$ toxin molecules be internalized before a cell will undergo apoptosis (26). Furthermore, it was established that this barrier was common to all gelonin immunotoxins tested regardless of cell type, antigen targeted, or binding affinity. We utilized the same techniques to characterize the intracellular barrier in the presence of potentiator. The number of anti-CEA immunotoxins internalized by HT-29 cells increased with proportionally with treatment concentration and incubation time (Figure 3.7A). However, the number is still significantly less than would be necessary to induce cytotoxicity without of potentiator, yet loss of viability is observed in treatment cells (Figure 3.7B).

When we combine data from internalization and cytotoxicity measurements we get internalized cytotoxicity curves that indicate TN_{50} values less than 10^4 molecules, a several order of magnitude drop in the delivery barrier mediated by the presence of potentiator (Figure 3.7C). In fact, we are unable to directly ascertain the true TN_{50} in the presence of potentiator because the fluorescent signal from so few molecules is indiscernible from autofluorescence of the cells. To give a sense of the magnitude of the enhancement of intracellular delivery due to potentiator we've plotted internalized cytotoxicity measurements for anti-CEA immunotoxins on HT-1080(CEA) and HT-29 cells in the presence of CEA or EGFR potentiator respectively alongside the curve-fit for unpotentiated TN_{50} from our previous work (26) (Figure 3.8).

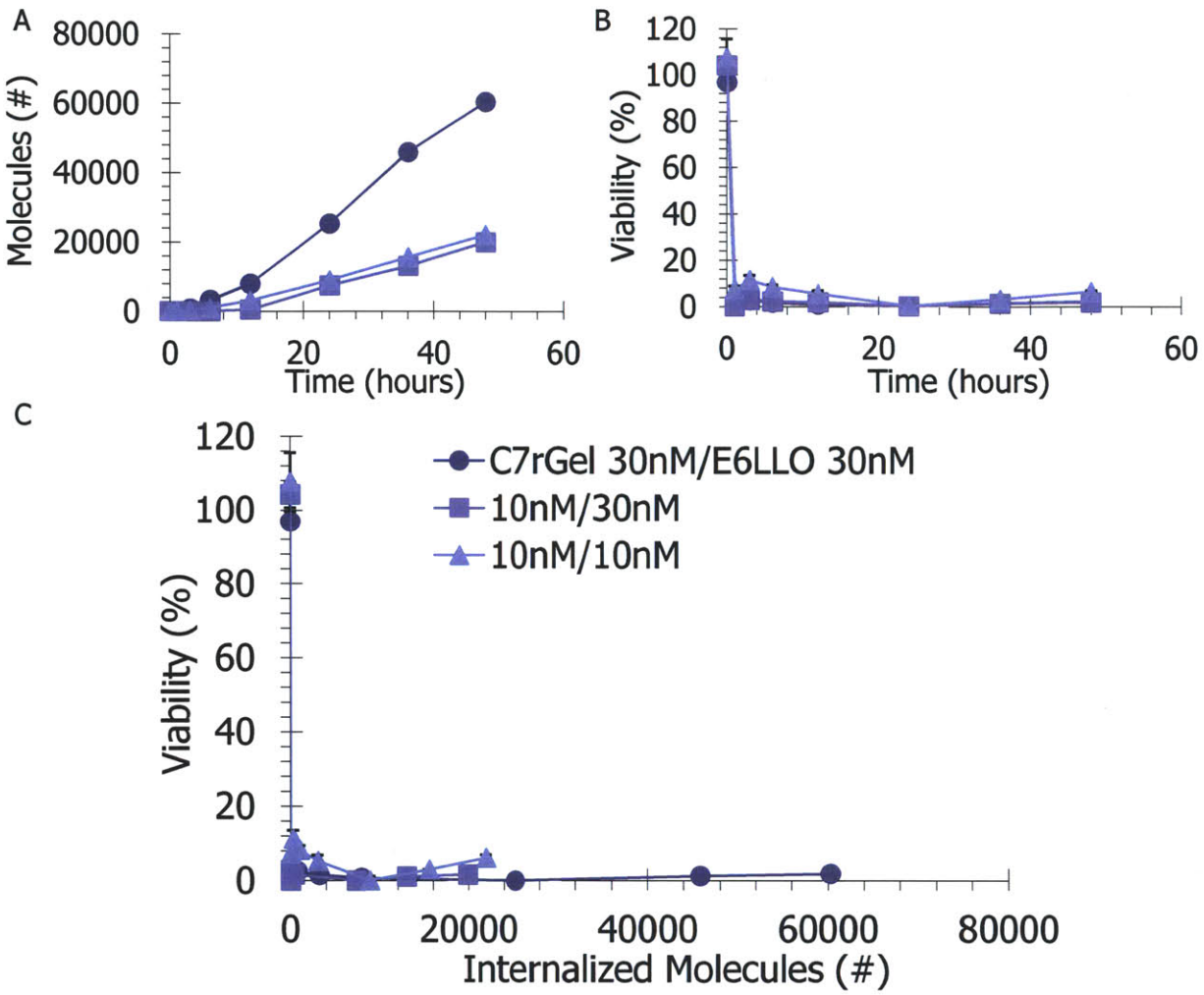

Figure 3.7 – Potentiaion of internalized cytotoxicity and reduction of TN_{50}. Immunotoxins were fluorescently labeled and their internalization by antigen positive cells was measured and quantified for the precise number of toxins inside. In the absence of potentiator, ~$5x10^6$ toxins must be internalized on average before a cell will undergo apoptosis. (A) HT-29 cells treated with independently non-toxic levels of immunotoxin which shows concentration and time dependent internalization in the presence of potentiator. (B) HT-29 cells treated with equivalent doses show concentration and time dependent loss of viability. (C) Combined data sets comparing loss of viability with respect to uptake indicates that fewer than $5x10^3$ immunotoxins were sufficient to induce apoptosis. The single legend applies to all plots.

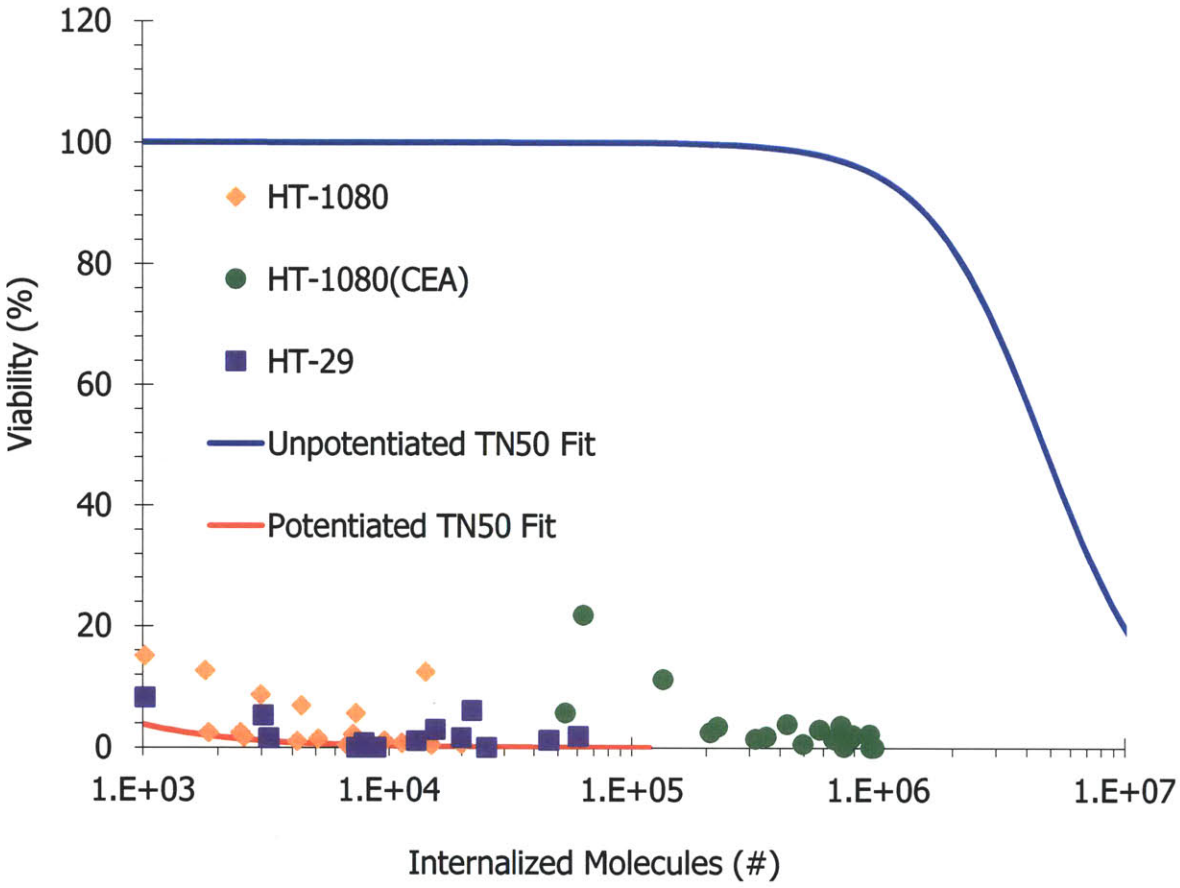

Figure 3.8 – Combined potentiated internalized cytotoxicity. Internalized cytotoxicity data from HT-1080, HT-1080(CEA) and HT-29 cells treated with C7rGel and E6LLO are fitted to a dose response curve, but assay limitations prevent determination of a potentiated TN_{50} $<10^4$. This is compared to the unpotentiated curve fit (26) with a TN_{50} of $\sim 5 \times 10^6$. In the presence of potentiator, significantly less immunotoxin uptake is required to induce loss of viability.

3.4.5 – Delayed exposure cytotoxicity

Much like differential targeting of two antigens, we envisioned a system in which two agents might be dosed independently *in vivo* to reduce non-specific uptake of both agents simultaneously by antigen-negative cells. We tested the possibility of this approach *in vitro* by treating cells for a fixed period of time with growth media containing one agent, then removing it and replacing it with new media containing the appropriate second agent. A431 cells were treated with anti-EGFR E4rGel immunotoxin and then non-competitive anti-EGFR E6LLO potentiator with increasing delay times (Figure 3.9A). Similarly, HT-29 cells were exposed to differentially targeted immunotoxin (CEA) and potentiator (EGFR) at order of magnitude higher concentrations, resulting in stronger but consistent results (Figure 3.9B). Treatment concentrations for each agent were non-toxic when exposed independently. For both cell lines, immunotoxin, and potentiator combinations, potentiating activity was strongest for simultaneous exposure and was abrogated as delay time increased but could still be observed even after 48 hours separation.

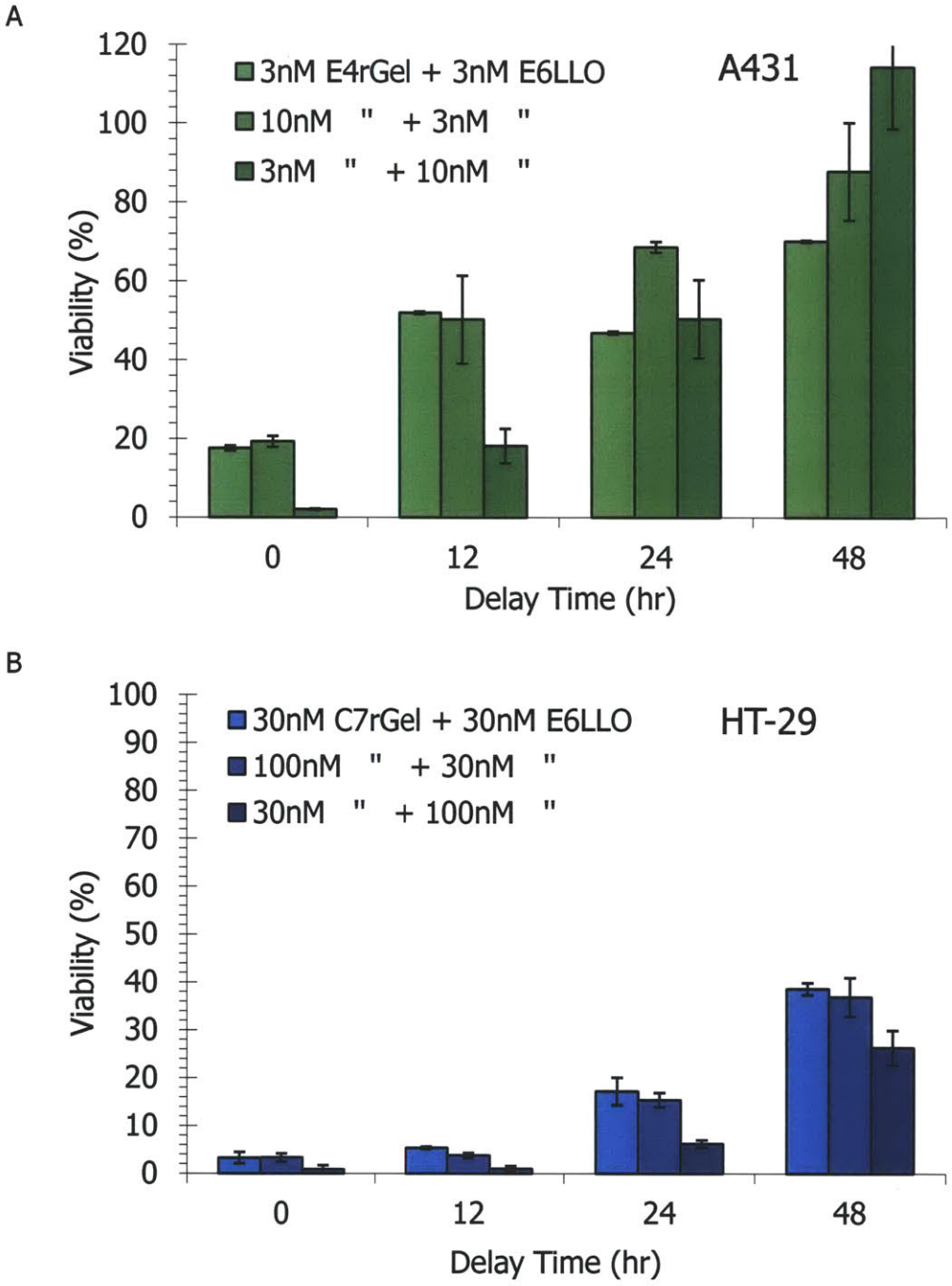

Figure 3.9 – Delayed exposure potentiation of cytotoxicity. In these experiments cells were exposed to a concentration of immunotoxin for 12 hours and a concentration of potentiator for 24 hours with potentiator exposure starting at either the same time (t= 0) or delayed by 12, 24, or 48 hours. (A) A431 cells treated with E4rGel immunotoxin and E6LLO potentiator, both non-competitively targeting EGFR. (B) HT-29 cells treated with C7rGel immunotoxin targeting CEA and E6LLO potentiator targeting EGFR. We observe that potentiators can be effective even after a 48 hour delay in treatments depending on concentration.

3.5 – Discussion

The importance of targeted intracellular delivery to the advancement of numerous therapeutic agents is well appreciated (3). While there has been some use of cholesterol-dependent cytolysins in this area, our studies are the first to use cytolysins as targeted *in trans* delivery agents together with a therapeutic that targets a second, different cell-surface target. One benefit of this approach is that targeting two independent antigens may improve *in vivo* tissue specificity. Additionally, when two agents are delivered *in trans*, they can be dosed independently, which can reduce unwanted side effects.

Our two agent approach was conceived of with the intention of directing a biotherapeutic and a potentiator towards different antigen targets. While it may be more convenient to target both components (*i.e.*, the therapeutic agent, such as Fn3-rGel, and a potentiating agent, such as Fn3-LLO or Fn3-PFO) to the same cell-surface molecule, and while such a design would ensure colocalization, we were interested in taking advantage of the additional specificity that targeting two different antigens might confer *in vivo*. Prior to doing so we sought to confirm that our two antigens of interest would colocalize within endosomes. We found that in HT-29 cells, CEA and EGFR will colocalize. This is not entirely unexpected since other cell surface antigens have been shown to colocalize (35) and most internalization pathways converge in early endosomes (36). Moreover, scaling analysis reveals that, in the absence of a preferential internalization mechanism, two antigens are more likely to colocalize than not. Examining the current system

where an average sized cell expresses ~10^5 copies of either antigen per cell, if we assume a random surface distribution of antigens and unbiased internalization, then each endosome would contain ~10 copies of each antigen, effectively ensuring colocalization of any two targets.

We have described the synthesis of novel targeted fusion proteins incorporating Fn3 and LLO or PFO. These fusions are expressed in *E. coli* and can be readily purified. Fn3 clones affinity matured for binding EGFR and CEA retained most of their affinity in the potentiator constructs, conserving nM binding constants. In cytotoxicity tests these potentiators showed antigen specificity and moderate cytotoxicity with IC_{50}'s around 100 nM for LLO fusions and 10 pM for PFO fusions. Analysis of the hemolytic activity of the fusions showed consistency with previous reports of the different cytolysins' activity. LLO fusions showed significant pH dependence and optimum activity at endosomal pH while PFO fusions exhibited greater potency but limited pH dependence. The EC_{50}'s at physiological pH corresponded roughly with the non-specific cytotoxicity, while that at endosomal pH was consistent with the antigen positive cell potentiating activity.

We proceeded to validate the ability of our Fn3-cytolysin to mediate increased cytoplasmic delivery. When our immunotoxins targeting EGFR and CEA were titrated in the presence of Fn3-cytolysin targeting the same antigen competitively or non-competitively, or targeting an independent antigen, the immunotoxins displayed IC_{50}'s several orders of magnitude lower than in the absence of the potentiating agent. Potency at these scales significantly improves the forecast for

use of type I immunotoxins in the treatment of cancer. The degree to which potency of a particular targeted biotherapeutic is enhanced by Fn3-cytolysin will be directly tied to its inherent potency in the cytoplasm. We believe that these enhancements in potency and selectivity will be broadly applicable to the delivery of any targeted biotherapeutic without its own translocation mechanism.

Having established a metric for determining the relative barrier to cytoplasmic delivery (26), we were interested in determining how Fn3-cytolysin might lower this barrier. Fundamentally, our assay queries the integrity of subcellular compartments in general, because it does not consider specific subcellular localization and merely approximates cytoplasmic release with cytotoxicity. Thus, an agent capable of enhancing the release of immunotoxin through either pore formation or membrane destabilization should quantitatively differentiate itself in this assay. We find that Fn3-LLO fusions are so effective in this setting as to reach the lower limit of detection for the method. In fact, so few molecules were required to be internalized prior to observing cytotoxicity that the signal from the internalized immunotoxins did not surpass background fluorescence of the cells. As a result we are forced to approximate the TN_{50} for our immunotoxins in the presence of potentiating Fn3-LLO fusions at less than 10^4 molecules. This shift in the TN_{50} value is consistent with the observed shifts in cytotoxicity when compared to the TN_{50} for our immunotoxins in the absence of potentiator (~$5x10^6$).

Our experiments showed the potentiation of our gelonin immunotoxins by Fn3-cytolysin fusions also exposed their synergy against antigen negative cells. This discovery further motivated us towards the use of delayed dosing *in vivo*. To test the possibility of such an approach, we used a delayed exposure assay in which cells were treated with immunotoxin for a fixed period of time followed by exposure to a potentiating agent after increasing delay times. We found that at low concentrations, a 48 hour delay between exposures was sufficient to abrogate potentiated cytotoxicity, but that at higher concentrations, even on cells expressing low levels of antigen, potentiation was still possible and even potent after the same delay. These experiments suggest that, given a sufficient *in vivo* dose, administration might be delayed by equally long times, which should be sufficient for the first agent to be cleared from the plasma, thereby reducing simultaneous exposure of antigen-negative cells subject to the highest concentrations of either agent.

Notes – This chapter was reproduced in part from Pirie C.M., Liu D.V., Wittrup K.D. (2011) Submitted.

3.6 – Citations

1. Shim, M. S., and Kwon, Y. J. (2010) *FEBS J* **277**, 4814-4827
2. Lares, M. R., Rossi, J. J., and Ouellet, D. L. (2010) *Trends Biotechnol* **28**, 570-579
3. Varkouhi, A. K., Scholte, M., Storm, G., and Haisma, H. J. (2011) *J Control Release* **151**, 220-228

4. Nishikawa, M., Hashida, M., and Takakura, Y. (2009) *Adv. Drug Deliv. Rev* **61**, 319-326

5. Zhao, M., Biswas, A., Hu, B., Joo, K.-I., Wang, P., Gu, Z., and Tang, Y. (2011) *Biomaterials* **32**, 5223-5230

6. Paterson, Y., Guirnalda, P. D., and Wood, L. M. (2010) *Semin. Immunol* **22**, 183-189

7. Foster, S., Duvall, C. L., Crownover, E. F., Hoffman, A. S., and Stayton, P. S. (2010) *Bioconjug. Chem* **21**, 2205-2212

8. Stirpe, F., and Barbieri, L. (1986) *FEBS Lett* **195**, 1-8

9. Kelley, V. E., Bacha, P., Pankewycz, O., Nichols, J. C., Murphy, J. R., and Strom, T. B. (1988) *Proc. Natl. Acad. Sci. U.S.A* **85**, 3980-3984

10. Bjorn, M. J., Groetsema, G., and Scalapino, L. (1986) *Cancer Res* **46**, 3262-3267

11. Seon, B. K. (1984) *Cancer Res* **44**, 259-264

12. Wu, M. (1997) *Br. J. Cancer* **75**, 1347-1355

13. Wu, Y. N., Gadina, M., Tao-Cheng, J. H., and Youle, R. J. (1994) *J. Cell Biol* **125**, 743-753

14. Vitetta, E. S., Cushley, W., and Uhr, J. W. (1983) *Proc. Natl. Acad. Sci. U.S.A* **80**, 6332-6335

15. Greenfield, L., Johnson, V. G., and Youle, R. J. (1987) *Science* **238**, 536-539

16. Goldmacher, V. S., Blättler, W. A., Lambert, J. M., McIntyre, G., and Stewart, J. (1989) *Mol. Pharmacol* **36**, 818-822

17. FitzGerald, D. J., Trowbridge, I. S., Pastan, I., and Willingham, M. C. (1983) *Proc. Natl. Acad. Sci. U.S.A* **80**, 4134-4138

18. Schnupf, P., and Portnoy, D. A. (2007) *Microbes Infect* **9**, 1176-1187

19. Geoffroy, C., Gaillard, J. L., Alouf, J. E., and Berche, P. (1987) *Infect. Immun* **55**, 1641-1646

20. Sun, X., Provoda, C., and Lee, K.-D. (2010) *J Control Release* **148**, 219-225

21. Giles, R. V., Spiller, D. G., Grzybowski, J., Clark, R. E., Nicklin, P., and Tidd, D. M. (1998) *Nucleic Acids Res* **26**, 1567-1575

22. Walev, I., Bhakdi, S. C., Hofmann, F., Djonder, N., Valeva, A., Aktories, K., and Bhakdi, S. (2001) *Proc. Natl. Acad. Sci. U.S.A* **98**, 3185-3190

23. Provoda, C. J., Stier, E. M., and Lee, K.-D. (2003) *J. Biol. Chem* **278**, 35102-35108

24. Bergelt, S., Frost, S., and Lilie, H. (2009) *Protein Sci* **18**, 1210-1220

25. Tweten, R. K. (2005) *Infect. Immun* **73**, 6199-6209

26. Pirie, C. M., Hackel, B. J., Rosenblum, M. G., and Wittrup, K. D. (2011) *J. Biol. Chem* **286**, 4165-4172

27. Geiser, M., Cèbe, R., Drewello, D., and Schmitz, R. (2001) *BioTechniques* **31**, 88-90, 92

28. Kim, Y.-S., Bhandari, R., Cochran, J. R., Kuriyan, J., and Wittrup, K. D. (2006) *Proteins* **62**, 1026-1035

29. Henry, S. M., El-Sayed, M. E. H., Pirie, C. M., Hoffman, A. S., and Stayton, P. S. (2006) *Biomacromolecules* **7**, 2407-2414

30. Chou, T.-C., and Talalay, P. (1983) *Trends in Pharmacological Sciences* **4**, 450-454

31. Chou, T. C., and Talalay, P. (1984) *Adv. Enzyme Regul* **22**, 27-55

32. Yan, H., Zhang, B., Li, S., and Zhao, Q. (2010) *BMC Syst Biol* **4**, 50

33. Webb, J. (1963) in *Enzyme and Metabolic Inhibitors* pp. 55-79 [online] New York: Academic Press.

34. Jones, S., and Portnoy, D. A. (1994) *Infect. Immun* **62**, 5608-5613

35. Xing, Y., Smith, A. M., Agrawal, A., Ruan, G., and Nie, S. (2006) *Int J Nanomedicine* **1**, 473-481

36. Mayor, S., and Pagano, R. E. (2007) *Nat. Rev. Mol. Cell Biol* **8**, 603-612

Chapter 4 – Pharmacokinetics and *in vivo* efficacy

4.1 - Abstract

There are an extensive number of *in vitro* assays available for characterization of biotherapeutics, but there remains a set of critical pharmacokinetic traits that are best, if not exclusively, determined by *in vivo* experimentation. We undertook a rigorous assessment of the *in vivo* characteristics and therapeutic potential of our independently-targeted intracellular delivery system. Maximum tolerated dose escalation was performed for each drug, with CEA-targeted C7rGel showing no limitations up to 16 mg/kg, and EGFR-targeted cytolysins E6LLO and E6PFO having maximum doses of 0.6 mg/kg and 0.2 mg/kg respectively. The same therapeutics were rapidly cleared with from the plasma: all agents had α-phase half-lives from 30-120 minutes and ß-phase half-lives around 12 hours. These rates are consistent with gelonin immunotoxin being cleared primarily by the liver and cytolysin fusions being cleared primarily by the liver. We found that based on *in vivo* imaging data and minimum dose separation experiments that a 6 hour separation between immunotoxin and potentiator doses was optimal. Subcutaneous tumor xenograft growth was inhibited and in fact regressed when treated with our therapeutic combination. *in vivo* validation of this system further supports the clinical potential of this approach. Future work should reveal whether this system can be applied to alternative active biotherapeutics other than a plant toxin.

4.2 – Introduction

Murine models of cancer have become standard practice in the progressive assessment of promising therapeutics (1). Morevoer, the tumor xenograft model in which human cancer cells are implanted into an immune compromised mouse has been used consistently in pre-clinical development of new oncology drugs (2). As scientific understanding of the complexity of biology continues to improve alongside our ability to capture it through mathematical models, someday mouse models may be replaced by computational models with better predictive capability for clinical success. But until then we will continue to test new therapeutic strategies with existing tools.

Tumor xenografts are the most common tool for *in vivo* testing of immunotoxin efficacy. By selecting appropriate cell lines expressing the target antigen, a wide array of immunotoxins can be tested (3-5). However, variations in growth rate, mutation rate, and other phenotypes can drastically alter the robustness of any xenograft study. Furthermore, the field lacks a consistent standard with respect to beginning xenograft size or treatment regimen, making it exceedingly difficult to compare the relative efficacy of immunotoxins in different studies. Some of the key points to a rigorous xenograft experiment are addressed by Seigall in his 1994 review (6): pointing out that vascularization is a key parameter, suggesting that tumors between 50 and 100 mm^3 are appropriate, and emphasizing that treatment should be initiated not concurrent to tumor cell implantation but rather sometime after the tumor has become established and vascularized. As

many oncology drugs showing pre-clinical efficacy continue to fail in late-stage trials, drug developers have focused on the fact that in xenografts tumor growth inhibition is a necessary but not sufficient measure of success, instead, tumor regression is the more relevant marker (7).

In recent years our group has become increasingly advanced in our use of mouse models ranging from adoptive T-cells (8) to an array of different xenografts (9, 10). Xenografts have been effective at allowing us to assess the pre-clinical efficacy of various therapeutic modalities as well as the predictive or informative powers of our pharmacokinetic biodistribution and tumor targeting models. We've utilized that experience to interrogate the pharmacokinetics and *in vivo* efficacy of our independently targeted intracellular delivery system to potentiate immunotoxin activity against tumor xenografts.

4.3 – Methods

4.3.1 – in vivo model system

All *in vivo* studies used 6-8 week old athymic N_{cr} (nu/nu) nude mice obtained from Taconic (Hudson, NY). This is the standard model for National Cancer Institute studies and many pharmaceutical and oncology screening programs. Their outbred background originates from BALB/c and NIH(s) stocks.

4.3.2 – *Large scale protein expression*

Protein production required for *in vivo* experiments was accomplished using the same protocol executed at 2L and 10L scales in Bioflo bioreactors (New Brunswick Scientific, Edison, NJ) with oxygen control supplied by filtered air at 0.5 (vvm) and agitation adjusted to maintain dissolved oxygen levels above 30%. pH was controlled at 7.0 using 6N NaOH. Cells were grown to OD600 = 0.8 before induction as before. Purification was carried out as described previously.

4.3.2 – Dose escalation

Dose escalation was carried out for all *in vivo* applied fusion proteins using the canonical "3+3 method" in which 3 mice are dosed at a particular concentration and if no dose limiting toxicity is observed then the dose is raised, if one of three mice exhibit limiting toxicity then a new cohort of three mice are treated at the same dose, and if two or more mice show limiting toxicity then escalation is stopped and the previous dose is deemed the maximum tolerated dose. Here, in the absence of any informed basis on which to select a starting dose, a logarithmically spaced escalation was employed where after limiting toxicity was observed a linear escalation was continued from the last tolerated dose.

4.3.3 – Plasma clearance

Fusion proteins were labeled with Li-Cor 800CW dye (Li-Cor Biosciences, Lincoln, NE) by N-hydroxyl succinimide ester reaction with free amine groups. Labeled

proteins were injected at their respective maximum tolerated doses into three mice and blood samples taken at logarithmically spaced time points by tail clipping. Blood was collected into heparin coated capillary tubes and imaged on a Li-Cor Odyssey Imaging System (LiCor Biosciences). Imaging sensitivity was adjusted so as to maximize signal-to-noise ratio without saturating the fluorescence channel. Fluorescent signals were averaged across mice at each time point and fitted with a bi-exponential function for retro-orbital injections and with a tri-exponential for intraperitoneal injections to determining absorption and clearance constants as well as plasma half-lives.

4.3.4 – Dose separation

Using clearance information as a basis we applied the same "3+3 method" as for dose escalation to determine the minimum separation time between doses. Gelonin immunotoxin was dosed first by retro-orbital injection at its independent maximum tolerated dose. After the defined amount of time targeted cytolysin was dosed at its own independent maximum tolerated dose either by retro-orbital injection in the opposite eye or by intraperitoneal injection. Mice were monitored for toxicity for 72 hours following the second injection.

4.3.5 – IVIS Imaging

Therapeutic proteins C7rGel and E6LLO were labeled with the near-infrared fluorophores Dylight 680 and Dylight 800 (Thermo Scientific, Rockland, IL),

respectively, according to the manufacturers' instructions. Maximum tolerated doses of both proteins were administered by retro-orbital injection at a separation time of 24 hours. While under anesthesia, HT-29 tumor bearing mice were imaged periodically on an IVIS 200 Imaging System (Caliper Life Sciences, Hopkinton, MA) across a range of excitation and emission bandwidths to allow for spectral deconvolution. Images were taken with greater frequency immediately following each injection. Mice with variable tumor sizes were used to account for differences in the size of the antigen sink provided by the tumor. Regions of interest were drawn around tumors and opposing flanks without tumors and radiant efficiency (photons/cm^2/sec) was used to quantify the relative amount of each drug in the tumor versus elsewhere in the mice.

4.3.6 – Tumor xenograft growth inhibition

Mice received subcutaneous injections of $3x10^6$ HT-29 cells in the right flank on day 0. Digital caliper measurements to determine tumor volume were begun on day 7 and taken every other day for the duration of the study. On day 7 measurements were used to divide mice into treatment groups to balance the average tumor volume for each group. Four groups were used: phosphate buffered saline (PBS)/PBS, C7rGel/PBS, PBS/E6PFO, and C7rGel/E6PFO as primary/secondary respectively. Treatments in the study were given on day 7 and 11 with 3 hour and 6 hour separations between primary retro-orbital injection and secondary intraperitoneal injection.

4.3.7 – Histology and immunofluorescent staining

At various time points, mice were euthanized and their HT-29 xenografts removed. Tumors were then frozen in plastic cartridges filled with Tissue-Tek O.C.T. Compound (Sakura Finetek USA, Torrance, CA). To freeze at the appropriate rate, cartridges containing freezing compound and a suspended tumor xenograft were placed in a bath of 2-methylbutane (Sigma-Aldrich, St. Louis, MO) which was then placed in a bath of liquid nitrogen until the freezing compound turned an opaque white. Cartridges were store at -80 °C until sectioned into 8 μm slices at the Koch Institute Swanson Biotechnology Center. Haematoxylin and eosin (H&E) staining was also performed by the Center and unstained slides containing tumor sections were provided and used for immunofluorescent staining. H&E images were taken by a digital camera adapted to a Zeiss Axiovert 40c with a 20x lens.

To stain, frozen slides were thawed for 30 min at room temperature. A pap pen was used to draw a border around the entire slide. Cells were fixed with a 5% formalin solution in phosphate buffered saline (PBS) for 10 min. Slides were then washed repeatedly with PBS. A blocking solution of 5% goat serum in PBS was applied to the cells for 1 hr. Primary antibodies against either CD-31 (BD Biosciences, Franlin Lakes, NJ), a vascular marker, and/or cleaved caspase-3 (Cell Signaling Technology, Danvers, MA), an apoptosis marker, were diluted 1:100 in PBS with 5% goat serum and incubated on slides overnight at 4 °C. Again cells were washed repeatedly with PBS and then secondary antibodies specific to the species of the respective primary antibodies were diluted 1:200 in PBS with 0.1%

Tween 20 detergent and incubated for 1 hr at room temperature. More PBS washes were conducted before slides were mounted with Vectashield Mounting Medium with DAPI (Vector Laboratories, Burlingame, CA) and a coverslip then sealed with clear nail polish. Images were taken under 10x or 60x magnification on an inverted Olympus X71 Deltavision deconvolution microscope.

4.4 – Results

4.4.1 – Independent dosing and clearance

Nude mice were dosed by the "3+3 method" with increasing amounts of either gelonin or cytolysin immunotoxins until dose limiting toxicity was observed. For CEA-targeted C7rGel no substantial toxicity was observed up to doses of 16 mg/kg while for E6LLO and E6PFO dose limiting toxicities were reached above 0.6 and 0.2 mg/kg respectively (Table 4.1).

We evaluated plasma half-lives of our therapeutic proteins to better inform dose separation. Bi-exponential fitting of protein clearance data from retro-orbital injections yielded alpha-phase half-lives and beta-phase half-lives of 30 minutes and 12.2 hours for C7rGel, 124 minutes and 11.5 hours for E6LLO, and 34 minutes and 13.3 hours for E6PFO. Tri-exponential fitting of data from intraperitoneal injections revealed a plasma absorption half-time of 65 minutes. Examples of clearance data and curve fitting results are provided (Figure 4.1)

C7rGel Dose (mg/kg)	Morbidity	E6LLO Dose (mg/kg)	Morbidity	E6PFO Dose (mg/kg)	Morbidity
0.2	0/3	0.02	0/3	0.02	0/3
0.8	0/3	0.08	0/3	0.08	0/3
2	0/3	0.2	0/3	0.2	0/3
8	0/3	0.8	2/3	0.8	3/3
12	0/3	0.4	0/3	0.4	2/3
16	0/3	0.6	0/3	-	-

Table 4.1 – Independent dose escalation of therapeutic proteins. The "3+3 method" was used to assess dose limiting toxicities as each agent to be used for *in vivo* testing was administered at increasing levels. We found that for C7rGel substantial doses could be given without toxicity but that for E6LLO and E6PFO the maximum tolerated dose was less than 1 mg/kg.

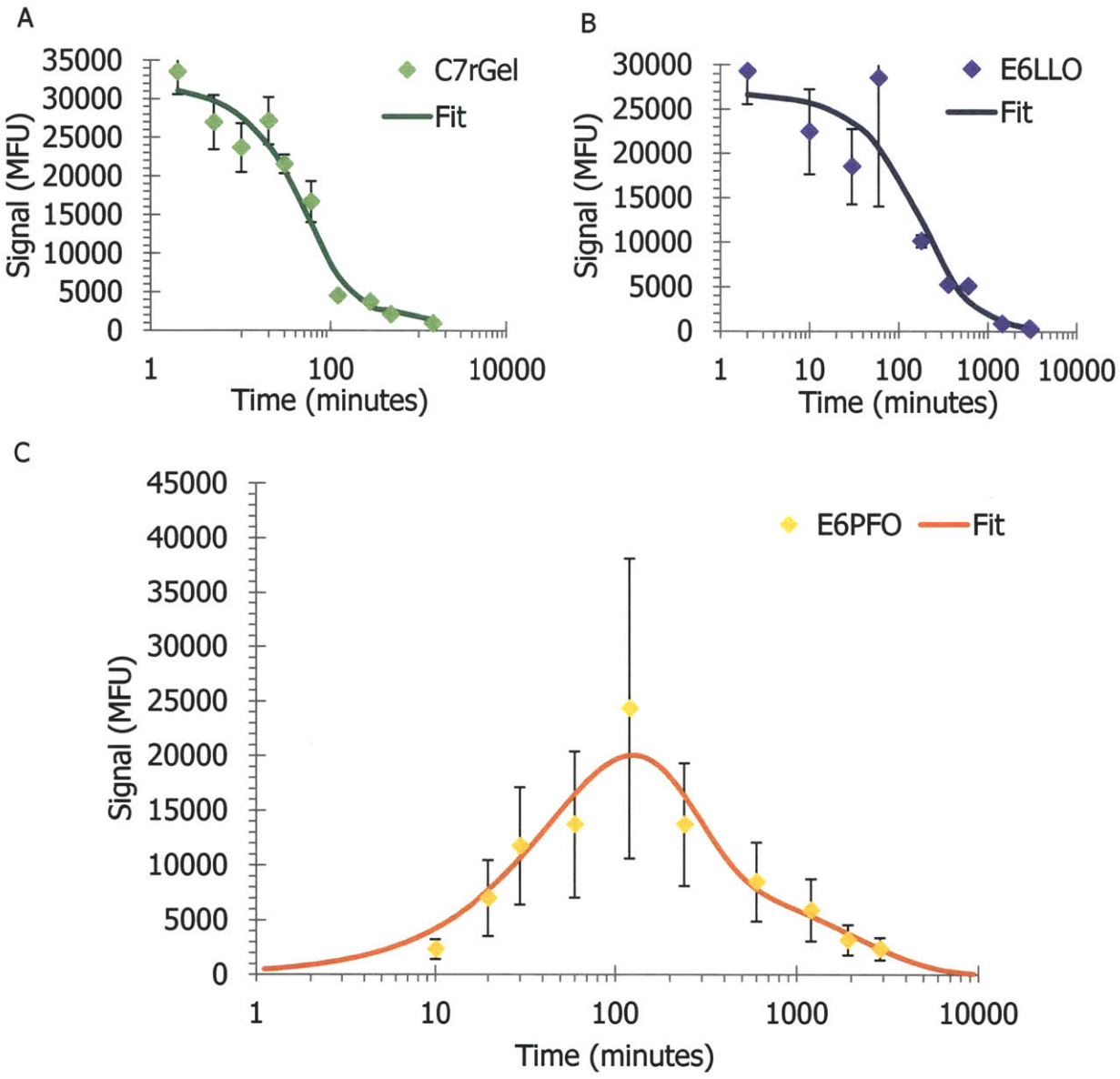

Figure 4.1 – Plasma clearance of immunotoxin and potentiators. Proteins used for *in vivo* testing were labeled with infra-red dye and injected into groups of three mice. Blood samples were collected at logarithmically spaced time points from the tail. (A) C7rGel injected retro-orbitally. (B) E6LLO injected retro-orbitally. (C) E6PFO injected intraperitoneally.

4.4.2 – Biodistribution and tumor targeting

Near-infrared imaging of mice allowed us to track the biodistribution and clearance mechanism of both C7rGel and E6PFO. Images taken within the first 8 hours following retro-orbital injection of C7rGel exemplified the primary renal clearance of the ~40 kDa therapeutic. At later time points the liver and bladder also showed elevated levels of the gelonin immunotoxin. Data from region of interest analysis show that the maximum fluorescent signal in the tumor is achieved between 20 and 60 minutes after injection (Figure 4.2A). Tumor fluorescence signals were divided by radiant efficiency data from an identical region on the opposite flank giving a tumor to skin ratio. In contrast to the direct tumor signal, the ratio was highest approximately 4 hours after the injection, likely due to the more rapid clearance of the therapeutic from the plasma compared to the tumor (Figure 4.2B).

Whole animal images were taken 8 hours following injection of labeled gelonin immunotoxin show distinct tumor localization dependent on tumor volume (Figure 4.3A). Two hours after injection of labeled, targeted cytolysin we observed strong signal from the liver implicating it as the primary clearance organ but fail to mimic the differentiable tumor retention of C7rGel (Figure 4.3B).

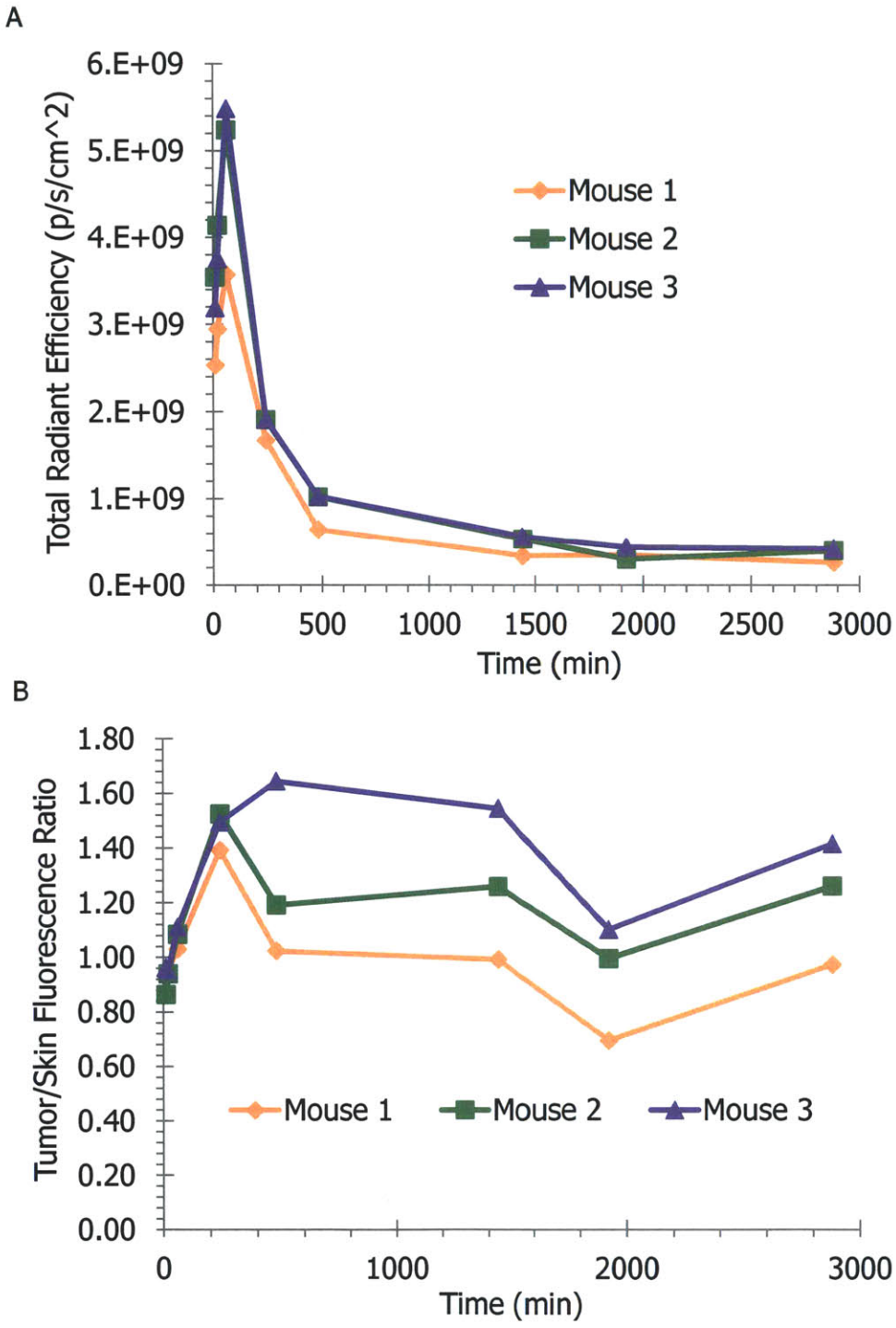

Figure 4.2 – IVIS imaged tumor accumulation of gelonin immunotoxin. (A) Total radiant efficiency from regions of interest drawn around tumors. (B) Time dependent ratio of radiant efficiency from tumors and opposing flank.

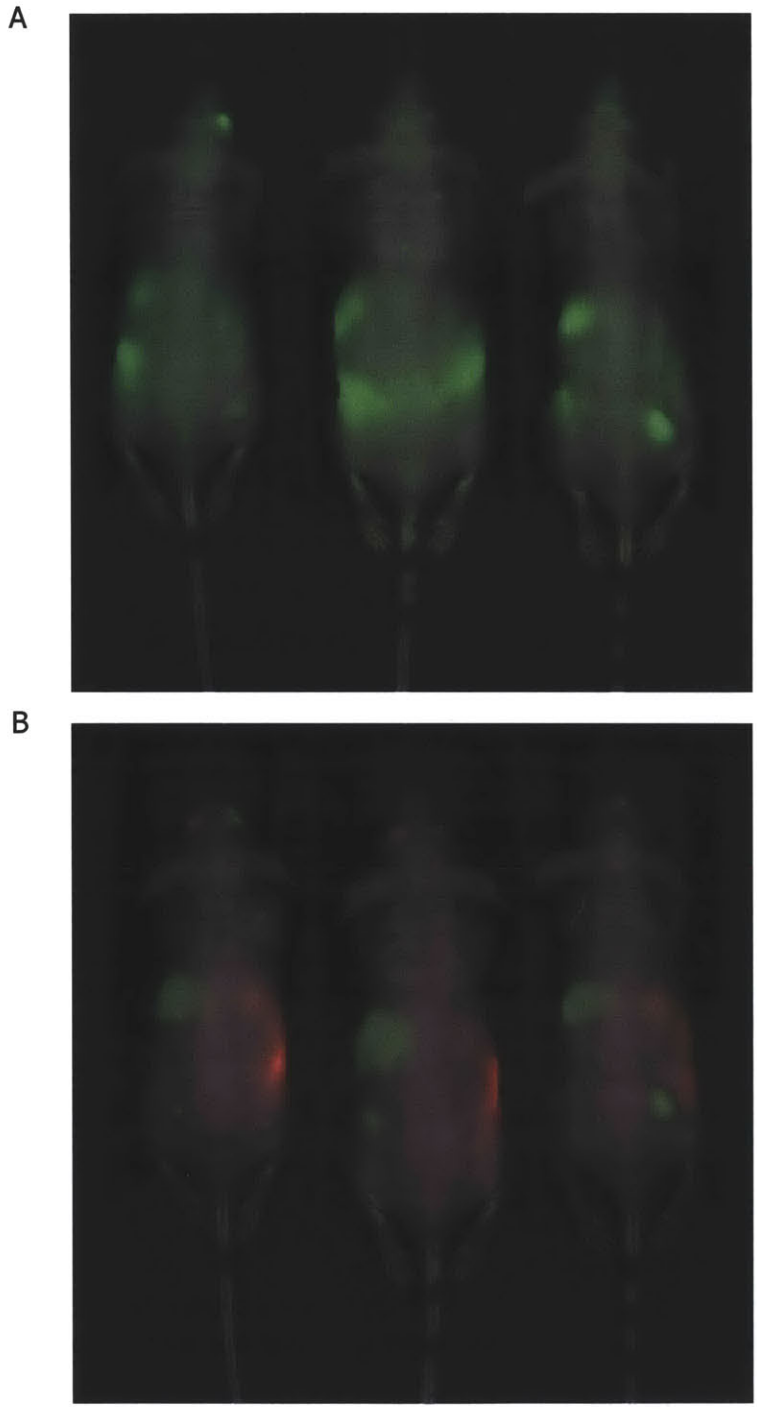

Figure 4.3 – Spectral deconvolution of IVIS images. (A) Dylight 680 labeled C7rGel biodistribution 8 hours after retro-orbital injection. Primary signal areas are injection sites, tumors (right flank), and what is likely the gallbladder. (B) Images taken 2 hours after injection of Dylight 800 labeled E6PFO show a similar distribution of C7rGel but a lack of tumor localization of the targeted cytolysin and primary liver clearance.

4.4.3 – Combination treatment of tumor xenografts.

Dual agent treatment was performed initially with retro-orbital injection of both agents with C7rGel injected first and E6LLO or E6PFO injected second. We shrank separation time linearly, again using the "3+3 method" until dose separation limiting toxicity was observed. Results indicated that when using this route of administration E6LLO could only be dose no sooner than 12 hours after C7rGel injection and the minimum delay with E6PFO was 24 hours (Table 4.2). Based on these limitations and our understanding of the clearance rate of C7rGel, we investigated the possibility of intraperitoneal injection of targeted cytolysins secondary to injection of gelonin immunotoxin. We hoped that like injection of other protein therapeutics into the peritoneal cavity we might be able to achieve a more gradual uptake into the plasma while gelonin immunotoxins were still residing in the tumor (11). When administering C7rGel by retro-orbital injection followed by intraperitoneal injection of targeted cytolysin we found that E6LLO and E6PFO doses could follow as little as 6 hours after (Table 4.2).

	Dose Separation Time (hours) – Morbidity				
RO C7rGel + RO E6LLO	24 – 0/3	18 – 0/3	12 – 0/3	6 – 3/3	-
RO C7rGel + RO E6PFO	24 – 0/3	18 – 2/3	-	-	-
RO C7rGel + IP E6LLO	-	-	-	6 – 0/3	3 – 1/3
RO C7rGel + IP E6PFO	24 – 0/3	18 – 0/3	12 – 0/3	6 – 0/3	3 – 2/3

RO = Retro-orbital
IP = Intraperitoneal

Table 4.2 – Determining minimum delay between doses of synergistic agents. When administering by retro-orbital injection which results in an almost instantaneous maximum plasma concentration we found that subsequent doses required at least a 12 hour delay. Alternatively when we administered secondary injections of targeted cytolysins into the peritoneal cavity where absorption into the plasma was slowed, we found that doses could be given with as little as 3 hours delay.

Once we had determined the maximum tolerated dose and minimum dose separation time we used these to test for efficacy in a tumor xenograft model. Nude mice bearing established HT-29 colorectal carcinoma xenografts were dosed with PBS & PBS, C7rGel & PBS, PBS & E6PFO, or C7rGel & E6PFO. Control groups were run in parallel to confirm that neither C7rGel, nor E6PFO alone could control tumor growth. Individual therapeutic treatments resulted in no reduction in the logarithmic growth rate of the xenografts, and no statistically significant difference between mean tumor volumes (Figure 4.4).

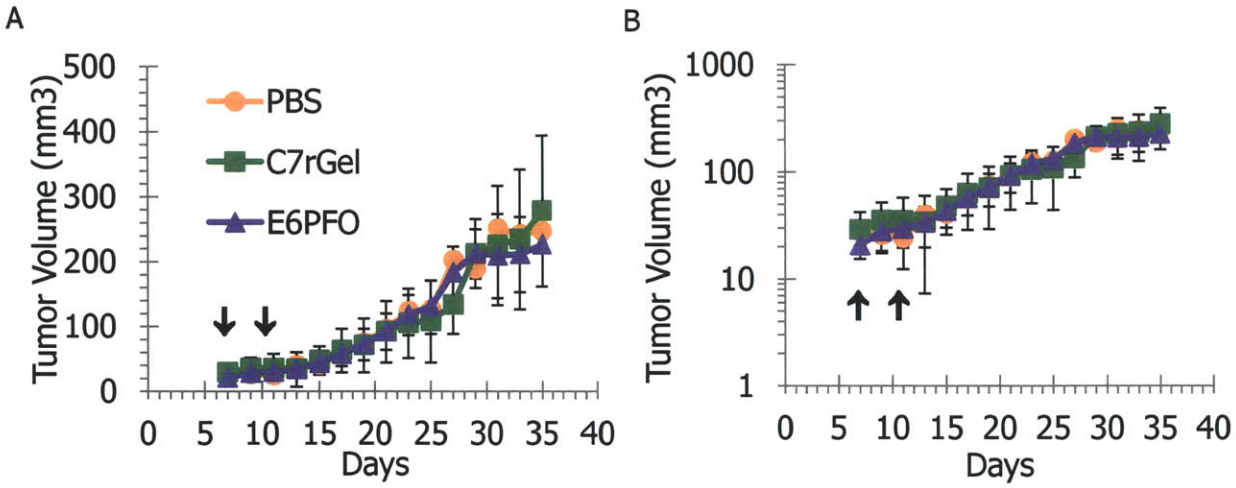

Figure 4.4 – Individual therapeutic tumor control impotency. C7rGel or E6PFO dosed twice at their respective maximum tolerated dose was incapable of controlling tumor growth when compared to a PBS control group growth. Legend applies to both plots. (A) Tumor volume measurements over the course of the study and (B) a semi-log representation of the data to convey logarithmic growth rate.

In contrast, when we dosed mice with a retro-orbital injection of C7rGel and an intraperitoneal injection of E6PFO separated by 3 hours on day 7 and 6 hours on day 11, we observed a statistically significant reduction in tumor volume and growth rate (Figure 4.5A/B). Unfortunately, one of three mice had to be sacrificed at day 13 due to treatment related morbidity, but we did attain a durable response in one of the two remaining mice (Figure 4.5C). Recurrent rounds of treatment appear to have had a cumulative toxicity effect not observed in preliminary dose limiting experiments. Repeated measures ANOVA of PBS versus combination treatments yield a P-value of 0.053 and an F-value of 9.71.

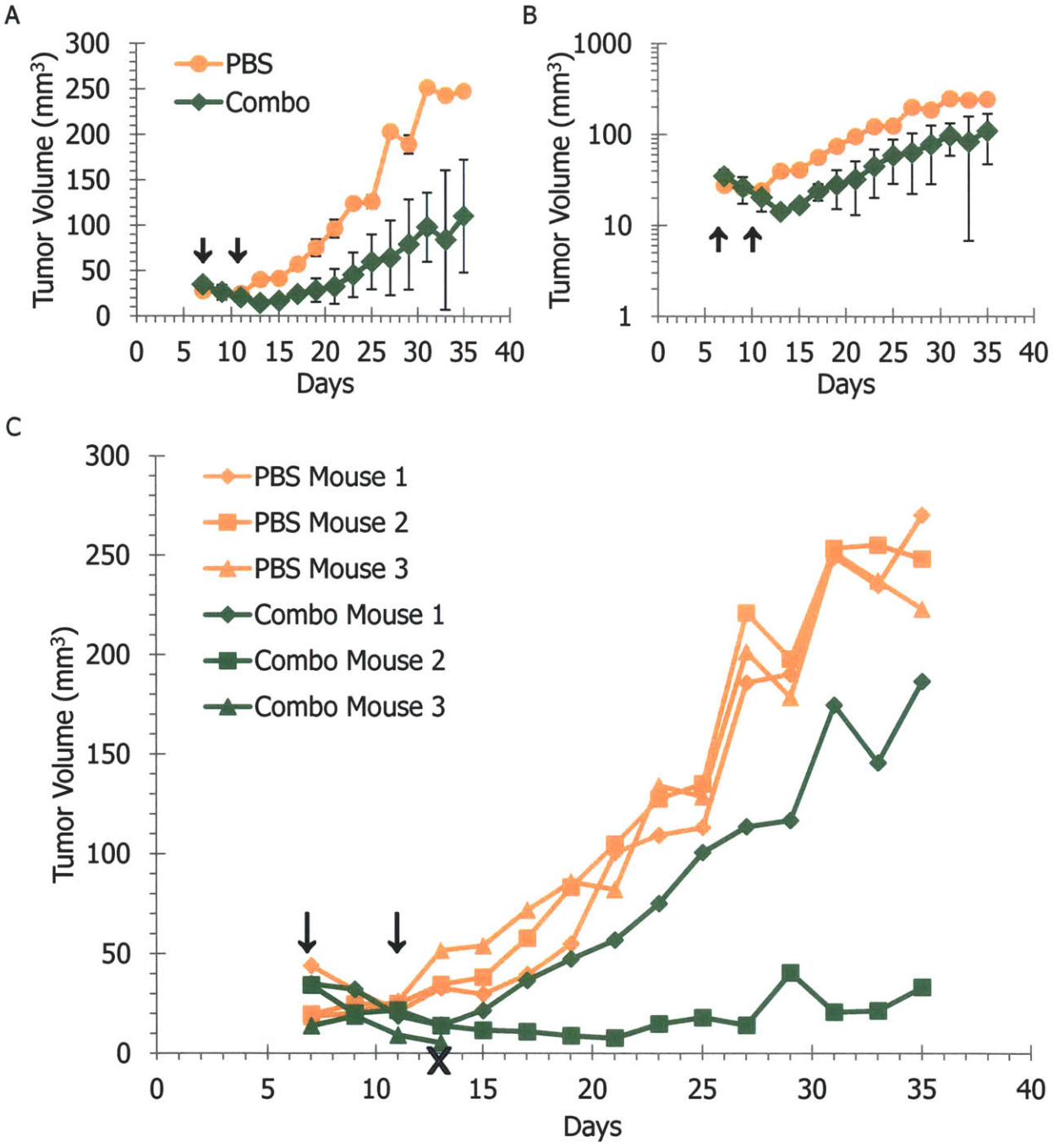

Figure 4.5 – Synergistic combination therapy. Treatment with our therapeutic combination resulted in (A) a reduction of the average tumor volume and during treatment; (B) tumor growth rate is not just stabilized, but in fact showed regression.(C) The growth curves of individual mice in each group are very consistent for PBS treated mice, but treatment related toxicity and inconsistent responses across the combination group cause the large error observed.

Histological analysis of control and treated tumors are rather remarkable. H&E images show distinctive loss of healthy morphology and gross physiological changes compared to untreated tumor samples (Figure 4.6). Tumors were excised 24 hours after initial injection. Sections from the same tissue sample were labeled by immunofluorescence for the apoptosis marker cleaved caspase-3 and images showed strong cellular staining (Figure 4.7A). When mice given injections of fluorescently labeled immunotoxin and cytolysin fusion under standard dosing conditions were euthanized 2 hours after cytolysin injection, tumor immunofluorescence indicated the continued presence of both agents in capillaries, colocalizing with a CD31 stain, while also showing strong cellular association and combined colocalization measured by a strong Pearson's coefficient.

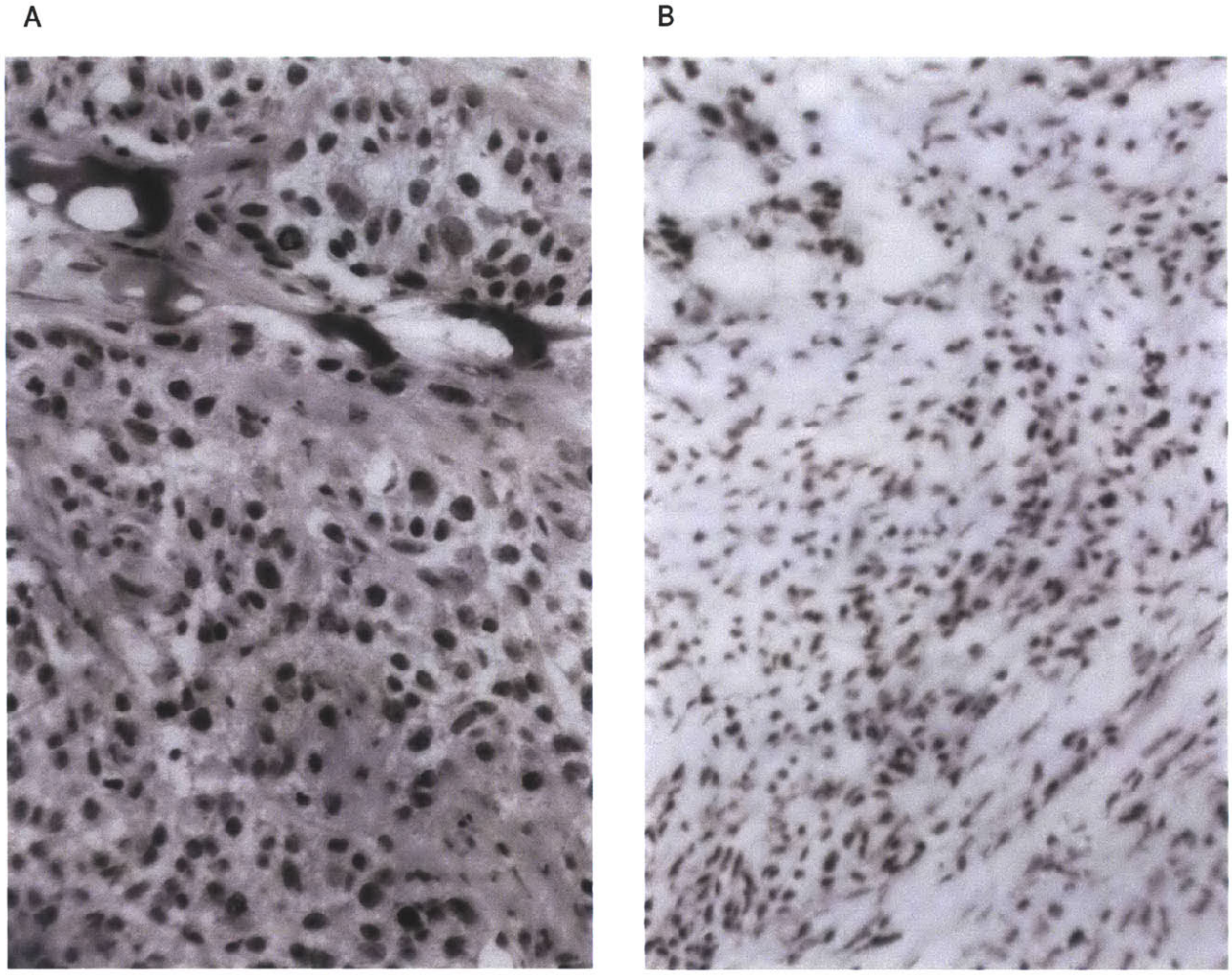

Figure 4.6 – HT-29 xenograft H&E staining. (A) Healthy tumor cells treated with PBS display good cell-cell connections, large nuclei, and blood vessels. (B) Tumor cells treated with C7rGel and E6PFO have classical apoptotic phenotypes with rounded morphology and DNA condensation (small nuclei). Fragmentation is difficult to observe at this magnification.

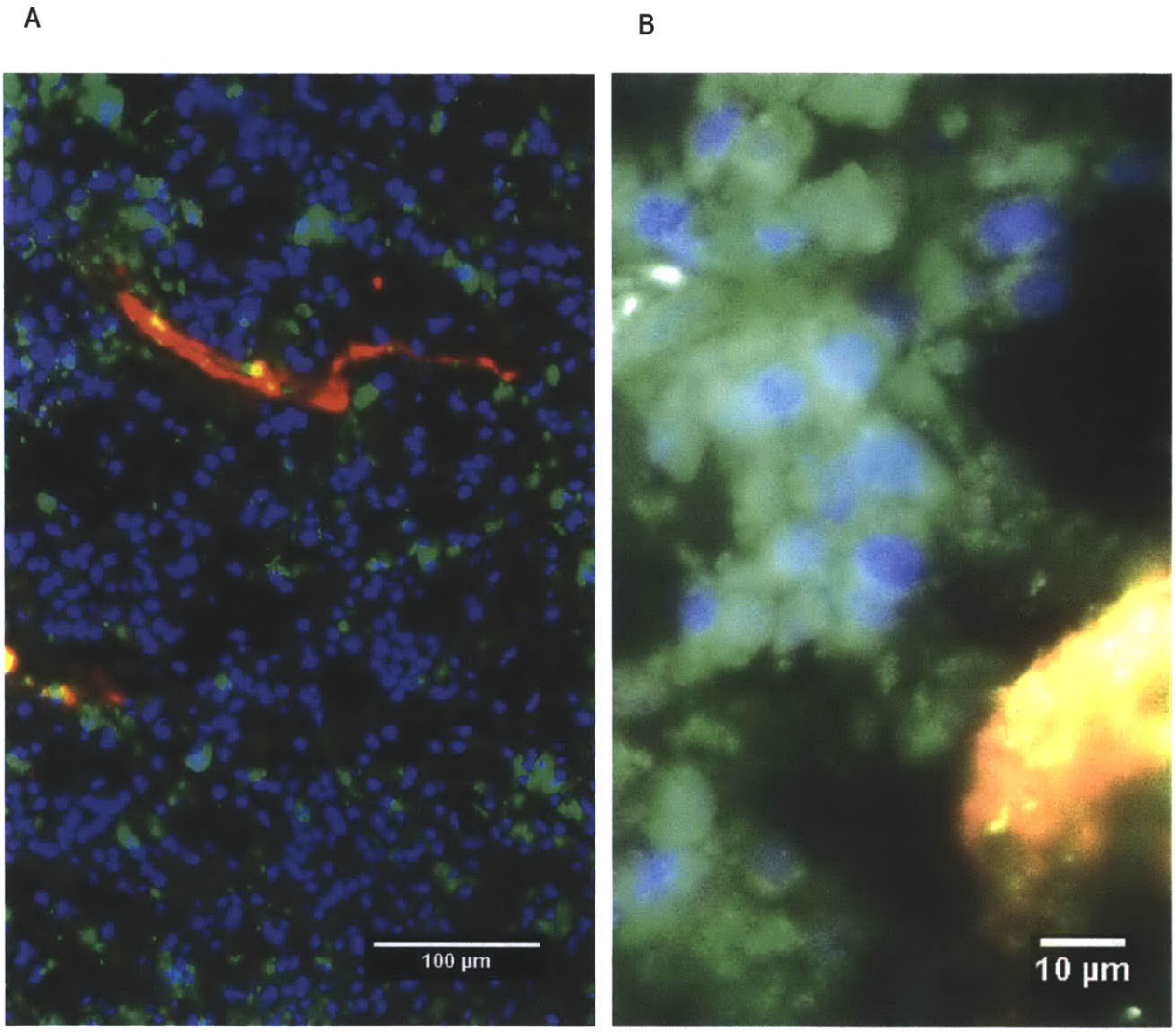

Figure 4.7 – Immunofluorescence of apoptosis and dual agent exposure. (A) Two-color fluorescence of apoptotic marker cleaved caspase-3 (green) and capillary endothelial marker CD31 (red) under 10x magnification. The majority of tumor cells show strong apoptotic signal. (B) Four-color fluorescence of CD31 (red), nuclear staining with DAPI (blue), Alexa Fluor 647 labeled C7rGel (white), and Alexa Fluor 488 labeled E6PFO (green) under 60x magnification.

4.5 – Discussion

The canonical progression from therapeutic development to clinical trials is based on pre-clinical studies in animal models that move from mice to a non-human primate. And while many drugs that show early success *in vivo* fail at various points in the process thereafter, this is still the standard approach. Here, we've taken the first steps towards proving the clinical potential of our independently targeted intracellular delivery system.

Results of independent therapeutic dose escalation were consistent with our expectations as informed by *in vitro* studies and historical use of these same agents *in vivo*. Rosenblum *et al.* dosed scFv-gelonin as high as 20 mg/kg (12), Geoffroy *et al.* found the 50% lethal dose of LLO to be 0.027 mg/kg (13), and it has been shown that PFO has the same specific activity as LLO but without any time-dependent inactivation at neutral pH suggesting that it's MTD should be lower (14). It was this inactivation property that urged us towards the use of PFO fusions for our preliminary tumor xenograft experiments because we were concerned that E6LLO would be inactivated at the neutral pH of the plasma before reaching the tumor, binding, and internalizing. The relative dosing limits found here are consistent with the *in vitro* and *in vivo* work of others with these proteins, even if their absolute values differ somewhat. Those differences may be attributable to difference in molecular weight of our targeted fusion proteins (when considering mg/kg) or possible destabilization of the native cytolysin folding resulting from

incorporation in the fusion construct similar to that observed for the binding of our Fn3's and scFv's or the toxicity of gelonin in fusions.

Differences in plasma clearance rates between fusion proteins correlated with molecular weight as expected for C7rGel and E6LLO, but for E6PFO we measured a much more rapid clearance rate that may be due to interactions with circulating cell or endothelial cell membranes leading to active clearance beyond normal filtration or hepatocellular uptake. Using intraperitoneal injection as an alternative to retro-orbital injection and as a way to control plasma uptake, E6PFO was able to intravasate, but it is difficult to assess from these data precisely what percentage of IP dose becomes bioavailable. Both absolute dose and the volume of injection will likely play a part in the degree of bioavailability (11) adding yet another variable that should be optimized as this therapeutic approach is further developed.

IVIS imaging was utilized as one way to address whether both agents were capable of being localized and retained in tumor xenografts. In these experiments fluorescently labeled C7rGel localized to tumors and was retained there longer than in naïve, non-specific tissues. However we were unable to show any tumor-specific localization or retention of E6PFO. It is possible that this is a result of the drastically lower dose of E6PFO relative to C7rGel not generating a strong enough signal (~100x molar difference in dose) although the primary clearance organ does produce a strong signal even at this dose.

When shrinking the separation time between doses, minimum separation times for retro-orbital injection of both agents correlated with the potency of the

respective targeted cytolysin. Intraperitoneal injection of targeted cytolysin allowed for shorter separation times, likely attributable to the slower time to maximum plasma concentration and perhaps lower overall bioavailability. Interestingly, the minimum delay for either cytolysin fusion by this administration route was the same despite their differences in independent potency and toxicity.

One of the primary motivations for developing this therapeutic approach was the inability of our immunotoxins targeted against either carcinoembryonic antigen or epidermal growth factor receptor to mediate antigen-dependent cytotoxicity against the HT-29 cell line *in vitro*. Thus it is not surprising that, even when given at quite a high dose, C7rGel is unable to inhibit tumor growth in a xenograft model using the same cells. The result is also consistent with predictions made in our pharmacokinetic model (Chapter 5) with respect to the number of internalized immunotoxin molecules relative to the previously defined threshold for induction of apoptosis (Chapter 2). From a clinical perspective, not all tumors that over express a particular antigen will do so at a level necessary for independent activity of immunotoxin, therefore a system that can induce targeted cytotoxicity against cells expressing tumor antigens at only modest levels is desirable.

The high toxicity of E6PFO might be expected to yield some independent tumor xenograft control, but our results show that it does not. This might be due again to a loss of significant amounts of the dosed material to non-specific membrane interactions. It is clear that at least a minimally potentiating concentration of targeted cytolysin does reach the tumor because of the significant

synergistic activity observed in combination as controlling of tumor xenograft growth. Despite the mixed results of tumor xenograft control, we are encourage by the follow up histology which showed that combination treated tumors resulted in colocalization of both therapeutics in the tumor interstitium and induction of widespread apoptosis. Anecdotally, we observed that induction of apoptosis depended on the size of the tumor being treated. These very preliminary *in vivo* therapeutic efficacy experiments provide a hint of the potential of this approach but also serve to emphasize the substantial amount of work that remains to be done to fully harness that potential.

Notes – This chapter was inspired by Pirie C.M., Liu D.V., Wittrup K.D. (2011) Submitted

4.6 – Citations

1. Cheon, D.-J., and Orsulic, S. (2011) *Annu Rev Pathol* **6**, 95-119
2. Troiani, T., Schettino, C., Martinelli, E., Morgillo, F., Tortora, G., and Ciardiello, F. (2008) *Crit. Rev. Oncol. Hematol* **65**, 200-211
3. Cao, Y., Marks, J. D., Marks, J. W., Cheung, L. H., Kim, S., and Rosenblum, M. G. (2009) *Cancer Res* **69**, 8987-8995
4. Zhou, X.-X., Ji, F., Zhao, J.-L., Cheng, L.-F., and Xu, C.-F. (2010) *J. Gastroenterol. Hepatol* **25**, 1266-1275
5. Kuroda, K., Liu, H., Kim, S., Guo, M., Navarro, V., and Bander, N. H. (2010) *Prostate* **70**, 1286-1294
6. Siegall, C. B. (1994) *Cancer* **74**, 1006-1012

7. Mallon, R., Feldberg, L. R., Lucas, J., Chaudhary, I., Dehnhardt, C., Santos, E. D., Chen, Z., dos Santos, O., Ayral-Kaloustian, S., Venkatesan, A., and Hollander, I. (2011) *Clin. Cancer Res* **17**, 3193-3203

8. Higham, E. M., Shen, C.-H., Wittrup, K. D., and Chen, J. (2010) *J. Immunol* **184**, 5954-5958

9. Orcutt, K. D., Slusarczyk, A. L., Cieslewicz, M., Ruiz-Yi, B., Bhushan, K. R., Frangioni, J. V., and Wittrup, K. D. (2011) *Nucl. Med. Biol* **38**, 223-233

10. Schmidt, M. M., and Wittrup, K. D. (2009) *Mol. Cancer Ther* **8**, 2861-2871

11. Barrett, J. S., Wagner, J. G., Fisher, S. J., and Wahl, R. L. (1991) *Cancer Res* **51**, 3434-3444

12. Rosenblum, M. G., Cheung, L. H., Liu, Y., and Marks, J. W. (2003) *Cancer Res* **63**, 3995-4002

13. Geoffroy, C., Gaillard, J. L., Alouf, J. E., and Berche, P. (1987) *Infect. Immun* **55**, 1641-1646

14. Portnoy, D. A., Tweten, R. K., Kehoe, M., and Bielecki, J. (1992) *Infect. Immun* **60**, 2710-2717

Chapter 5 – Pharmacokinetic modeling of combination therapy

5.1 - Abstract

Use of computational models can provide insight into complex biological systems. Here we use a two-compartment deterministic model to address the difficulty of simultaneously monitoring the multitude of variables that might be present in a particular *in vivo* experiment. Pharmacokinetic parameters were used as inputs and the time dependent levels of numerous molecular species or complexes of interest were tracked. Exposure of the tumor compartment to immunotoxin was simulated and depended on the dose separation time and route of administration of potentiating agent. Tumor overlap exposure varied by as much as 20% under different dose limiting conditions *in vivo*. At toxicity limited doses of immunotoxin, endothelial cell internalization does not appear to be a source of toxicity and depending on the average separation between capillaries in the tumor, the average tumor cell internalizes only enough immunotoxin to overcome the potentiated threshold for apoptosis. These results support particular dosing regimens for future *in vivo* studies and provide insight into the possible sources of dose limiting toxicity for gelonin immunotoxins.

5.2 - Introduction

Mathematical modeling continues to gain traction in the biological sciences, where its uses range from structural protein-protein interaction models (1) to cellular level systems modeling (2, 3) to physiological models of pharmacokinetics (4, 5). As this trend develops we may begin to see more and more experimental effort replaced by validated models with reliable predictive capabilities. In fact, the FDA has even begun accepting model based data to accompany, and in some cases replace, pre-clinical data (6, 7). Compartmental models, consisting of well-mixed "compartments" representing organs or tissues of the body can be useful for simplification of the otherwise complex process of biodistribution. When an agent's movement into and out of a compartment is defined by kinetic rate parameters, then the instantaneous or time dependent amount of that agent in each compartment can be calculated.

Others have used mathematical models to investigate immunotoxin properties on both physiological and cellular scales. One of the earliest examples is Sung *et al.* who modeled the tumor distribution and cell surface binding of blocked diphtheria toxin and a transferrin receptor binding antibody based immunotoxin thereof (8). Much of the related work has been done in the Murphy Lab at the University of Wisconsin. For almost a decade their studies addressed immunotoxin binding, internalization, and translocation not unlike our own initial work (Chapter 2) and their models predicted translocation kinetics that were supportive of our experimental results (9-12). The most recent model developed by Chen *et al.*

combines tumor distribution and cellular kinetics resulting in model predictions of tumor xenograft growth inhibition (13).

Ideally, a model describing the dosing, pharmacokinetics, and tumor biodistribution of two independently targeted protein therapeutics would inform *in vivo* experiments to eliminate much of the costs associated with such work (namely animal life). But the complexities of *in vivo* systems are such that it can be quite difficult to execute representative *in vitro* experiments the results of which can be used to validate and support model outputs. As we strove to characterize the fibronectin targeted fusion proteins to gelonin and cholesterol-dependent cytolysins, we lacked appropriate *in vitro* systems to address or even query limits of *in vivo* toxicity or putative efficacy. In this modeling work we focused on the same set of therapeutics that we used for *in vivo* efficacy experiments. These therapeutics consisted of a primary treatment of carcinoembryonic antigen-targeted gelonin immunotoxin (C7rGel) followed by a secondary treatment with a potentiating epidermal growth factor receptor-targeted cholesterol-dependent cytolysin (E6LLO or E6PFO), against a cell line expressing only modest levels of either antigen.

Our model builds upon the foundational work in the group conducted by Thurber, Schmidt, and Wittrup (14, 15). Their compartmental model strove to analyze the limitations to antibody transport in tumors and to assess the effect of molecular size on tumor biodistribution. Here, we build upon the principles they established in understanding biodistribution of antibodies and antibody fragments and apply them to the biodistribution of our fusion proteins and the effects it has on

dosing and compartmental colocalization of two different targeted proteins in tumors.

5.3 – Methods

5.3.1 – Core model

Original MATLAB (The Mathworks, Natick, MA) code for a compartmental, Krogh cylinder model describing the pharmacokinetics and tumor biodistribution of antibodies was graciously provided by Dr. Michael Schmidt. Briefly, the fundamental equations of that code describe the diffusivity of protein out of the capillary as a two-pore system, the tumor void fraction using the same self-consistent representation, the resulting size-dependent permeability of the capillary to the protein, clearance of protein from the bloodstream as a single exponential with a rate proportional to renal and non-renal clearance rates. From those inputs, uptake into the tumor interstitial space, and the time to maximum therapeutic concentration in the tumor were calculated (16, 17). This code was used as a basis for the modifications described herein (Figure 5.1).

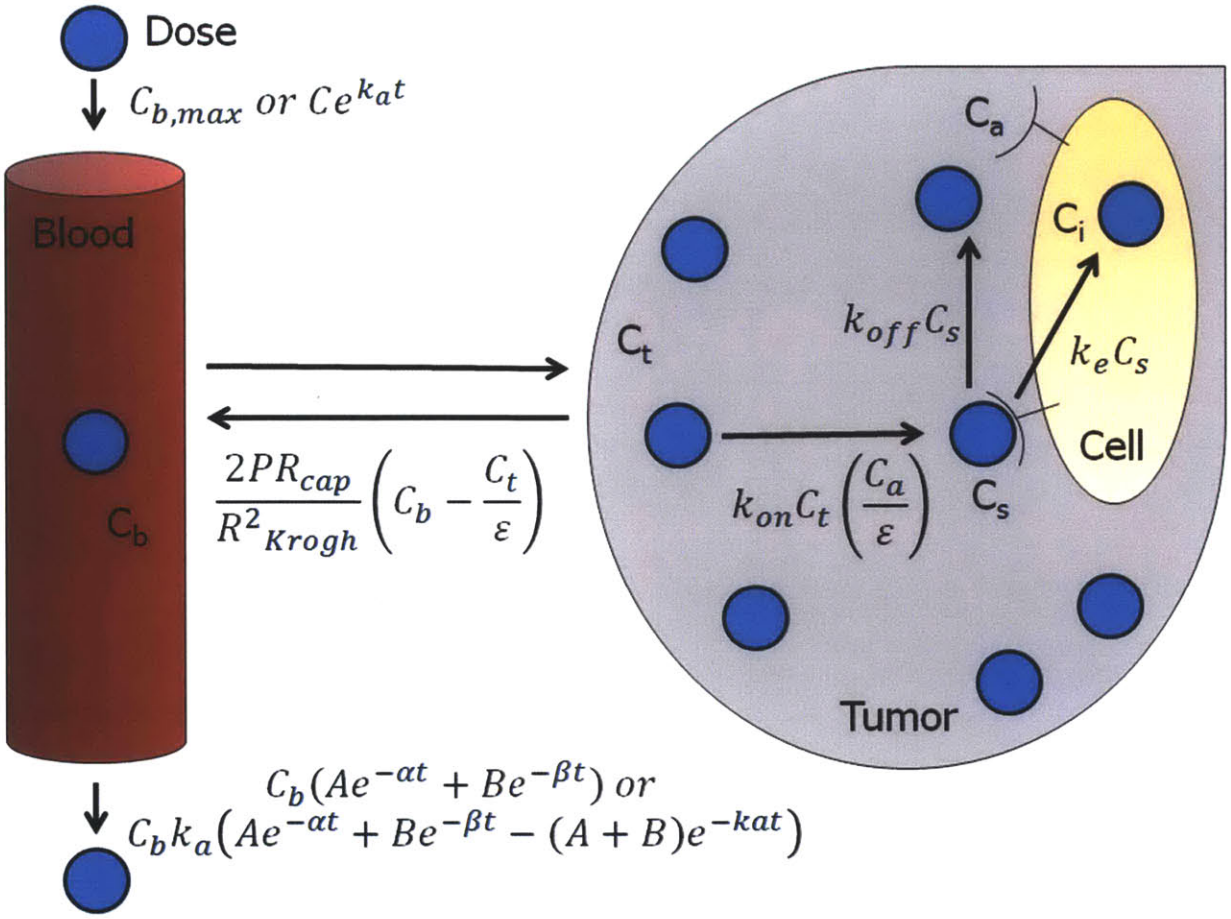

Figure 5.1 – A multi-compartment dual therapeutic model. Modified from Schmidt *et al.,* concentrations of therapeutic protein and other species in different compartments are monitored: C_b (in blood), C_t (in tumor), C_s (bound), C_i (internalized), and C_a (antigen concentration). P is the capillary permeability, R_{cap} is the capillary radius, R_{Krogh} is the Krogh cylinder radius, ε is the tumor void fraction, k_{on} and k_{off} are the binding rates for the antigen/protein interaction, k_e is the endocytosis rate, A and B are the clearance fractions, α and ß are the clearance rates, and k_a is the absorption rate. Two different equations are provided for either accumulation or removal from the blood stream depending on the route of administration.

5.3.2 – Model parameter determination

In some cases, model parameters we determined empirically from data collected in previous chapters. Many parameter values were derived from the online calculator designed in our lab (http://tumormodel.org/) (17). When necessary, parameters were obtained from literature sources which are cited where appropriate.

5.3.3 – Clearance equations

Where in the core model a single exponential clearance equation had been used we built in a bi-exponential equation:

$$C_b = C_{max}\left(Ae^{-\alpha t} + Be^{-\beta t}\right)$$

where A, B, α, and ß were fitted to experimental plasma clearance data measured from mice injected retro-orbitally. And tri-exponential:

$$C_b = C_{max}k_a\left(Ae^{-\lambda_1 t} + Be^{-\lambda_2 t} - (A+B)e^{-k_a t}\right)$$

where A, B, λ_1, λ_2, and k_a were fitted to experimental data from intraperitoneal injections. These equations more accurately represent and use parameters coordinated with *in vivo* data collected (Chapter 4) following either retro-orbital or intraperitoneal injections, respectively.

5.3.4 – Dual agent dosing

To most accurately represent our *in vivo* system and develop a model with the most clinical relevance, it was important to build in the delayed dosing

approach we used experimentally. In the computational setup this was achieved by iterating the model with a time shift to simulate dual retro-orbital injections and to replace the simple bi-exponential decay rate in the plasma with a tri-exponential plasma concentration equation in the delayed iteration, to simulate a secondary intraperitoneal injection.

Time delays used in the model were based on the minimum dose separations that were determined empirically (Table 5.1). We ran simulations of dual retro-orbital injections for C7rGel primary and for either E6LLO or E6PFO secondary. For secondary intraperitoneal injections we only simulated E6PFO.

Table 5.1 – Secondary time shifts for simulations

Secondary (Route)	Time shift (hrs)
E6LLO (retro-orbital)	12
E6PFO (retro-orbital)	24
E6PFO (intraperitoneal)	6

5.3.5 – Calculation of tumor exposure overlap

From a physiological perspective one of the most important goals of this approach is to achieve the maximum tumor exposure to both agents in combination without such exposure to the vascular endothelium. To quantify the strength of dual exposure, we calculated the area under curve (AUC) for immunotoxin in the tumor interstitial space while in the presence of potentiator for each dosing condition. This was achieved using the cumulative trapezoidal method in MATLAB

(Z = cumtrapz(Y)) to get an integral approximation for each agent across time increments at which the concentration of the potentiator was non-zero.

5.3.6 – Endothelial versus tumor internalization

Internalization of immunotoxin by both capillary endothelial cells and tumor cells was modeled. Antigen dependent internalization was a component already incorporated into the core model but in order to address cumulative uptake we had to remove the signal decay component originally used to describe the loss of scintillation signal over time. Furthermore, to obtain a quantitative measure of the average uptake per cell across a tumor cross section, it was necessary to approximate the number of cells within the computationally simulated cross-section of the Krogh cylinder radius. We first defined the volume of the cross-section:

$$V = d_{cell} \times \pi(r_{outer} - r_{inner})^2$$

based on the diameter of an average cell (d_{cell}) and the cross-sectional radii (r_{outer} and r_{inner}) and approximated then the number of cells (N_{cells}) in that cross section as a generalization from the average cell density of a tumor (ρ_{tumor}) in cells/volume :

$$N_{cells} = V \times \rho_{tumor}$$

From there the average number of therapeutic molecules internalized by each cell (N_i) was calculated from volume, the internalized concentration (C_i) output from the core model, Avogadro's number (N_{av}), and N_{cells}:

$$N_i = \frac{C_i V N_{av}}{N_{cells}}$$

In the case of antigen-negative cells, specifically those of the vascular endothelium, we approximated non-specific uptake (U) by integrating the plasma concentration of the therapeutic over time and multiplying it by a generalized pinocytic uptake rate (k_u) :

$$U = k_u \int_0^t C_b \, dt$$

Internalized molecule calculations were compared to measurements of molecular cytotoxicity *in vitro* (Chapters 2/3).

5.4 – Results

5.4.1 – Parameter assignment

Model parameters that were not dependent on the particular biotherapeutic used are listed and when determined from the literature, citations are provided (Table 5.2). For tumor radius, which here refers to the same dimension as the Krogh cylinder, we reference two citations but also base the number on work in our own group using immunofluorescence and advanced image analysis to determine the median distance between capillaries in tumor xenografts.

Table 5.2 – Parameter values independent of protein characteristics

Parameter	Symbol	Value	Reference
Endothelial pinocytosis rate	E_{up}	23×10^{-15} L/hr	(18)
Antigen endocytosis rate	k_e (CEA)	3×10^{-5} s^{-1}	(19)
	k_e (EGFR)	1.5×10^{-5} s^{-1}	(20)
Effective antigen concentration	C_a	550×10^{-9} M	(21, 22)
Tumor radius	R_T	150×10^{-6} m	(23, 24)
Capillary radius	R_C	8×10^{-6} m	(25)
Tumor cell density	ρ_{tumor}	7×10^{8} cells/ml	(18)

Additional parameters for individual agents dosed *in vivo* were obtained from primary data, literature, or other sources (Table 5.3). Here, all clearance parameters were taken from infra-red labeled protein measurements in plasma samples collected as described (Chapter 4). The rather rapid clearance of these therapeutic proteins is likely a result of their relatively small size. At 40 kDa, fibronectin targeted gelonin is within the glomerular filtration cut-off and, as we observed in whole animal imaging, is cleared primarily by the kidneys. In contrast, E6LLO has a slightly longer half-life and both it and E6PFO are cleared primarily by the liver.

Table 5.3 – Parameter values specific to individual therapeutics

Parameter	Symbol	Value C7rGel / E6LLO / E6PFO	Reference
Dose	$[C_{max}]$	$4.5x10^{-6}$ / $1.3x10^{-7}$ / $2x10^{-8}$ (M)	*
Antigen binding on rate	k_{on}	$5x10^{5}$ (M^{-1} s^{-1})	(26)
Antigen binding off rate	k_{off}	10^{-3} / $2.5x10^{-3}$ / (s^{-1})	†
Capillary permeability	P	6.73 / 5.03 / 5.18 ($x10^{-7}$ cm/s)	‡
Tumor diffusivity	D	5.7 / 4.11 / 4.29 ($x10^{-7}$ cm^2/s)	‡
Tumor void fraction	ε	0.319 / 0.287 / 0.291	‡
Plasma alpha fraction	A	0.82 / 0.85 / 0.95	*
Alpha decay rate	α	0.023 / 0.0056 / 0.02	*
Plasma beta fraction	B	0.18 / 0.15 / 0.05	*
Beta decay rate	β	0.00095 / 0.00099 / 0.0009	*
IP intravasation rate	k_a	- / - / 0.0106 (min^{-1})	*
IP primary coefficient	L_1	- / - / 8.95	*
IP lambda primary	Λ_1	- / - / 0.0089	*
IP secondary coefficient	L_2	- / - / 0.39	*
IP lambda secondary	Λ_2	- / - / 0.00048	*

* Determined by empirical measurement

† K_d's were measured (Chapter 3) and $k_{off} = k_{on} * K_d$

‡ Obtained from online tumor uptake predictor (tumormodel.org)

5.4.2 – Plasma clearance and tumor targeting

Simulations accurately reproduced the plasma clearance kinetics measured *in vivo* for both retro-orbital and intraperitoneal injections (Figure 5.2). Consistent with *in vivo* data, the model reproduced the rapid clearance of each different therapeutic from the plasma after retro-orbital injection with characteristic bi-exponential curves. After intraperitoneal injection the plasma concentration remains elevated for a greater duration due to the slow intravasation from the peritoneal cavity.

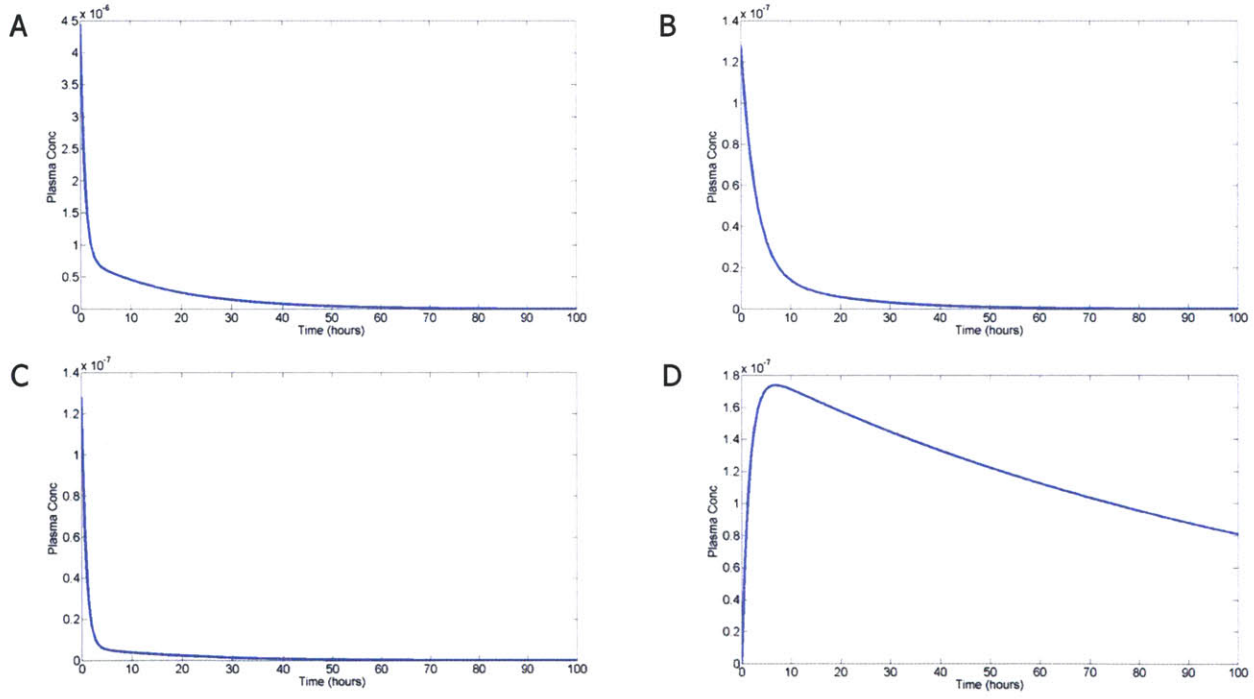

Figure 5.2 – Simulation of biotherapeutic plasma concentration. (A) Plasma clearance following retro-orbital injection of C7rGel, (B) E6LLO, or (C) E6PFO and (D) following intraperitoneal injection of E6PFO.

5.4.3 – Dual dosing and exposure calculations

To better understand how dosing schedules and schemes influence the exposure of either vascular endothelium or tumor to both therapeutics simultaneously, we simulated dual agent dosing and monitored the plasma concentrations (Figure 5.3) and the tumor concentrations (Figure 5.4). A common theme amongst these simulations, which is consistent with *in vivo* results is the rapid appearance of therapeutic in either the plasma or tumor interstitial space following retro-orbital injection and the relatively longer time to achieve maximum concentration in those same compartments for therapeutic injected into the peritoneal cavity.

From these simulations we also quantified overlap of immunotoxin and potentiator in the tumor interstitial space. AUC calculations of C7rGel across times of dual exposure for 6, 12, or 24 hour separation times were 4.92×10^{-7}, 4.66×10^{-7}, 4.09×10^{-7} M•hrs, respectively. This result suggests that by using alternative routes of administration that allow for shorter separation times we can increase overlapping exposure in the tumor by twenty percent.

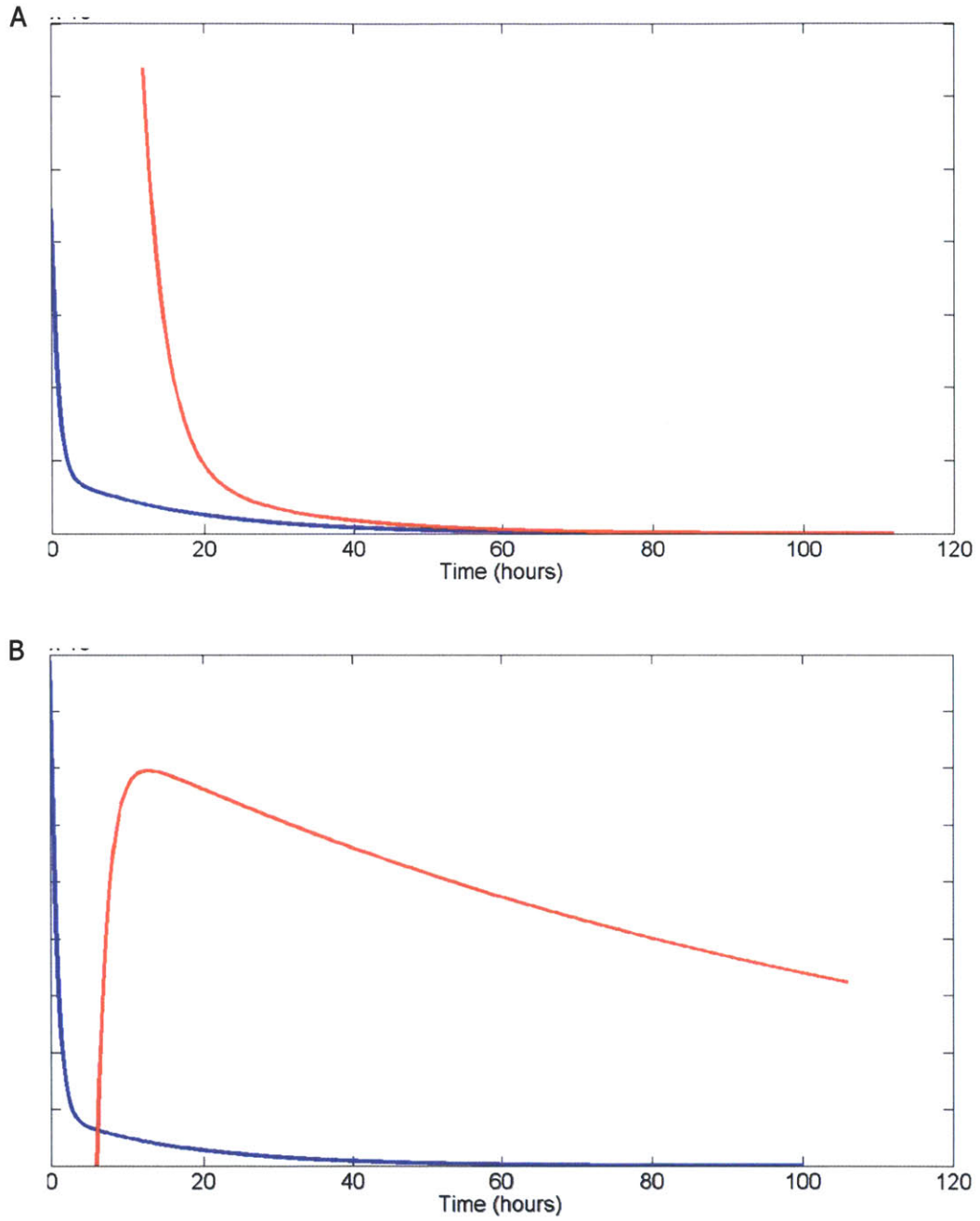

Figure 5.3 – Modeling therapeutic overlap in the plasma. Combination treatments are simulated on arbitrary scales with different dose separations and routes of administration. C7rGel concentration is plotted in blue and potentiator concentration is plotted in red. (A) E6LLO retro-orbital injection with 12 hour delay. (B) E6PFO intraperitoneal injection with 6 hour delay.

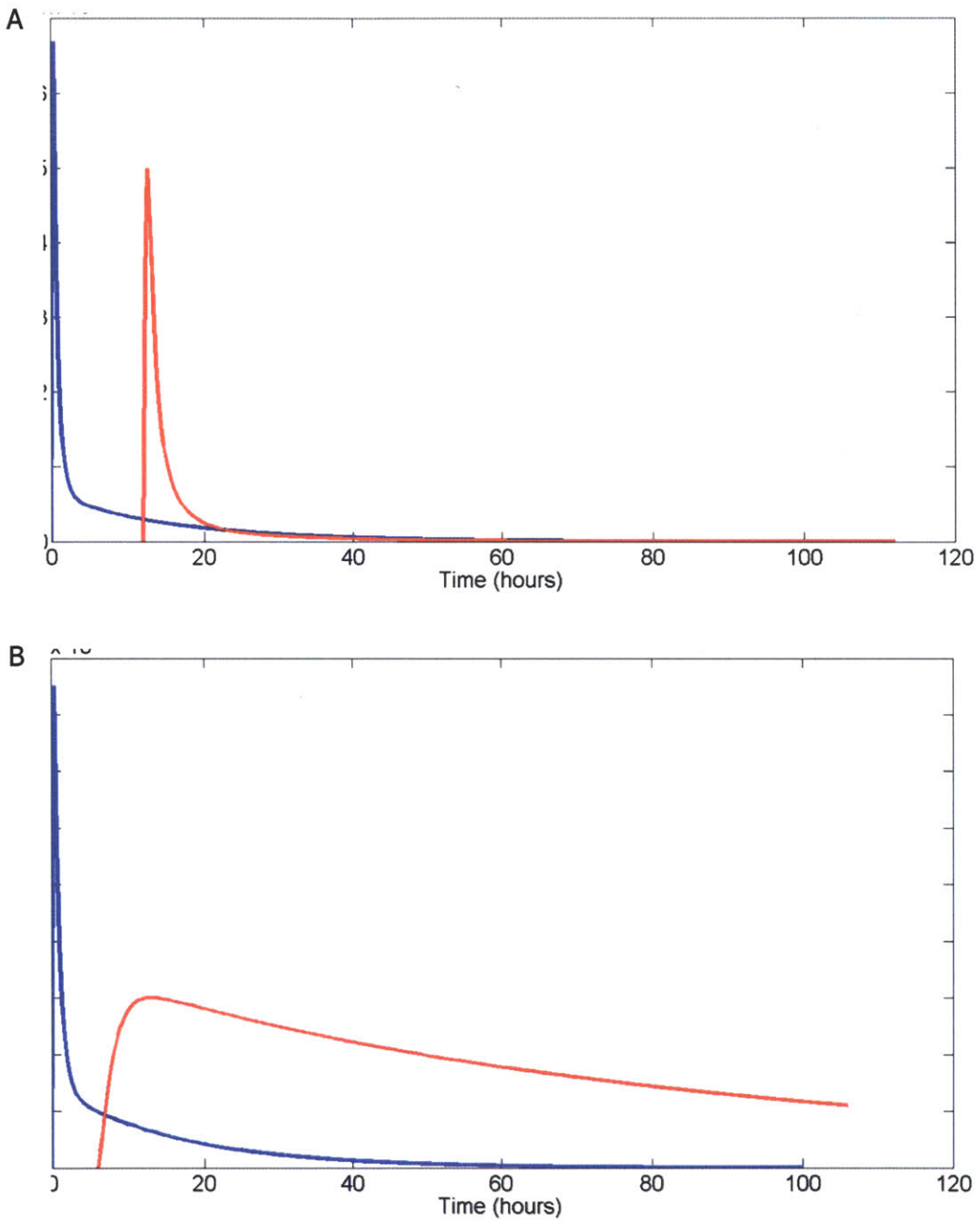

Figure 5.4 – Therapeutic concentrations in the tumor interstitium. Simulated tumor overlap for C7rGel (blue lines) and potentiator (red lines) with either (A) E6LLO by retro-orbital injection after 12 hour delay or (B) E6PFO by intraperitoneal injection after 6 hour delay.

5.4.4 – Internalization by vascular endothelium and tumor cells

As is generally accepted in the field and known intimately to us from our earliest investigations of immunotoxin activity, potency is intimately tied to internalization (27, 28). Ultimately, it is internalization that leads to cytotoxicity, whether targeted or non-specific. To this end, we sought to capture the accumulated number of internalized molecules by cells in the vascular endothelium and tumor. Like our dose overlap calculation, we focused on internalization occurring after dosing of the potentiation agent. We found that fewer than 200 molecules of immunotoxin are pinocytosed by cells of the vascular endothelium while the average tumor cell internalizes 3.1×10^6 molecules. This number is just under the $\sim 5 \times 10^6$ internalized molecule threshold for apoptosis determined in our earlier work (Chapter 2) but well above the $\sim 10^4$ molecule threshold found in the presence of a potentiating cytolysin (Chapter 3). It is important to note however the strength of the relationship between tumor cell internalization of immunotoxin and the Krogh cylinder radius. The calculation represents an average internalization meaning that cells near the capillary likely internalize a greater number and there are cells that don't internalize nearly as many. When Krogh cylinder radius is varied between 50 and 200 μm there is a non-linear effect on the tumor cell internalization of immunotoxin ranging from 2.3×10^7 to 2×10^6.

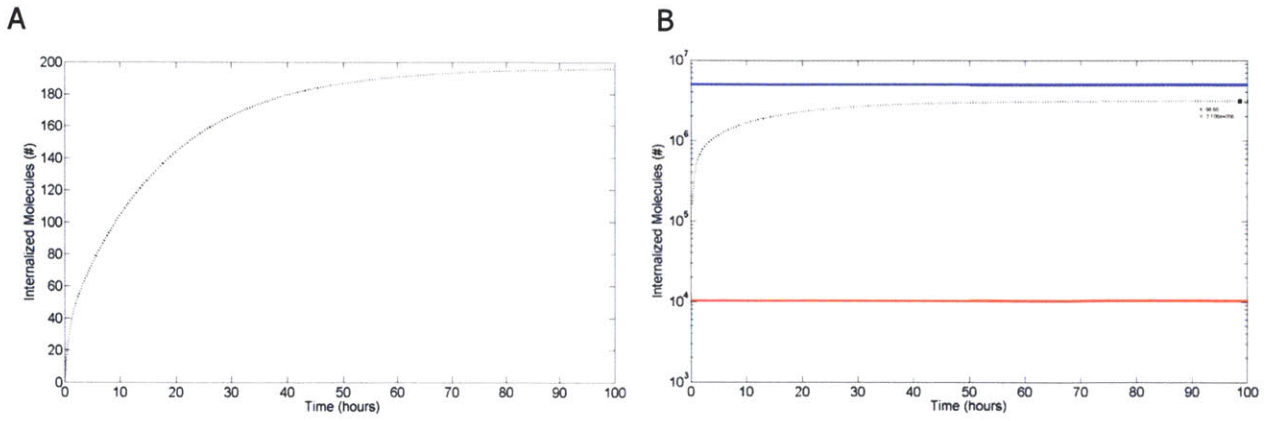

Figure 5.5 – Immunotoxin uptake simulation. Model outputs for internalization in (A) the vascular endothelium and (B) by tumor cells. Outputs were considered surrogates for non-specific toxicity and efficacy *in vivo*. The red and blue lines represent the thresholds for internalized cytotoxicity in the presence or absence of potentiator.

5.5 – Discussion

Building upon the pioneering work of others from our group (17, 18) we have been able to characterize the basic pharmacokinetics of our two novel therapeutics in a two-compartment model system. Our mathematical modeling was both informed by and motivated *in vivo* experimentation (Chapter 4). We supplemented empirically determined model parameters where necessary with metrics derived from literature sources. Results indicated that in the situation in which E6PFO was used as the potentiating agent and administered by intraperitoneal injection, the allowed shorter delay time increased the amount of immunotoxin available in the tumor to be potentiated by approximately 20% over the dual retro-orbital injection strategy.

Remarkably, increased overlap in the plasma following intraperitoneal injection of potentiator does not result in increased morbidity. Our hypothesis had been that combination therapeutic toxicity *in vivo* resulted from non-specific uptake of both agents by vascular endothelial cells, but this modeling result suggests that it may arise from common clearance organs internalizing both agents. If we recall our whole animal imaging results (Chapter 4), it seems clear that such toxicity would have to arise in the liver or one of the secondary clearance organs. Unfortunately, the current model does not simulate hepatocellular uptake of immunotoxin.

When we take overlap in exposure a step further to consider the cumulative internalization of immunotoxin by cells either of the vascular endothelium or of the tumor, we find that thanks to antigen specific binding, a vastly greater number of immunotoxins are internalized by tumor cells. That internalization is insufficient on average to induce cytotoxicity in the absence of potentiator, but more than overcomes the threshold for apoptosis in the presence of potentiator. The potentiator itself is also internalized at significant levels, but without supporting *in vitro* data correlating uptake with cytotoxicity it is impossible to predict the impact of these particular levels. The influence of the Krogh cylinder radius parameter on tumor cell internalization of immunotoxin is quite significant; for physiologically relevant ranges, changes to the Krogh cylinder parameter can cause the average number of immunotoxins internalized to be either above or below the apoptotic threshold in the absence of potentiator.

Despite these promising conclusions derived from our mathematical model, *in vivo* experiments show that repeated doses at the levels described here result in varying levels of toxicity. This further supports the idea that *in vivo* toxicity is the result of clearance organ damage rather than vascular leak syndrome which is a common dose limiting toxicity in clinical trials of immunotoxins (29, 30). Others have found toxicities associated with elevated transaminase levels (usually correlated with liver damage) following immunotoxin treatments (31, 32) which are likely to be accentuated when subsequently dosing with a potentiating agent whose primary clearance organ is the liver.

5.6 – Citations

1. Lippow, S. M., Wittrup, K. D., and Tidor, B. (2007) *Nat. Biotechnol* **25**, 1171-1176
2. Kreeger, P. K., and Lauffenburger, D. A. (2010) *Carcinogenesis* **31**, 2-8
3. Emmert-Streib, F., and Dehmer, M. (2011) *IET Syst Biol* **5**, 185-207
4. Roskos, L. K., Schneider, A., Vainshtein, I., Schwickart, M., Lee, R., Lu, H., Faggioni, R., and Liang, M. (2011) *Bioanalysis* **3**, 659-675
5. Sim, H., Bibee, K., Wickline, S., and Sept, D. (2011) *Cancer Res* **71**, 686-692
6. US Department of Health and Human Services, F. and D. A. (1999) *Guidance for Industry: Population Pharmacokinetics*, [online] http://www.fda.gov/downloads/ScienceResearch/SpecialTopics/WomensHealthResearch/UCM133184.pdf.
7. Gobburu, J. V., and Marroum, P. J. (2001) *Clin Pharmacokinet* **40**, 883-892
8. Sung, C., Youle, R. J., and Dedrick, R. L. (1990) *Cancer Res* **50**, 7382-7392
9. Yazdi, P. T., and Murphy, R. M. (1994) *Cancer Res* **54**, 6387-6394

10. Yazdi, P. T., Wenning, L. A., and Murphy, R. M. (1995) *Cancer Res* **55**, 3763-3771

11. Wenning, L. A., Yazdi, P. T., and Murphy, R. M. (1998) *Biotechnol. Bioeng* **57**, 484-496

12. Wenning, L. A., and Murphy, R. M. (1999) *Biotechnol. Bioeng* **62**, 562-575

13. Chen, K. C., Kim, J., Li, X., and Lee, B. (2008) *Ann Biomed Eng* **36**, 486-512

14. Thurber, G. M., Schmidt, M. M., and Wittrup, K. D. (2008) *Adv. Drug Deliv. Rev* **60**, 1421-1434

15. Thurber, G. M., Schmidt, M. M., and Wittrup, K. D. (2008) *Trends Pharmacol. Sci* **29**, 57-61

16. Schmidt, M. M., and Wittrup, K. D. (2009) *Mol. Cancer Ther* **8**, 2861-2871

17. Schmidt, M. M. (2010) [online] http://hdl.handle.net/1721.1/61239.

18. Thurber, G. M. (2008) [online] http://hdl.handle.net/1721.1/43216.

19. Schmidt, M. M., Thurber, G. M., and Wittrup, K. D. (2008) *Cancer Immunol. Immunother* **57**, 1879-1890

20. Wiley, H. S. (2003) *Exp. Cell Res* **284**, 78-88

21. Conaghan, P., Ashraf, S., Tytherleigh, M., Wilding, J., Tchilian, E., Bicknell, D., Mortensen, N. J., and Bodmer, W. (2008) *Br. J. Cancer* **98**, 1217-1225

22. Spangler, J. B., Neil, J. R., Abramovitch, S., Yarden, Y., White, F. M., Lauffenburger, D. A., and Wittrup, K. D. (2010) *Proc. Natl. Acad. Sci. U.S.A* **107**, 13252-13257

23. Ginj, M., Zhang, H., Waser, B., Cescato, R., Wild, D., Wang, X., Erchegyi, J., Rivier, J., Mäcke, H. R., and Reubi, J. C. (2006) *Proc. Natl. Acad. Sci. U.S.A* **103**, 16436-16441

24. Wicki, A., Wild, D., Storch, D., Seemayer, C., Gotthardt, M., Behe, M., Kneifel, S., Mihatsch, M. J., Reubi, J.-C., Mäcke, H. R., and Christofori, G. (2007) *Clin. Cancer Res* **13**, 3696-3705

25. DeNardo, G. L., Natarajan, A., Hok, S., Perkins, J., Cosman, M., DeNardo, S. J., Lightstone, F. C., Mirick, G. R., Miers, L. A., and Balhorn, R. L. (2007) *J. Nucl. Med* **48**, 1338-1347

26. Schreiber, G. (2002) *Curr. Opin. Struct. Biol* **12**, 41-47
27. Du, X., Beers, R., Fitzgerald, D. J., and Pastan, I. (2008) *Cancer Res* **68**, 6300-6305

28. Kuo, S.-R., Alfano, R. W., Frankel, A. E., and Liu, J.-S. (2009) *Bioconjug. Chem* **20**, 1975-1982

29. Kreitman, R. J., Hassan, R., Fitzgerald, D. J., and Pastan, I. (2009) *Clin. Cancer Res* **15**, 5274-5279

30. Schindler, J., Gajavelli, S., Ravandi, F., Shen, Y., Parekh, S., Braunchweig, I., Barta, S., Ghetie, V., Vitetta, E., and Verma, A. (2011) *Br. J. Haematol* **154**, 471-476

31. Garland, L., Gitlitz, B., Ebbinghaus, S., Pan, H., de Haan, H., Puri, R. K., Von Hoff, D., and Figlin, R. (2005) *J. Immunother* **28**, 376-381

32. Wayne, A. S., Kreitman, R. J., Findley, H. W., Lew, G., Delbrook, C., Steinberg, S. M., Stetler-Stevenson, M., Fitzgerald, D. J., and Pastan, I. (2010) *Clin. Cancer Res* **16**, 1894-1903

Appendix A – Amino acid sequences of proteins

Chapter 2

A.1 – rGel (recombinant gelonin)

ISEFGSSRVDLQGLDTVSFSTKGATYITYVNFLNELRVKLKPEGNSHGIPLLRKK
CDDPGKCFVLVALSNDNGQLAEIAIDVTSVYVVGYQVRNRSYFFKDAPDAAYEG
LFKNTIKTRLHFGGSYPSLEGEKAYRETTDLGIEPLRIGIKKLDENAIDNYKPTEI
ASSLLVVIQMVSEAARFTFIENQIRNNFQQRIRPANNTISLENKWGKLSFQIRTSG
ANGMFSEAVELERANGKKYYVTAVDQVKPKIALLKFVDKDPK

A.2 – C7rGel (anti-CEA Fn3 – recombinant gelonin)

ISEFASVSDGTLSRDLGVVAATPTSLLISWYYSYSHHYSSYRITYGETGGNSPVQE
FTVPRYRAFATISGLKPGVDYTITVYAVTSSSSYSYPISINYRTEIDKPSQGSGGGG
SGLDTVSFSTKGATYITYVNFLNELRVKLKPEGNSHGIPLLRKKCDDPGKCFVLV
ALSNDNGQLAEIAIDVTSVYVVGYQVRNRSYFFKDAPDAAYEGLFKNTIKTRLHF
GGSYPSLEGEKAYRETTDLGIEPLRIGIKKLDENAIDNYKPTEIASSLLVVIQMVS
EAARFTFIENQIRNNFQQRIRPANNTISLENKWGKLSFQIRTSGANGMFSEAVEL
ERANGKKYYVTAVDQVKPKIALLKFVDKDPK

A.3 – E4rGel (anti-EGFR Fn3 – recombinant gelonin)

ISEFASVSDVPRDLEVVAATPTSLLISWYHPFYYVAHSYRITYGETGGNSPVQEFT
VPRSPWFATISGLKPGVDYTITVYAVTDSNGSHPISINYRTEIDKPSQGSGGGGSG
LDTVSFSTKGATYITYVNFLNELRVKLKPEGNSHGIPLLRKKCDDPGKCFVLVAL
SNDNGQLAEIAIDVTSVYVVGYQVRNRSYFFKDAPDAAYEGLFKNTIKTRLHFG
GSYPSLEGEKAYRETTDLGIEPLRIGIKKLDENAIDNYKPTEIASSLLVVIQMVSE
AARFTFIENQIRNNFQQRIRPANNTISLENKWGKLSFQIRTSGANGMFSEAVELE
RANGKKYYVTAVDQVKPKIALLKFVDKDPK

A.4 – 3ErGel (anti-CEA ds-scFv – recombinant gelonin)

AMADIEFASQVKLEQSGAEVVKPGASVKLSCKASGFNIKDSYMHWLRQGPGQC
LEWIGWIDPENGDTEYAPKFQGKATFTTDTSANTAYLGLSSLRPEDTAVYYCNE
GTPTGPYYFDYWGQGTLVTVSSGGGGSGGGGSGGGGSENVLTQSPSSMSVSVG
DRVTIACSASSSVPYMHWLQQKPGKSPKLLIYLTSNLASGVPSRFSGSGSGTDYS
LTISSVQPEDAATYYCQQRSSYPLTFGCGTKLEIKAAAGSSRVDGGGGSGGGGSL
QGLDTVSFSTKGATYITYVNFLNELRVKLKPEGNSHGIPLLRKKCDDPGKCFVL
VALSNDNGQLAEIAIDVTSVYVVGYQVRNRSYFFKDAPDAAYEGLFKNTIKTRLH
FGGSYPSLEGEKAYRETTDLGIEPLRIGIKKLDENAIDNYKPTEIASSLLVVIQMV
SEAARFTFIENQIRNNFQQRIRPANNTISLENKWGKLSFQIRTSGANGMFSEAVE
LERANGKKYYVTAVDQVKPKIALLKFVDKDPK

A.5 – FErGel (anti-CEA ds-scFv – recombinant gelonin)

AMADIEFASQVKLEQSGAEVVKPGASVKLSCKASGFNIKDSYMHWLRQGPGQC
LEWIGWIDPENGDTEYAPKFQGKATFTTDTSANTAYLGLSSLRPEDTAVYYCNE
GTPTGPYYFDYWGQGTLVTVSSGGGGSGGGGSGGGGSENVLTQSPSSMSASVG
DRVTIACSASSSVPYMHWFQQKPGKSPKLLIYSTSNLASGVPSRFSGSGSGTDYS
LTISSVQPEDAATYYCQQRSSYPLTFGCGTKLEIKAAAGSGGGGSGLDTVSFSTK
GATYITYVNFLNELRVKLKPEGNSHGIPLLRKKCDDPGKCFVLVALSNDNGQLA
EIAIDVTSVYVVGYQVRNRSYFFKDAPDAAYEGLFKNTIKTRLHFGGSYPSLEGE
KAYRETTDLGIEPLRIGIKKLDENAIDNYKPTEIASSLLVVIQMVSEAARFTFIEN
QIRNNFQQRIRPANNTISLENKWGKLSFQIRTSGANGMFSEAVELERANGKKYY
VTAVDQVKPKIALLKFVDKDPK

Chapter 3

A.6 – C7LLO (anti-CEA Fn3 – listeriolysin O)

ISEFASVSDGTLSRDLGVVAATPTSLLISWYYSYSHHYSSYRITYGETGGNSPVQE
FTVPRYRAFATISGLKPGVDYTITVYAVTSSSSYSYPISINYRTEIDKPSQGSGGGG
SKKIMLVFITLILVSLPIAQQTEAKDASAFNKENLISSMAPPASPPASPKTPIEKKH
ADEIDKYIQGLDYNKNNVLVYHGDAVTNVPPRKGYKDGNEYIVVEKKKKSINQ
NNADIQVVNAISSLTYPGALVKANSELVENQPDVLPVKRDSLTLSIDLPGMTNQD
NKIVVKNATKSNVNNAVNTLVERWNEKYAQAYPNVSAKIDYDDEMAYSESQLI
AKFGTAFKAVNNSLNVNFGAISEGKMQEEVISFKQIYYNVNVNEPTRPSRFFGK
AVTKEQLQALGVNAENPPAYISSVAYGRQVYLKLSTNSHSTKVKAAFDAAVSGK
SVSGDVELTNIIKNSSFKAVIYGGSAKDEVQIIDGNLGDLRDILKKGATFNRETPG
VPIAYTTNFLKDNELAVIKNNSEYIETTSKAYTDGKINIDHSGGYVAQFNISWDEI
NYDPEGNEIVQHKNWSENNKSKLAHFTSSIYLPGNARNINVYAKECTGLAWEW
WRTVIDDRNLPLVKNRNISIWGTTLYPKYSNSVDNPIE

A.7 – E6LLO (anti-EGFR Fn3 – listeriolysin O)

ISEFASVSDVPRDLEVVAATPTSLLISWFDYAVTYYRITYGETGGNSPVQEFTVPG
WISTATISGLKPGVDYTITVYAVTDNSRWPFRSTPISINYRTEIDKPSQGSGGGGS
KKIMLVFITLILVSLPIAQQTEAKDASAFNKENLISSMAPPASPPASPKTPIEKKH
ADEIDKYIQGLDYNKNNVLVYHGDAVTNVPPRKGYKDGNEYIVVEKKKKSINQ
NNADIQVVNAISSLTYPGALVKANSELVENQPDVLPVKRDSLTLSIDLPGMTNQD
NKIVVKNATKSNVNNAVNTLVERWNEKYAQAYPNVSAKIDYDDEMAYSESQLI
AKFGTAFKAVNNSLNVNFGAISEGKMQEEVISFKQIYYNVNVNEPTRPSRFFGK
AVTKEQLQALGVNAENPPAYISSVAYGRQVYLKLSTNSHSTKVKAAFDAAVSGK
SVSGDVELTNIIKNSSFKAVIYGGSAKDEVQIIDGNLGDLRDILKKGATFNRETPG
VPIAYTTNFLKDNELAVIKNNSEYIETTSKAYTDGKINIDHSGGYVAQFNISWDEI
NYDPEGNEIVQHKNWSENNKSKLAHFTSSIYLPGNARNINVYAKECTGLAWEW
WRTVIDDRNLPLVKNRNISIWGTTLYPKYSNSVDNPIE

A.8 – C7PFO (anti-CEA Fn3 – perfringolysin O)

SASVSDGTLSRDLGVVAATPTSLLISWYYSYSHHYSSYRITYGETGGNSPVQEFTV
PRYRAFATISGLKPGVDYTITVYAVTSSSSYSYPISINYRTEIDKPSQGSGGGGSSS
KDITDKNQSIDSGISSLSYNRNEVLASNGDKIESFVPKEGKKAGNKFIVVERQKR
SLTTSPVDISIIDSVNDRTYPGALQLADKAFVENRPTILMVKRKPININIDLPGLK
GENSIKVDDPTYGKVSGAIDELVSKWNEKYSSTHTLPARTQYSESMVYSKSQISS
ALNVNAKVLENSLGVDFNAVANNEKKVMILAYKQIFYTVSADLPKNPSDLFDDS
VTFNDLKQKGVSNEAPPLMVSNVAYGRTIYVKLETTSSSKDVQAAFKALIKNTDI
KNSQQYKDIYENSSFTAVVLGGDAQEHNKVVTKDFDEIRKVIKDNATFSTKNPA
YPISYTSVFLKDNSVAAVHNKTDYIETTSTEYSKGKINLDHSGAYVAQFEVAWDE
VSYDKEGNEVLTHKTWDGNYQDKTAHYSTVIPLEANARNIRIKAREATGLAWE
WWRDVISEYDVPLTNNINVSIWGTTLYPGSSITYNGSHHHHHH

A.9 – E6PFO (anti-EGFR Fn3 – perfringolysin O)

SASVSDVPRDLEVVAATPTSLLISWFDYAVTYYRITYGETGGNSPVQEFTVPGWI
STATISGLKPGVDYTITVYAVTDNSRWPFRSTPISINYRTEIDKPSQGSGGGGSSS
KDITDKNQSIDSGISSLSYNRNEVLASNGDKIESFVPKEGKKAGNKFIVVERQKR
SLTTSPVDISIIDSVNDRTYPGALQLADKAFVENRPTILMVKRKPININIDLPGLK
GENSIKVDDPTYGKVSGAIDELVSKWNEKYSSTHTLPARTQYSESMVYSKSQISS
ALNVNAKVLENSLGVDFNAVANNEKKVMILAYKQIFYTVSADLPKNPSDLFDDS
VTFNDLKQKGVSNEAPPLMVSNVAYGRTIYVKLETTSSSKDVQAAFKALIKNTDI
KNSQQYKDIYENSSFTAVVLGGDAQEHNKVVTKDFDEIRKVIKDNATFSTKNPA
YPISYTSVFLKDNSVAAVHNKTDYIETTSTEYSKGKINLDHSGAYVAQFEVAWDE
VSYDKEGNEVLTHKTWDGNYQDKTAHYSTVIPLEANARNIRIKAREATGLAWE
WWRDVISEYDVPLTNNINVSIWGTTLYPGSSITYNGSHHHHHH

Appendix B – Alternative approaches to targeted intracellular delivery

Introduction

The field of intracellular delivery is rife with tools designed to selectively permeabilize subcellular compartments without cytotoxic effects. Substantial research efforts have been devoted to the advancement of delivery tools derived from small molecules (1), lipids (2), or polymers (3-5). But as alluded to earlier in this work (Chapters 2 & 3), one of the keys to success in this area is the ability to target that delivery.

Small molecules are probably the easiest of the intracellular delivery tools to target. Much like the recently popularized antibody drug conjugate technologies (6, 7), small molecules like monensin, chloroquine, or retinoic acid can be amenable to chemical conjugation to an antibody to direct their release inside a specific cell type. The same methodology can also be applied to conjugation of lipids (8) or polymers (9).

We set out to develop a tool for mediating targeted, *in trans*, intracellular biotherapeutic delivery. In doing so, we took an open minded approach as to which membrane active molecules might be most easily targeted using our lab's antigen binding protein scaffolds. Here we describe the various conjugates and fusion proteins we produced that showed only limited, or a total lack, of potentiating activity in our immunotoxin model system. And while this should not be taken as strict indictment of these active molecules, we believe to have learned a bit about the importance of potency in any targeting effort.

Methods

PAMAM dendrimer conjugation & purification

Poly-amidoamine dedrimers are branched polymers containing a combination of primary and tertiary amines which serve destabilize membranes by direct interaction or by buffering endosomal acidification, respectively (10, 11). Dan Bonner of the Hammond Lab at MIT kindly provided functionalized generation 4 or 5 dendrimers for conjugation and testing (12). These dendrimers were built on a disulfide-bonded, bifunctional initiator that was reduced to expose free sulfhydryl groups for reaction with maleimide groups at the end of poly(ethylene glycol) chains conjugated to anti-CEA and anti-EGFR IgG (sm3E and 225).

Prior work conducted under this same collaboration revealed that naïve dendrimer shows high levels of non-specific cytotoxicity specific to primary amine membrane interaction. Thus, for many conjugations, we used dendrimers with primary amines capped by acetylation to varying degrees, usually 50%.

IgG-dendrimer conjugates were purified using Protein A – Agarose resin (Thermo Scientific) and were characterized qualitatively by SDS-PAGE. Binding was assayed by flow cytometry on fixed, antigen-positive cells labeled with a fluorophore conjugated secondary antibody against the Fc domain of the dendrimer conjugated IgG. Cytotoxicity of dendrimer conjugates alone or in the presence of gelonin immunotoxins was assessed as described previously (Chapter 2)

Targeted fusion peptide construction & synthesis

In nature, viruses have evolved some of the most efficient mechanisms for intracellular delivery. Part of that success is built upon small fusogenic peptides whose ability to mediate intracellular delivery in other settings is recognized (13). Other have used peptides directly fused or conjugated to an active molecule to mediate delivery (14-16) and Wadia *et al.* were able to mediate *in trans* intracellular delivery of cre recombinase using TAT peptide as an internalization mechanism (17).

We hoped to mimic this result in a targeted manner using our engineered Fn3 domains with either N-terminal or C-terminal fusions to the peptides. Specifically, we chose to test the hemaglutinin (HA), gp41 (GP), flavivirus (Dengue – DN), and leucine zipper (LZ) peptides (Table B.1) for targeted potentiator activity. Using the overlap-extension PCR method described by Geiser *et al.* (18) we inserted codon optimized sequences encoding the aforementioned peptides either 5' or 3' of engineered Fn3 sequences in a pET24b derived vector.

Table B.1 – Fusogenic peptides tested for targeted membrane disruption.

Peptide (Abbreviation)	Sequence	Reference
Hemaglutinin (HA)	GLFGAIAGFIENGWEG	(19)
gp41 (GP)	GVFVLGFLGFLATAGS	(19)
Flavivirus (DN)	DRGWGNGCGLFGKGSL	(20)
Leucine Zipper (LZ)	ALEALAEALEALAEALA	(21)

Fn3's designed with fusogenic peptide arms were synthesized and purified as described previously (22) and their characterization in our model system was conducted in the same manner as for the other potentiators.

Other potentiators tested for in trans delivery activity

In addition to the agents described above for targeted potentiation we also tested a number of other small molecules, peptides, and polymers for *in trans* delivery capabilities in the absence of any targeting modality. These included the synthetic peptide INF7 (GLFEAIEGFIENGWEGMIDGWY – AnaSpec, Fremont, CA) (23), a poly(propyl-acrylic acid)-b-(butyl-methacrylate-co-pyrridyl-disulfide methacrylate) polymer kindly donated by the Stayton Lab (University of Washington, Seattle, WA) (9), stapled peptides generously provided by the Verdine Lab (Harvard University, Cambridge, MA) (24), poly(ethylenimine) (25), retinoic acid (Sigma-Aldrich) (1), and chloroquine (Sigma-Aldrich) (26).

Results

IgG-G5 Testing

Antibodies targeting either CEA (sm3E) or EGFR (225) were conjugated to G5 dendrimer hemispheres with 50% of their primary amines acetylated (G5Ac50) through bifunctional NHS-PEG-Maleimide. In these reactions, protein was used as the limiting reagent whose subsequent yield was quite high, but a strong excess of ~40% molar was used of the G5Ac50. SDS-PAGE of the Protein A purified IgG's

showed stepped bands that we hypothesize are representative of additional G5Ac50 reactions (Figure B.1)

These conjugates conferred modest independent cytotoxicity and some signs of synergy, but their combined effects appear mostly additive (Figure B.2A/B)

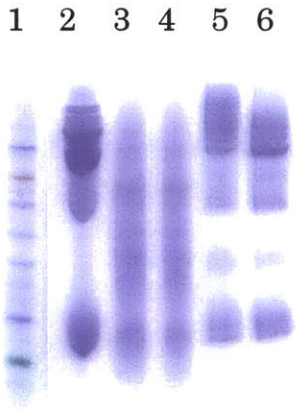

Figure B.1 – IgG-G5Ac50 characterization. Reducing SDS-PAGE was run with ColorPlus Prestained Protein Ladder (New England Biolabs, Ipswich, MA) (lane 1), 225 mAb (lane 2), protein A-agarose resin flow through from a 225/G5Ac50 reaction (lane 3) and a sm3E/G5Ac50 reaction (lane 4), the protein A-agarose resin purified 225-G5Ac50 (lane 5) and purified sm3E-G5Ac50 (lane 6). The protein ladder MW's from top to bottom are 150 kDa (barely visible), 100, 80, 60, 50, 40, 30, 25, and 20.

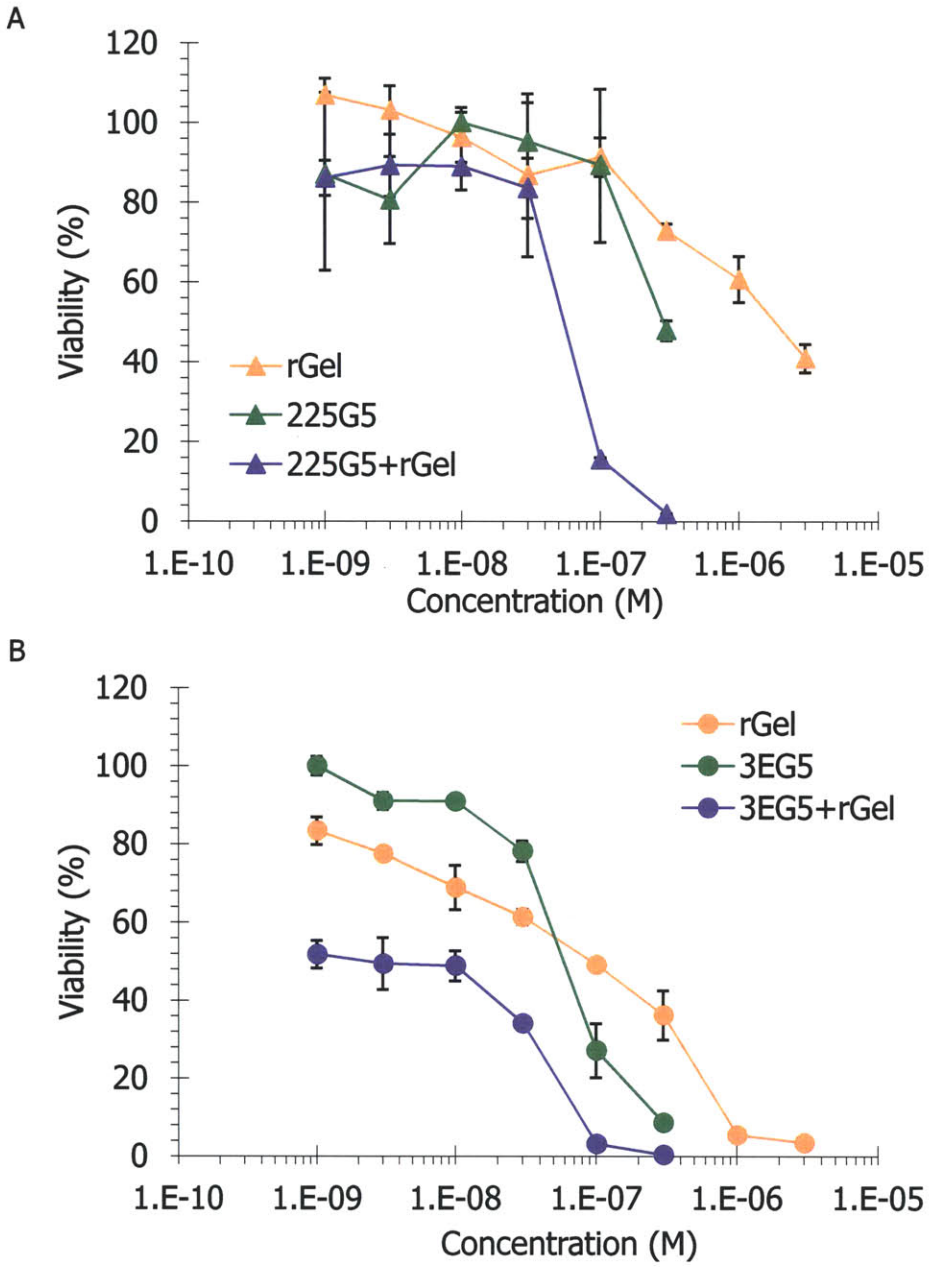

Figure B.2 – Cytotoxicity of IgG-G5Ac50 conjugate. (A) The EGFR-overexpressing cell line A431 is titrated with untargeted gelonin, 225-G5Ac50, and their combination titrated together. (B) HT-1080(CEA) over expressing CEA is titrated with untargeted gelonin, sm3E-G5Ac50, and their combination titrated together.

Targeted fusogenic peptide testing

Fusogenic peptides HA, GP, DN, and LZ were incorporated at either the N-terminus or C-terminus of CEA or EGFR targeted Fn3's depending on any perceived necessity for N-terminal exposure for activity. Consistent with their own independent expression levels, peptides fused to CEA-binding C743 (C7) were expressed at lower soluble levels, < 1 mg/L, than peptides fused to EGFR-binding E246 (E4) whose expression levels were around 5 mg/L.

We assayed targeted fusogenic peptides independent cytotoxicity and in combination with untargeted gelonin at levels where we might expect to see activity from both components. Example data are shown for various combinations of peptide and targeting Fn3. In some cases the targeted peptides show no independent cytotoxicity (Figure B.3A) and in those cases we didn't expect to see any synergistic activity with gelonin since at some level endosomal disruption should induce cytotoxicity or correlate with general membrane disruption. But even for those examples in which independent cytotoxicity was observed (Figure B.3B) there were no signs of synergy with gelonin.

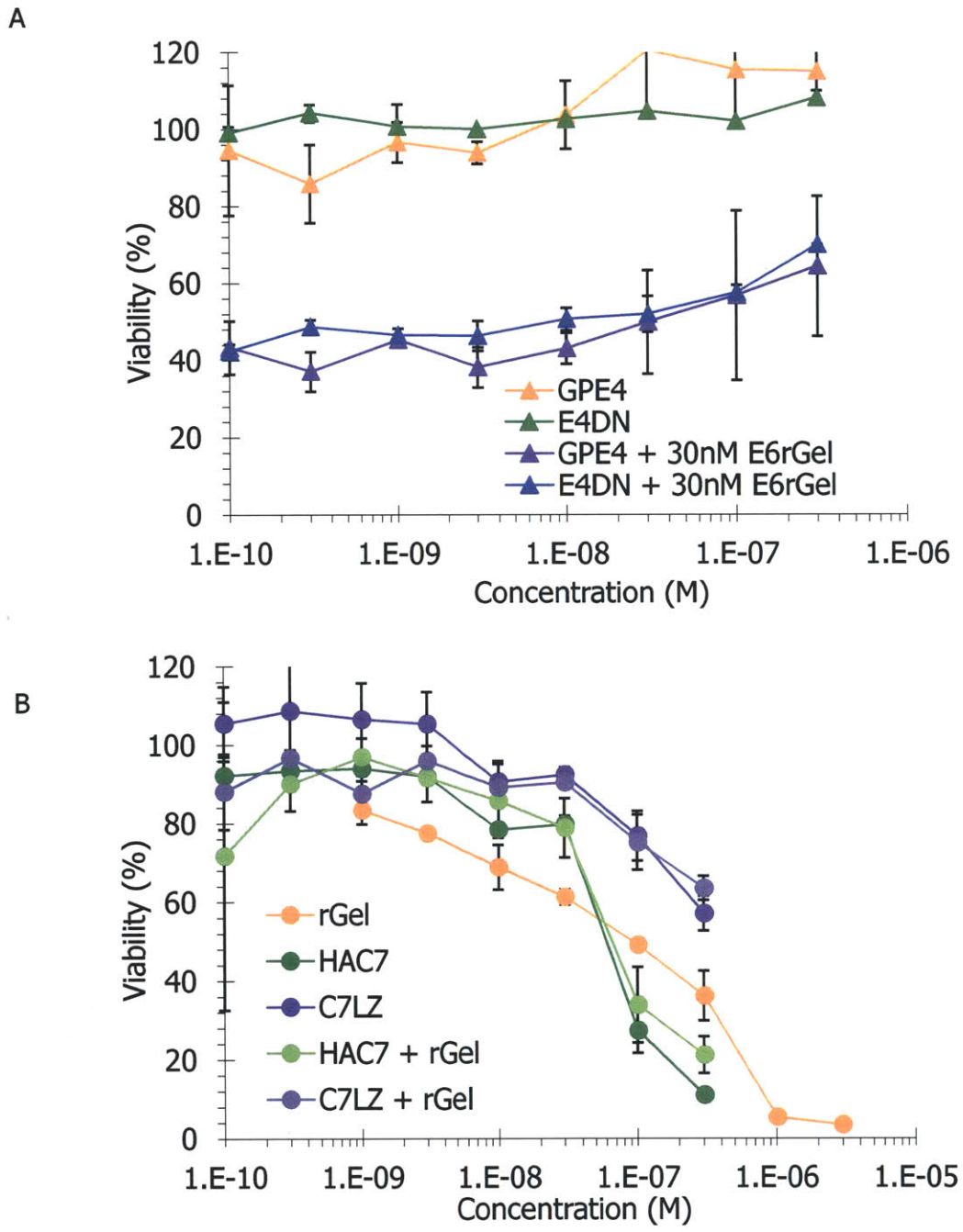

Figure B.3 – Targeted fusogenic peptide cytotoxicity. (A) EGFR-overexpressing A431 cells were treated with varying concentrations of GPE4 or E4DN in the presence or absence of a fixed, moderately cytotoxic concentration of non-competitively EGFR-targeted gelonin immunotoxin (E6rGel). (B) CEA-overexpressing HT-1080(CEA) cells were titrated with gelonin, HAC7, C7LZ, or a combination thereof.

Untargeted potentiator testing

Poly(propyl-acrylic acid) (PAAc) copolymer provided by the Stayton Lab and commercially obtained INF7 peptide showed modest enhancement of cytotoxicity when added to titrations of untargeted gelonin (Figure B.4). However when the roles were reversed (i.e. polymer or peptide titration with fixed, non-toxic concentration of gelonin) no potentiation was observed (data not shown). Attempts to conjugate PAAc polymer samples to Fn3 or IgG targeting proteins using Traut's reagent and disulfide bond formation with pyridyl groups were largely unsuccessful in our hands.

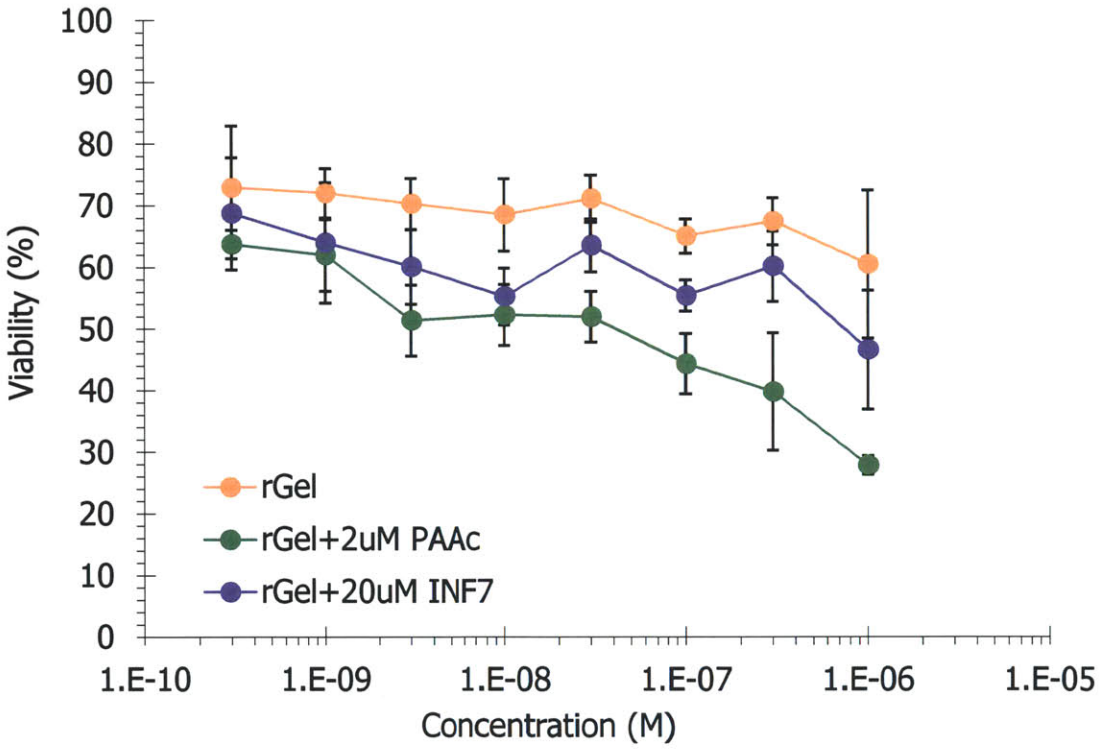

Figure B.4 – Potentiation of rGel cytotoxicity by polymer and synthetic peptide. Fixed concentrations of polymer or peptide were added to titrations of rGel on HT-1080 cells.

Stapled peptides given to us by the Verdine Lab showed additive cytotoxic effects when added at fixed concentrations to CEA-targeted gelonin immunotoxin titrations (Figure B.5A). They also were cytotoxic in their own right when titrated to concentrations above 1 μM (Figure B.5B).

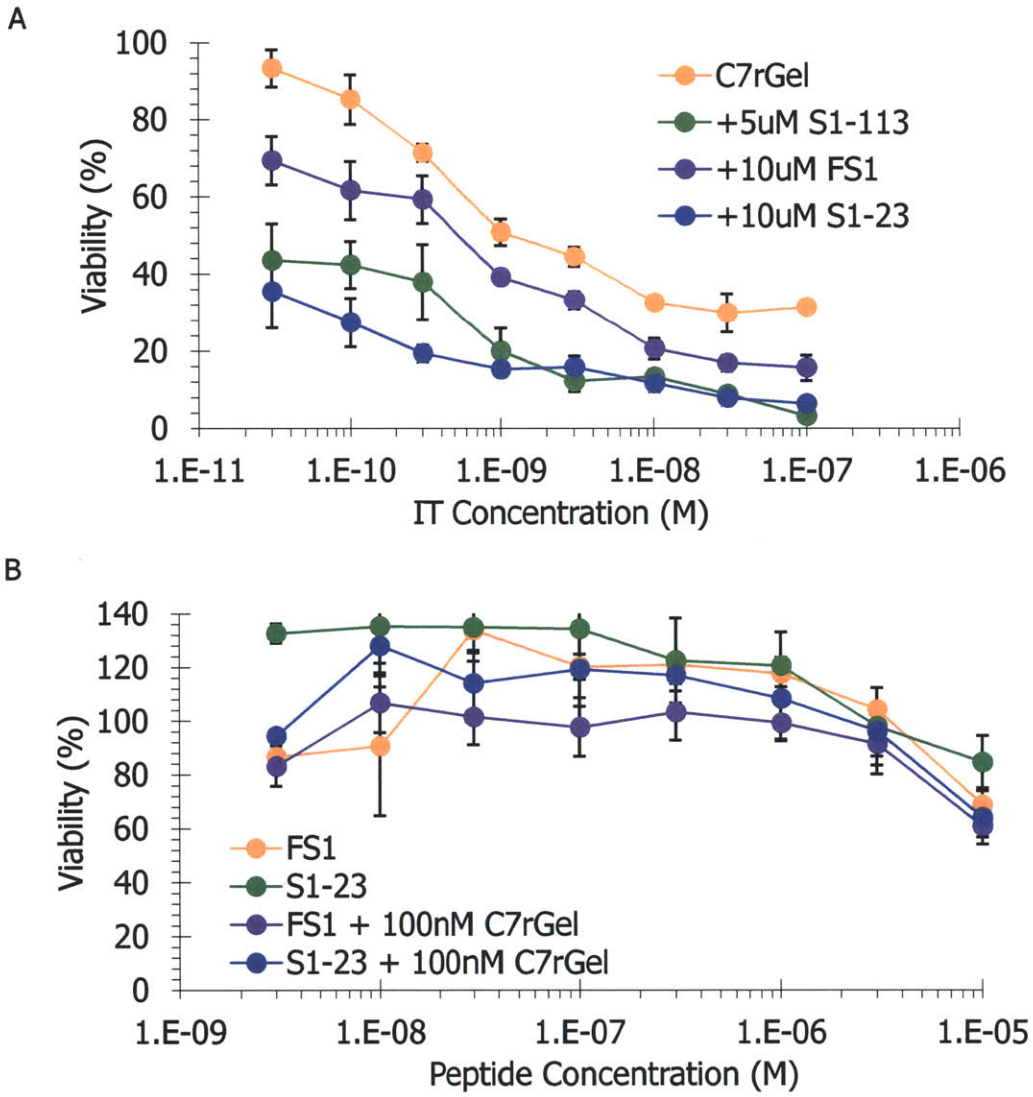

Figure B.5 – Additive and independent cytotoxicity of stapled peptides. (A) Stapled peptides are additive in their cytotoxicity when combined with CEA-targeted immunotoxin, but are also (B) independently cytotoxic at concentrations above one micromolar.

Small molecule enhancers were also tested for potentiating activity. We tested poly(ethylenimine) (PEI), chloroquine, and retinoic acid for independent cytotoxicity (Figure B.6A) finding that at 10 μM or higher, these molecules could induce cell death. When added to titrations of gelonin at non-toxic concentrations, only PEI and retinoic acid conferred even modest enhancement of cytotoxicity (Figure B.6B).

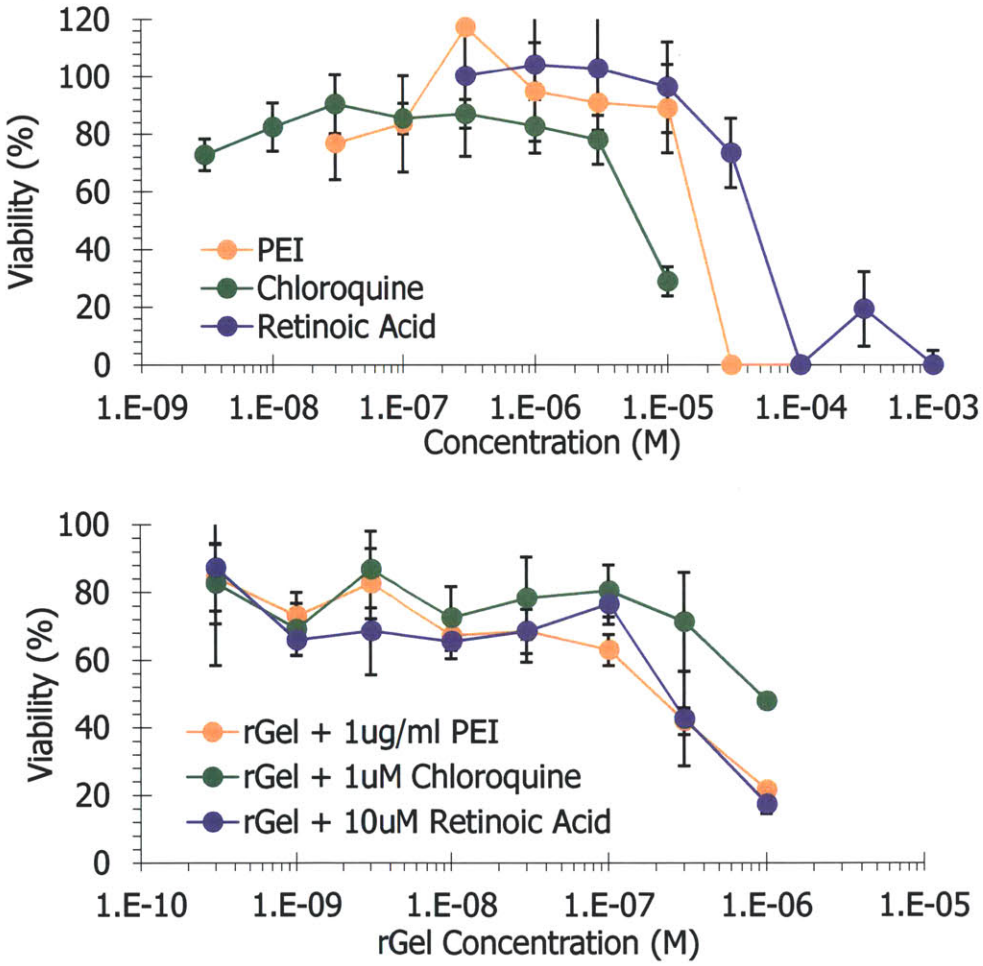

Figure B.6 – Small molecule potentiator cytotoxicity. (A) Independent cytotoxicity of small molecule potentiators. (B) Non-toxic concentrations of small molecules added to titrations of untargeted gelonin.

Discussion

Each of the different membrane active agents tested here has been implicated by others as such. However, in our hands and in our system they were not able to strongly potentiate the cytotoxic activity of either untargeted gelonin or gelonin immunotoxins. These data are supported by the fact that delivery mechanisms involving these molecules haven't progressed clinically. But this should not discourage others from attempting to target these molecules. If enough PAAc chains were conjugated to an appropriate targeting agent, then the binding and internalization of that agent might serve to increase the endosomal concentration of PAAc to active levels.

What is more important to take away from these experiments is the criticality of potency. Even if one of these molecules was capable of potentiating immunotoxin activity, if it did so only at a very high concentration, then it would be difficult to achieve the same type of activity in a targeted manner, the true goal of this work. If an average endosome has a diameter of 100 nm, then its volume is 4.2×10^{-18} L, and there would need to be ~25 molecules of an agent active at 10 μM to disrupt it. This same endosome, assuming it samples the cell membrane randomly and that antigen is distributed over that membrane randomly at ~10^5 copies per cell, will contain ~10 antigens. Such that even when saturating antigen with binding proteins, which is difficult to accomplish *in vivo*, those proteins would have to be decorated with > 2.5 active molecules each. This degree of labeling is not unrealistic, especially for IgG size proteins, but saturation can be hard to achieve.

Citations

1. Wu, Y. N., Gadina, M., Tao-Cheng, J. H., and Youle, R. J. (1994) *J. Cell Biol* **125**, 743-753

2. Musacchio, T., and Torchilin, V. P. (2011) *Front. Biosci* **16**, 1388-1412

3. Fox, M. E., Guillaudeu, S., Fréchet, J. M. J., Jerger, K., Macaraeg, N., and Szoka, F. C. (2009) *Mol. Pharm* **6**, 1562-1572

4. Henry, S. M., El-Sayed, M. E. H., Pirie, C. M., Hoffman, A. S., and Stayton, P. S. (2006) *Biomacromolecules* **7**, 2407-2414

5. Green, J. J., Zugates, G. T., Langer, R., and Anderson, D. G. (2009) *Methods Mol. Biol* **480**, 53-63

6. Lopus, M. (2011) *Cancer Lett* **307**, 113-118

7. Foyil, K. V., and Bartlett, N. L. (2010) *Curr Hematol Malig Rep* **5**, 140-147

8. Paliwal, R., Paliwal, S. R., Agrawal, G. P., and Vyas, S. P. (2011) *Mol. Pharm* **8**, 1314-1321

9. Foster, S., Duvall, C. L., Crownover, E. F., Hoffman, A. S., and Stayton, P. S. (2010) *Bioconjug. Chem* **21**, 2205-2212

10. Sonawane, N. D., Szoka, F. C., and Verkman, A. S. (2003) *J. Biol. Chem* **278**, 44826-44831

11. Funhoff, A. M., van Nostrum, C. F., Koning, G. A., Schuurmans-Nieuwenbroek, N. M. E., Crommelin, D. J. A., and Hennink, W. E. (2004) *Biomacromolecules* **5**, 32-39

12. Bonner, D. K., Leung, C., Chen-Liang, J., Chingozha, L., Langer, R., and Hammond, P. T. (2011) *Bioconjug Chem* [online] http://www.ncbi.nlm.nih.gov/pubmed/21761838 (Accessed August 15, 2011).

13. Fabre, J. W., and Collins, L. (2006) *Curr Gene Ther* **6**, 459-480

14. Meyer, M., Zintchenko, A., Ogris, M., and Wagner, E. (2007) *J Gene Med* **9**, 797-805

15. Martin, M. E., and Rice, K. G. (2007) *AAPS J* **9**, E18-29

16. Moore, N. M., Sheppard, C. L., Barbour, T. R., and Sakiyama-Elbert, S. E. (2008) *J Gene Med* **10**, 1134-1149

17. Wadia, J. S., Stan, R. V., and Dowdy, S. F. (2004) *Nat. Med* **10**, 310-315

18. Geiser, M., Cèbe, R., Drewello, D., and Schmitz, R. (2001) *BioTechniques* **31**, 88-90, 92

19. Skehel, J. J., Cross, K., Steinhauer, D., and Wiley, D. C. (2001) *Biochem. Soc. Trans* **29**, 623-626

20. Seligman, S. J. (2008) *Virol. J* **5**, 27

21. Turk, M. J., Reddy, J. A., Chmielewski, J. A., and Low, P. S. (2002) *Biochim. Biophys. Acta* **1559**, 56-68

22. Hackel, B. J., Kapila, A., and Wittrup, K. D. (2008) *J. Mol. Biol* **381**, 1238-1252

23. Esbjörner, E. K., Oglecka, K., Lincoln, P., Gräslund, A., and Nordén, B. (2007) *Biochemistry* **46**, 13490-13504

24. Moellering, R. E., Cornejo, M., Davis, T. N., Del Bianco, C., Aster, J. C., Blacklow, S. C., Kung, A. L., Gilliland, D. G., Verdine, G. L., and Bradner, J. E. (2009) *Nature* **462**, 182-188

25. Günther, M., Lipka, J., Malek, A., Gutsch, D., Kreyling, W., and Aigner, A. (2011) *Eur J Pharm Biopharm* **77**, 438-449

26. Yuan, X., Lin, X., Manorek, G., and Howell, S. B. (2011) *BMC Cancer* **11**, 61

Appendix C – Modeling cytotoxic synergy

Introduction

Our efforts in assessing the potentiating activity of membrane disruptive agents led us to question under what conditions that activity might be most easily observed. We hoped to inform the design of *in vitro* cytotoxicity experiments used for initial screening of different potentiators. Classically, simultaneous titration of both agents at a fixed molar ratio would be used (1, 2). But data collected in this way often requires statistical analysis to parse out synergistic interactions. We desired an approach where synergy might be more readily interpreted.

Methods

Equations defining cell viability and IC_{50} were derived from those of Chou and Talalay (1). The first equation gives the general definition of the combination index (CI) metric for two different drugs, D_1 and D_2:

$$CI = \frac{(D)_1}{(D_x)_1} + \frac{(D)_2}{(D_x)_2} + \frac{(D)_1(D)_2}{(D_x)_{1,2}}$$

where, D_x is a concentration for a fraction affected x, such as IC_{50} and:

$$CI = \frac{(f_a)_{1,2}}{(f_u)_{1,2}} = \frac{1-(f_u)_{1,2}}{(f_u)_{1,2}}$$

where f_a and f_u are the fraction affected and unaffected, respectively. Conveniently, f_u is directly quatified in our cytotoxicity assays. If we assume that the active concentrations of D_1 and D_2 are significantly different, then the right most term of

the CI definition is small compared to the other two terms. If we choose to ignore it completely and focus on a 50% fraction affected then:

$$\frac{1-V}{V} = \frac{D_1}{(D_{50})_1} + \frac{D_2}{(D_{50})_2}$$

where V is the viability (as a fraction). We can rearrage this equation and consider immunotoxin (IT) and potentiator (P) as D_1 and D_2 respectively to get a direct percent viability output to relate to our assays as:

$$V = \frac{1}{1+\frac{[IT]}{IT_{50}}+\frac{[P]}{P_{50}}}$$

This equation will define our combination cytotoxicity, but in order to address the affect of synergy, if any, on our cytotoxicity measurement then it will have to be incorporated into the equation as an influence of P on IT_{50}. Without a clear mechanistic way to define such an interaction, we arbitrarily selected a modified hyperbolic dose-effect curve shape:

$$IT_{50} = \frac{IT_{50}}{1+\left(\frac{P}{K_{D,P}} \times \frac{k_i}{k_{off}} \times \frac{k_{dis}}{k_{deg}}\right)}$$

Here, IT_{50} is dependent on $K_{D,P}$, the affinity of potentiator for a surface antigen, k_i / k_{off} the relative rate of internalization of the potentiator and antigen versus the antigen binding off-rate, and k_{dis} / k_{deg} the relative rate of endosomal disruption versus potentiator degradation. Parameter values were based on *in vitro* data or values understood to be reasonable from the literature. (Table C.1)

Table B.1 – Cytotoxic potentiation model parameters

Parameter	Value
IT_{50}	$2x10^{-8}$ M
P_{50}	$5x10^{-7}$ M
IT/P Concentrations	$0/10^{-10} - 10^{-7}$ M
$K_{D,P}$	$5x10^{-9}$
k_i	$2x10^{-5}$
k_{off}	$2x10^{-6}$
k_{dis}	$5x10^{-7}$
k_{deg}	$3x10^{-5}$

Results

A simulation was run using the parameters outlined above and the viability levels under each treatment concentration combination were output first for an assumption of only additive cytotoxic interactions (Figure C.1).

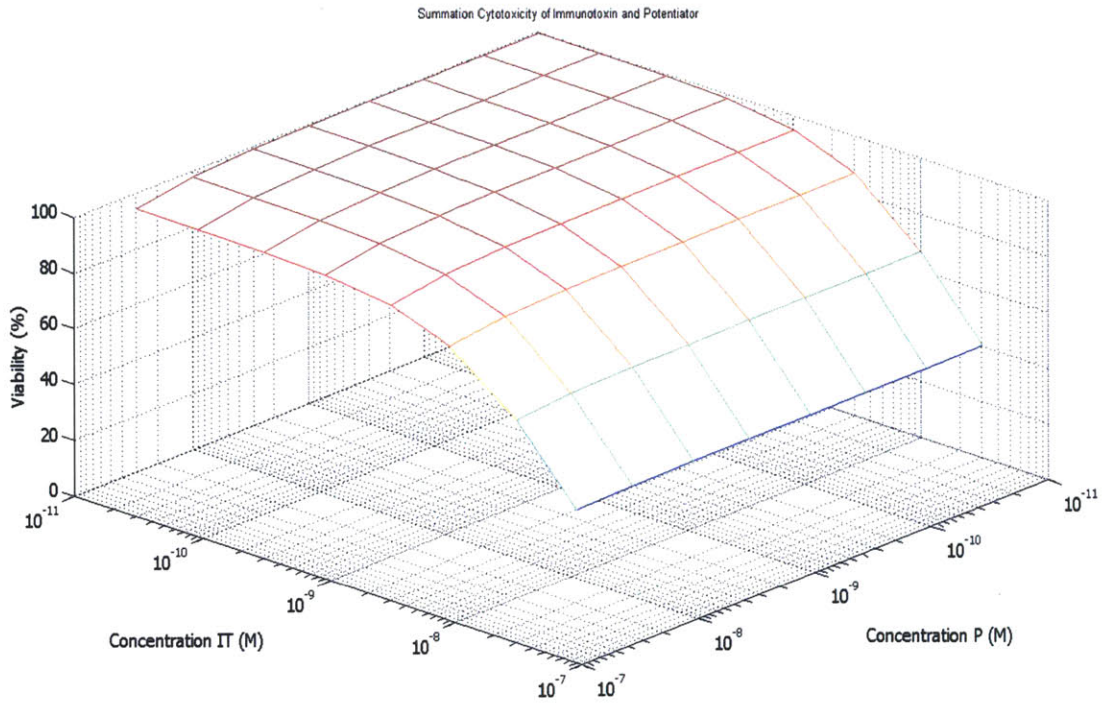

Figure C.1 – Additive cytotoxicity of immunotoxin and potentiator. Concentration dependent loss of viability is resolved across two therapeutic dimensions under conditions of no interaction between them.

Subsequently we interrogated the same loss of viability when factoring in the potentiative reduction of the IC_{50} of the immunotoxin. Using the modified hyperbolic dose-response equation to determine the affect of potentiator, we looked at the same range of concentrations for immunotoxin or potentiator for synergistic effects on viability (Figure C.2).

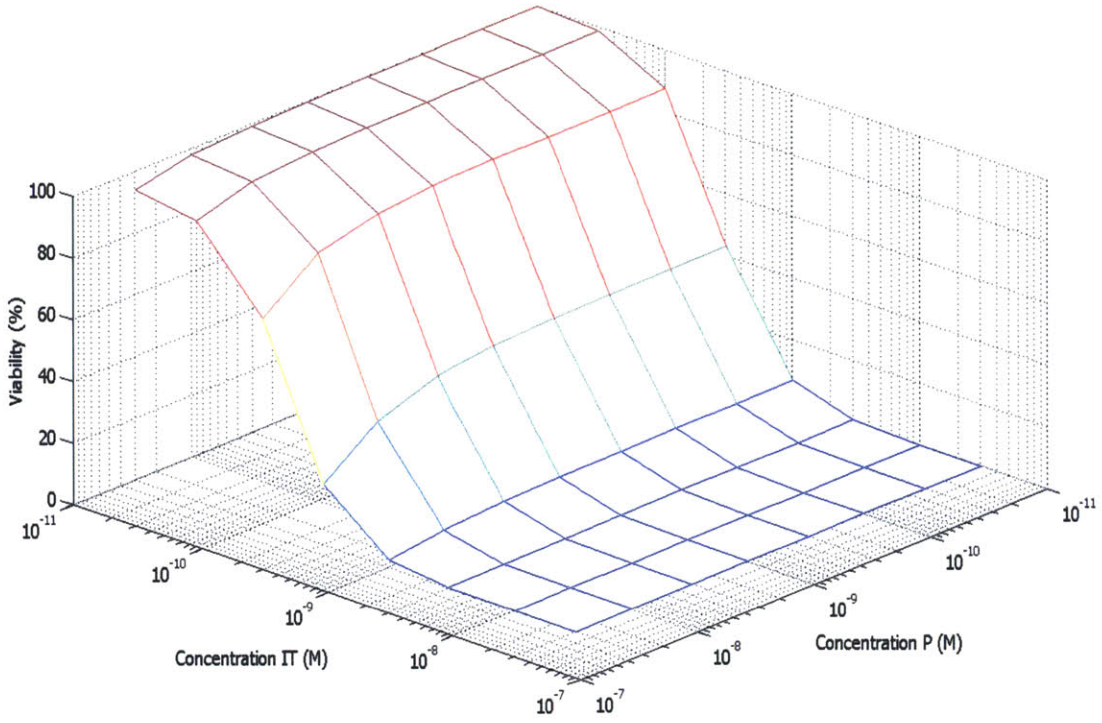

Figure C.2 – Synergistic loss of viability. When potentiator affects the IC_{50} of the immunotoxins there is a general reduction of viability across the screened two-dimensional concentration space.

Then to understand how to best observe the difference between putative potentiators that are either synergistic or merely additive, we simply subtracted the synergistic viability from the additive viability to understand the differential viability (Figure C.3).

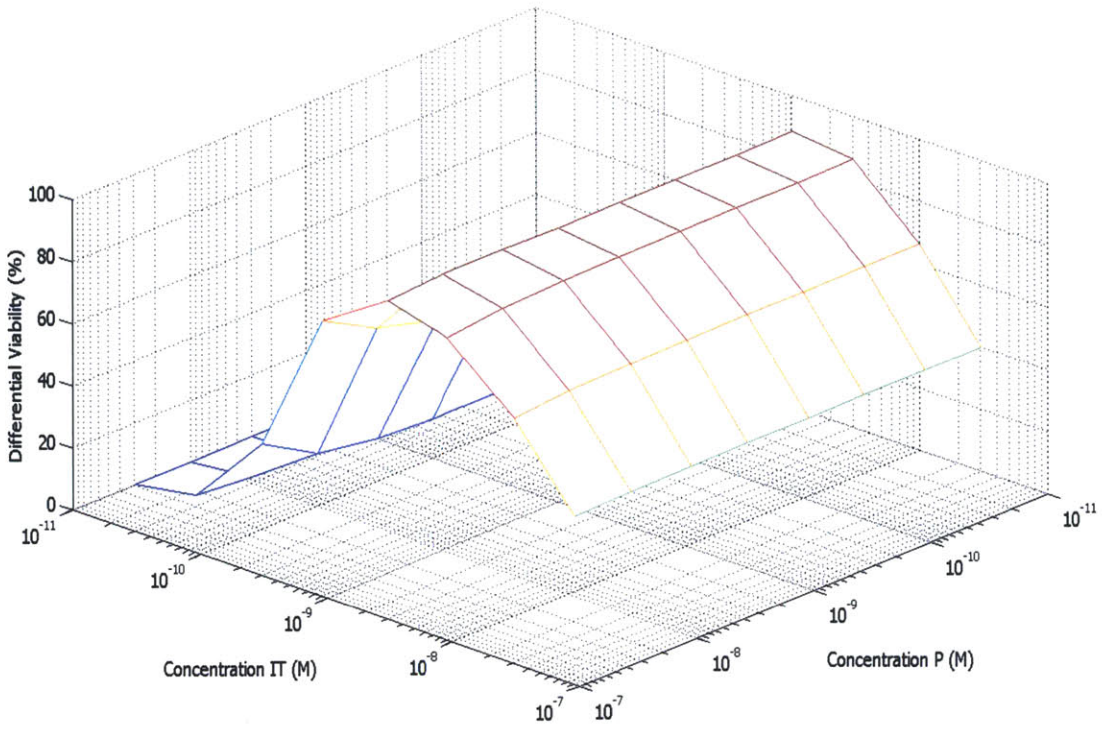

Figure C.3 – Differential viability. Synergistic viability is subtracted from additive viability across the range of concentrations for both species.

Discussion

When testing for synergistic activity between two therapeutic agents there are different statistical methods that can be applied to better understand the character of their interaction and it's strength (1-3). But sometimes, especially when searching a large number of potentiating candidates, it is valuable to be able to characterize synergy without having to calculate it. This rudimentary cytotoxicity model suggests that it should be possible to easily and directly observe potentiation from titrating a potentiator against a fixed, almost non-toxic concentration of immunotoxin. For such a titration through the concentration space, the differential viability is maximized.

Citations

1. Chou, T. C., and Talalay, P. (1984) *Adv. Enzyme Regul* **22**, 27-55

2. Chou, T.-C., and Talalay, P. (1983) *Trends in Pharmacological Sciences* **4**, 450-454

3. Yan, H., Zhang, B., Li, S., and Zhao, Q. (2010) *BMC Syst Biol* **4**, 50

This work was set in the Century typeface
which was derived from *Century Roman* in 1894 by Linn Boyd Benton.
Noted for its extreme legibility, it is the official font of the
United States Supreme Court.

Thank you for reading.